Space Sci Rev (2009) 142: 73–156
DOI 10.1007/s11214-008-9463-8

Alfvén Waves and Their Roles in the Dynamics of the Earth's Magnetotail: A Review

Andreas Keiling

Received: 30 April 2007 / Accepted: 26 August 2008 / Published online: 10 December 2008

Abstract The Earth's magnetotail is an extremely complex system which—energized by the solar wind—displays many phenomena, and Alfvén waves are essential to its dynamics. While Alfvén waves were first predicted in the early 1940's and ample observations were later made with rockets and low-altitude satellites, observational evidence of Alfvén waves in different regions of the extended magnetotail has been sparse until the beginning of the new millennium. Here I provide a phenomenological overview of Alfvén waves in the magnetotail organized by region—plasmasphere, central plasma sheet, plasma sheet boundary layer, tail lobes, and reconnection region—with an emphasis on spacecraft observations reported in the new millennium that have advanced our understanding concerning the roles of Alfvén waves in the dynamics of the magnetotail. A brief discussion of the coupling of magnetotail Alfvén waves and the low-altitude auroral zone is also included.

Keywords Alfvén wave · Magnetotail · Energy transport · Earth's magnetosphere

Contents

A. Keiling (✉)
Space Sciences Laboratory, University of California, Berkeley, USA
e-mail: keiling@ssl.berkeley.edu

1 Introduction

1.1 Brief Introduction to Alfvén Waves

Waves of any kind play three fundamental roles in physical systems. First, they act as an energy sink. For example, dropping a tennis ball vertically into a lake creates water waves which provide a mechanism for "absorbing" the ball's kinetic energy. Depending upon the intensity of the impact (e.g., the height of the fall), the transfer of the ball's kinetic energy into "wave energy" can be significant or minute in comparison to other participating energy absorbers. In a similar way, Alfvén waves "absorb" energy or are created by transferring energy during magnetospheric processes. In this regard, they provide the same function as water waves, a "sink" for energy. The extent of the participation for Alfvén waves in the energy balance of the various magnetospheric phenomena is still unknown. To act as an energy sink, an energy source and a mechanism that enables the energy transfer from the source onto the wave must exist. In the case of Alfvén waves, an example of an energy source is the stretched magnetotail and its reconfiguration via reconnection. Several mechanisms for energy transfer into Alfvén waves have been proposed and are the topic of intense investigation.

The second fundamental role of waves is to carry the absorbed energy to other—sometimes very remote—regions. One could argue that this is their most important role. For many diverse magnetospheric phenomena, it is recognized that Alfvén wave formation is an intermediate step in a sequence of energy transfer processes. For example, it has recently

been determined that during active geomagnetic conditions, Alfvén waves carry significant amounts of energy from the magnetotail to the ionosphere, in addition to plasma flows and static field-aligned currents (FAC). It can also be said that waves carry "information" about a local change to a remote location. In the case of Alfvén waves, information is carried regarding changes in currents, the magnetic field and/or convective ($\mathbf{E} \times \mathbf{B}$) flows that occur over time scales longer than an ion gyroperiod.

A third important aspect of waves is how they dissipate their energy, or, in other words, how the wave energy is transferred to other forms of energy. When waves travel, they interact with their environment in a manner that ultimately leads to wave dissipation, and this dissipation provides energy for other processes to take over. Several mechanisms have been proposed for the dissipation of Alfvén waves, most notable is the energization of electrons leading to spectacular auroras in the ionosphere. Both energy absorption and dissipation imply changes in course for energy flow inside the magnetosphere. Understanding such changes lies at the heart of every physical system. Since Alfvén waves are ubiquitous in the magnetosphere, they must play an integral role in its dynamics, and, in fact, their presence is evidence for the magnetosphere's dynamic behavior.

The three roles listed above can be found for any wave. What distinguishes the different kinds of waves (e.g., sound waves, water waves, Alfvén waves, etc.) are the unique environments in which they travel, and each environment leads to specialized wave roles. For example, surface ocean waves promote the exchange of gases such as carbon dioxide and oxygen; clearly, an important process (role) for the Earth's atmosphere, oceans, and living organisms. Alfvén waves, unlike surface ocean waves, require a magnetized plasma for propagation. The magnetosphere is such an environment which constitutes many different regions with different properties. Alfvén waves take on special roles in each of these magnetospheric regions. For example, the creation of field-aligned currents which help release magnetic stresses in the magnetotail is one such specialized role. Additional roles for Alfvén waves will be outlined in this review by presenting concrete examples. After reviewing these individual roles, I will revisit the three fundamental roles of waves, in Sect. 8, in order to evaluate the extent to which our understanding of these roles in association with Alfvén waves has increased over the last eight years.

In this day and age, Alfvén waves have been noted in popular, over-the-counter science magazines (e.g., *Scientific American* and *National Geographic*) as "wiggles" in the Earth's magnetic field, an expression which can be described as a type of "mental picture" also used by experts in the field. Utilization of this type of mental picture goes back to the concept of field lines developed by Michael Faraday and to the analogy of magnetic field line tension which can be exploited to propagate Alfvén waves. In qualitative terms, Alfvén waves are a transient electromagnetic-hydromagnetic phenomenon occurring within a magnetized plasma. They are traveling oscillations of ions and the magnetic field, $\delta\mathbf{B}$. The ion mass density provides the inertia and the magnetic field line tension provides the restoring force. Electrons also oscillate in an Alfvén wave but mostly along magnetic field lines, and they are the carriers of field-aligned currents in Alfvén waves. Since Alfvén waves are electromagnetic waves, they also have an oscillating electric field, $\delta\mathbf{E}$. Both $\delta\mathbf{E}$ and $\delta\mathbf{B}$ oscillate perpendicular to the ambient magnetic field; and due to this, the waves are also called shear Alfvén waves. Together, $\delta\mathbf{E}$ and $\delta\mathbf{B}$ yield a Poynting vector (Sect. 1.5) that represents the energy flow of the wave. In the large-scale (ideal MHD—magnetohydrodynamic) case, all frequency components of the electromagnetic field travel at the same speed, namely the Alfvén speed. At smaller scales the waves become dispersive and acquire small electric and magnetic field components parallel to the ambient magnetic field.

The first mathematical MHD description of Alfvén waves was given by Alfvén (1942). Since that time, much progress has been made regarding their theoretical description in the

non-ideal MHD case (i.e., dispersive Alfvén waves) which was reviewed by Stasiewicz et al. (2000). A commemorative biography of Hannes Alfvén, the scientist who predicted these waves ten years before their discovery, can be found in Fälthammar (1997).

1.2 Scope of Review

During 1999 and 2000, several review papers were published relating to specialized Alfvén wave topics. The review of Stasiewicz et al. (2000) discussed the theory of dispersive Alfvén waves and their relation to small-scale auroral structures. Glassmeier et al. (1999) discussed field line resonance (FLR), and Gekelman (1999) discussed laboratory experiments. Gekelman wrote, "in the past few years the quantum jump in data collection on the Freja and FAST (Fast Auroral Snapshot Explorer) missions have led to the reevaluation of the importance of these [Alfvén] waves in the highly structured plasma that was probed". Until the late 1990's, most work on Alfvén waves in the nightside was based on data from rockets and low-altitude ($<$10,000 km) satellites, and thus the significance of Alfvén waves in the extended magnetotail was not fully appreciated yet. Particularly, the low-altitude measurements of Alfvénic Poynting flux lacked a comparison with observations above the auroral acceleration region, which could provide information regarding the extent to which the Alfvénic Poynting flux is carried from the magnetotail into the auroral acceleration region, as well as information relating to the amount of Alfvénic dissipation. While Freja and FAST have continued to produce new results regarding Alfvén waves and their impacts on auroral electron acceleration, additional spacecraft missions (e.g., Geotail, Polar, and Cluster) have also led to new observations. The Polar spacecraft provided the first 3-dimensional measurements of the electric field above the auroral acceleration region, allowing an assessment for the electromagnetic energy flux of Alfvén waves. The use of conjunction studies has increased our knowledge of Alfvén wave dissipation along auroral field lines. The first FAST-Polar conjunction studies further characterized Alfvén wave coupling of the ionosphere and the magnetotail, making a strong case for the role of Alfvén waves in the creation of the aurora. Now, there is evidence that Alfvénic electron acceleration not only occurs in the auroral acceleration region, but also above it, and possibly along the entire plasma sheet boundary layer (PSBL). The UVI imager on Polar, designed to assess the energy input into the ionosphere, has strengthened the case for the Alfvén wave coupling of the magnetosphere–ionosphere system over the entire auroral oval. The other available space imager, IMAGE (Imager for Magnetopause-to-Aurora Global Exploration), together with FAST, has provided further information as to where in the auroral oval Alfvén waves contribute to the aurora. Polar and Cluster results have extended our knowledge of Alfvén waves in the seemingly "uninteresting" lobe region. Geotail studies have provided a comprehensive comparison of ion beam energies and Alfvén waves in the near-Earth tail, suggesting a causal link. The new Cluster mission and its multipoint measurement capabilities have, for the first time, allowed a description of the spatial and temporal scales of properties associated with Alfvén waves. Consequently, the combined results of these spacecraft missions have given new impetus for the study of Alfvén waves and their impacts. These, and other results, will be reviewed here.

The Earth's magnetosphere includes several distinct regions (Fig. 1). In spite of the vastly different plasma regimes found in these regions, Alfvén waves have been reported in all, with one caveat (see Sect. 6). The current review provides a phenomenological overview of Alfvén waves in the magnetotail with an emphasis on spacecraft observations reported since 2000 that have contributed to the advancement of our understanding for the roles of Alfvén waves in the dynamics of the magnetotail. The review includes observations from the central plasma sheet (CPS) (Sect. 2), the PSBL (Sect. 3), the plasmasphere (Sect. 4),

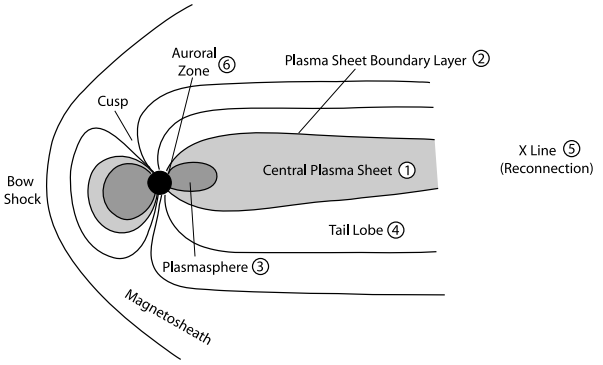

Fig. 1 Different magnetospheric regions. The numbered regions are reviewed here in the specified order (*1–6*)

the tail lobes (Sect. 5), the reconnection region (Sect. 6), and the auroral zone (Sect. 7) (see numbered regions in Fig. 1). There is also indirect evidence of Alfvén waves from many ground-based observations which are, however, not reviewed here. Concurrent with the new observations, model simulations regarding the acceleration of electrons by Alfvén waves have been compared with observational data, providing unambiguous evidence for parallel electron acceleration via Alfvén waves. Since a comprehensive review concerning recent advances in model simulations does not currently exist in the literature, such a review in the near future by another author would be advantageous. In this review, each section begins by briefly defining the region of discussion and giving a selective choice of an early (before 2000) Alfvén wave report regarding this region. Brief descriptions and early report are followed by subsections that review recent advances in the field of Alfvén waves in the specific space region discussed. The organization of Alfvén wave observations by regions is pedagogically useful for prospective students learning about each region and the effects of Alfvén waves, and for experts desiring current information for Alfvén waves in a particular region of space. An alternative approach to this organization scheme would be a review arranged by phenomena, as for past reviews. In the next section, I provide a brief review format of this type, where I list thirteen reasons why Alfvén waves are important, followed by two sections on how one identifies Alfvén waves and how the Alfvénic Poynting flux is calculated.

1.3 Importance (Roles) of Alfvén Waves

While threading the entire magnetosphere, Alfvén waves play many roles in the dynamics of the magnetosphere. Brief summaries of these various roles, some which overlap, are given below. More detail can be found in the subsequent sections where also the appropriate references are given; some references are given here if they do not appear later.

1.3.1 Magnetosphere–Ionosphere Coupling

The Earth's magnetic field connects the ionosphere with the outer magnetosphere (Fig. 2). Currents flowing along magnetic field lines are closed by perpendicular currents in these two regions, thus closing the auroral current circuit. Alfvén waves are the initial carrier of these field-aligned currents. The coupling of two vastly different regions, one collisionless and the other collisional, creates a special region, called the auroral acceleration region—the site of a rich phenomenology of plasma processes many of which are only partially understood and which require further investigation. Our understanding of the role of Alfvén waves in the magnetosphere–ionosphere coupling process is ever-increasing.

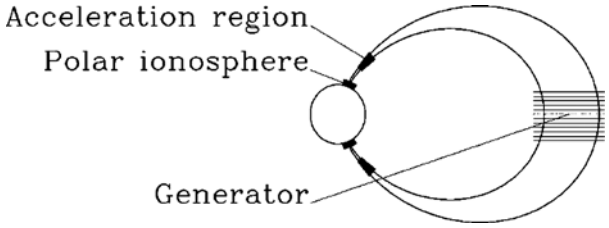

Fig. 2 Key regions of the auroral current circuit (from Vogt 2002)

1.3.2 Energy Carrier

Guided along magnetic field lines, Alfvén waves carry energy from one region to another. Recent results indicate that this mechanism is important for the transport of energy from the magnetotail towards the auroral acceleration region during the energy release of stored magnetic field energy at times of substorm expansion.

1.3.3 Parallel Electric Field

Large-scale Alfvén waves with perpendicular wavelength much larger than the electron inertial length or the ion acoustic gyroradius are, to a first approximation, governed by the ideal Ohm's law. Therefore, they do not contain any considerable electric field parallel to the ambient magnetic field. However, small-scale, kinetic Alfvén waves are accompanied by a parallel electric field which affects the interaction of the wave with its plasma environment.

1.3.4 Particle Accelerator

Hasegawa (1976) proposed that Alfvén waves launched from the magnetosphere could accelerate auroral electrons, and currently there is ample evidence for this early conjecture. Alfvén waves are also thought to transversely accelerate ions leading to their expulsion from the ionosphere.

1.3.5 Energy Sink

Alfvén waves are a type of sink for other forms of energy in the magnetosphere, and therefore help release stresses and/or overloading, a role intimately related to the generation mechanisms of Alfvén waves. One of the best established mechanisms for the generation of Alfvén waves is mode-coupling to compressional waves. Firsthand observational evidence also indicates that the energy release process during reconnection creates Alfvén waves.

1.3.6 Field-Aligned Currents (FAC)

Alfvén waves carry field-aligned currents and are also necessary for the establishment of quasi-static, field-aligned currents. The idea is that a sudden dynamic change in convection or resistivity in some region of the magnetosphere launches an Alfvénic front. This front propagates back and forth between the source and any potential boundary like the ionosphere, and, in time, a steady current is generated.

1.3.7 Auroral Arcs

Many proposed scenarios exist regarding the creation of auroral arcs (see review by Borovsky 1993). The causal connection between Alfvén waves and the aurora is one of them, and this connection is now well supported observationally for some classes of auroral structures. An example is the optical auroral modulation at the foot points of the FLR.

1.3.8 Field Line Resonance

The term field line resonance (FLR) is used in two ways. First, it describes the coupling process of fast mode waves and shear Alfvén waves at Alfvén velocity gradients perpendicular to the magnetic field direction. Second, it refers to standing Alfvén waves oscillating between two reflecting boundaries at the eigenfrequency of a particular magnetic field line. Unmistakable evidence from space now indicates that FLR exists. FLR is associated in various ways with substorms; for example, it can control luminosity fluctuations of the aurora, it can start at substorm onset and it might play a role in the triggering of substorms.

1.3.9 ULF Pulsations

Ultra-low frequency (ULF) pulsations encompass a broad range of wave phenomena. As first suggested by Dungey (1955), and now well established, some ULF pulsations are generated by Alfvén waves. The application of ULF pulsations to magnetospheric phenomena is manyfold (see review by Takahashi et al. 2006).

1.3.10 Substorm Dynamics

Alfvén wave activity during magnetospheric substorms has been reported from the ground and in space. A substorm is a highly dynamic period which involves, for example, the transport of energy, the acceleration of particles, the establishment of field-aligned currents, and the formation of the aurora. All of these processes are associated with Alfvén waves. Recent observations from space also correlate energetic Alfvén waves with the onset of the auroral break-up. Alfvén waves in the form of FLR are even thought to play a role in the initiation of substorms.

1.3.11 Energy Cascade, Turbulence, and Resistivity

Transferring energy from large scales to smaller scales is important for the dissipation of wave energy. This process operates in Alfvén waves and can lead to wave turbulence and anomalous resistivity. In turn, anomalous resistivity plays an important role in, as two examples, magnetosphere–ionosphere coupling and reconnection.

1.3.12 Reconnection

Kinetic Alfvén waves have been proposed to mediate reconnection. Recently, they have been observed in the reconnection region, which demonstrates that Alfvén waves at small scales are also an energy sink for the reconnection process. The full extent of their importance in all phases of reconnection (i.e., triggering, evolution, and dissipation) has not yet been observationally demonstrated.

1.3.13 Astrophysical and Geophysical Applications

The application of Alfvén waves extends beyond the magnetosphere. Alfvén waves have also been observed in the magnetosphere of other planets (e.g., Acuna et al. 1981), and their role is being investigated to solve problems related to the solar wind (review by Tu and Marsch 1995), solar flares (e.g., Melrose 1992), the solar corona (e.g., Tomczyk et al. 2007), and the Earth's core (Bloxham et al. 2002).

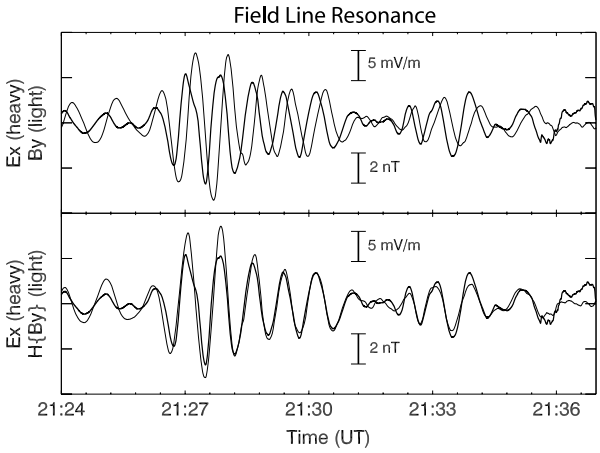

Fig. 3 (from Keiling et al. 2001b) The *top panel* shows the 90° phase shift between the perturbation fields of a standing Alfvén wave. The *bottom panel* illustrates the action of the Hilbert transform

1.4 Identification of Alfvén Waves

Several techniques with different degrees of confidence have been used in the literature to identify Alfvén waves from the ground and in space. Since this review is largely an observational review, it is appropriate to briefly describe in-situ and ground-based techniques, and to give some early references where these techniques have been applied.

1.4.1 Space-Based Techniques

1. To a first approximation, a shear Alfvén wave propagating along the magnetic field does not change the total magnetic field. Therefore, before electric field measurements were available in space, magnetic fluctuations (perpendicular to the background field) below the ion gyrofrequency, showing no variation in the total magnetic field, were interpreted as Alfvén waves (Hayward and Dungey 1983). The method did not allow one to determine differences in a system of field-aligned currents traversed by a fast-moving satellite (Gurnett et al. 1984).

2. A well accepted identification method for Alfvén waves relates to the ratio of the two perpendicular perturbation fields, δE and δB, in relation to the Alfvén speed, v_A (e.g., Mallinckrodt and Carlson 1978). In addition, the method requires that the wave frequency lies below the ion cyclotron frequency. For small-scale waves, the ratio is modified and includes parameters such as the ion gyroradius, the electron inertial length, and the perpendicular wavelength (e.g., Lysak and Lotko 1996). These parameters render a $\delta E/\delta B$ ratio larger than the local Alfvén speed (for examples see Louarn et al. 1994; Volwerk et al. 1996; and Wygant et al. 2002).

3. In the case of standing Alfvén waves, the $\delta E/\delta B$ ratio does not equal the Alfvén speed, but is modified because of the nodal structure of the E and B fields. In this case, a very convincing Alfvén wave signature results in a phase shift of 90° between the two corresponding perpendicular perturbation fields of a monochromatic Alfvén wave (Fig. 3) (e.g., Hughes and Grard 1984; and Cahill et al. 1986).

4. A standing Alfvén wave can contain several superposed frequency components. Dubinin et al. (1990) showed that for such a case, the wave fields δE and δB are related via the Hilbert transform (Fig. 4). This transform shifts all frequency components by 90° without changing their amplitudes. This technique is an extension of #3.

5. For a traveling Alfvén wave, the perturbation magnetic field and the fluid velocity are related by $v = \pm\delta B/\sqrt{\mu_0}$ (Lysak 1990). Hence, if no electric field measurements are

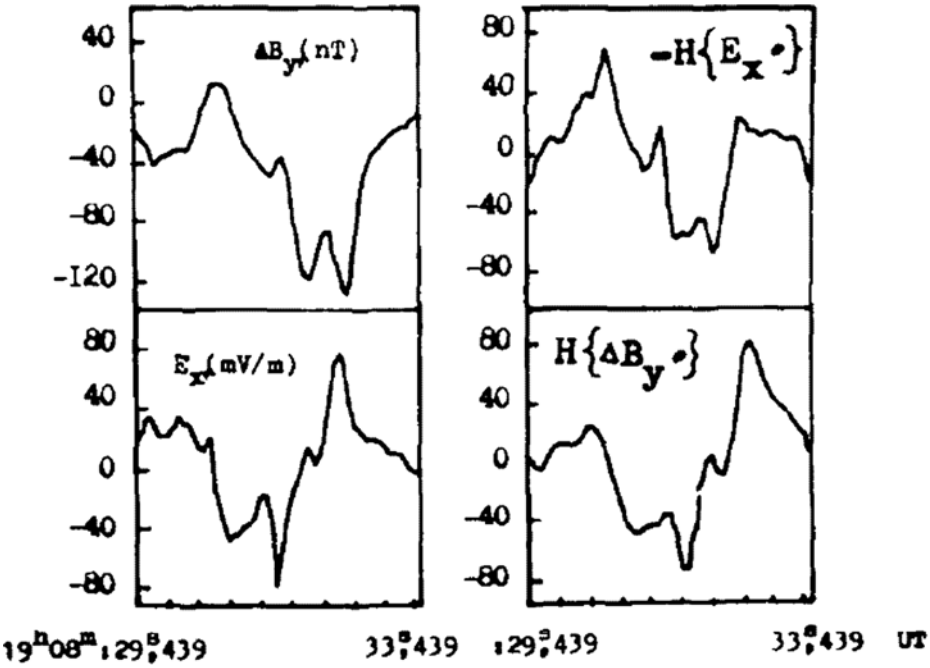

Fig. 4 (from Dubinin et al. 1990) The signals B_y and E_x show different waveforms. However, B_y and the Hilbert transform of E_x show very similar waveforms, demonstrating the existence of standing waves with several spectral components. Alternatively, one can take the Hilbert transform of B_y and compare it with E_x

available, $\delta\mathbf{B}$ and $\mathbf{v}$ can be compared. Of course, knowing $\mathbf{v}$ allows one to calculate the electric field, $\mathbf{E} = -\mathbf{v} \times \mathbf{B}_0$ via the frozen-in condition. Thus, this method is, in fact, similar to methods #2 through #4.

6. In turbulent wave fields, when none of the above techniques seem appropriate, a comparison of measured and theoretical wave dispersion curves can be made to infer the existence of Alfvén waves (Chaston et al. 2005; see Sect. 7 for an example).

7. The interaction of Alfvén waves of various temporal and spatial scales with the ionosphere or regions of parallel electric fields can lead to phase relationships between δE and δB more complicated than 90°; E/B ratios can also be affected in unpredictable ways (Lysak and Dum 1983; Knudsen et al. 1992; Vogt and Haerendel 1998; and Streltsov and Lotko 2003). Furthermore, Alfvén waves undergo dynamic changes driven by both the generator region and the region of interaction (e.g., the ionosphere and parallel electric field regions). Such temporal evolution of Alfvén waves is best determined with the use of numerical methods (model simulations). Comparisons of model simulation results and observations have, therefore, been used as an indirect method for identifying Alfvén waves (see Sect. 7.1).

8. It is now well established that Alfvén waves accelerate electrons, in particular, in the auroral zone. The signature of wave-accelerated electrons is different from those that are accelerated by a static field-aligned potential, for example. Therefore, as an indirect identification method, the simultaneous presence of these wave-accelerated electrons and turbulent wave fields have been used to identify the fields as the perturbation fields of Alfvén waves (see Sect. 7.3).

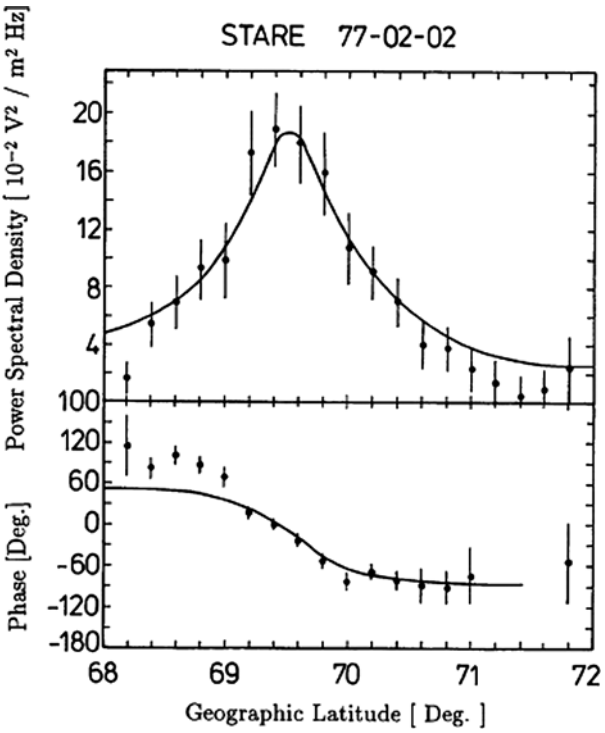

Fig. 5 Properties of the electric field of FLR in the auroral zone, inferred by radar (from Walker et al. 1979)

1.4.2 Ground-Based Techniques

The E/B ratio is ineffective for the identification of Alfvén waves in the ionosphere and on the ground. Hence, other techniques have been developed using ground-based magnetometer and radar data.

9. Ground magnetometer data alone do not allow one to distinguish between fast and Alfvén modes. The fundamental reason behind the lack of determination is that the magnetic field perturbation of an Alfvén wave undergoes a 90° rotation as the wave travels through the ionosphere to the ground (Hughes 1974). Since fast mode signals do not undergo a rotation, both the fast and Alfvén modes show the same magnetic field polarization. However, in the case of FLR, identifications can be achieved by analyzing the latitudinal variation in wave amplitude and polarization, since the amplitude is a maximum in the phase reversal region for a FLR (e.g., Samson et al. 1971; and Fukunishi 1975).

10. Similar to technique #9, electric fields associated with the FLR show the same amplitude and polarization pattern as magnetic fields (Fig. 5). This pattern has been verified by radar measurements of ionospheric electric fields in the north–south component (Walker et al. 1979).

11. Alfvén waves modulate and increase the intensities of plasma irregularities in the ionosphere. The irregularities can be measured in the backscatter of radars and can, therefore, be utilized to identify Alfvén waves. The technique was demonstrated in Yeoman and Lester (1990) and Yeoman et al. (1991).

1.5 Calculation of Alfvénic Poynting Flux

An important quantity associated with Alfvén waves is the Poynting flux. It is the Poynting flux that carries the wave energy and that can be converted into particle energy during dissipation processes. The Poynting flux also indicates the energy flow direction, which is not immediately apparent in **E** and **B** measurements alone. An early space application of this very useful quantity was demonstrated by Kelley et al. (1991) who applied it to large-scale currents. Later, other workers calculated the Poynting flux of Alfvén waves (e.g., Louarn et al. 1994; Volwerk et al. 1996; Nagatsuma et al. 1996; and Kletzing et al. 1996). Calculation of the Poynting flux is not trivial and erroneous results can occur. Here I describe some of the pitfalls in calculating this quantity, using excerpts from Keiling et al. (2002).

The relevant fields needed to calculate the Poynting vector, **S**, are the perturbation electric ($\delta\mathbf{E}$) and magnetic ($\delta\mathbf{B}$) fields: $\mathbf{S} = 1/\mu_0\ \delta\mathbf{E} \times \delta\mathbf{B}$. Strictly speaking, it is only the integral over a volume of the Poynting flux that is physically significant for dissipation and creation of the Poynting flux (Kelley et al. 1991). The existence of the Poynting flux at a particular location does not tell us whether this flux will ever dissipate, or whether it will simply circulate indefinitely. For space physics applications, it is often impractical to integrate over the volume at hand, because regions of mere energy flow and regions of energy dissipation can be separated by very large distances, and simultaneous measurements of electric and magnetic fields in the different regions are not available. However, physical insight into the problem may allow one to reason its relevance.

In the context of the magnetosphere, the measured magnetic field is $\mathbf{B} = \mathbf{B}_0 + \delta\mathbf{B}$, where $\mathbf{B}_0$ is the background magnetic field and $\delta\mathbf{B}$ is the perturbation field. Two sources for the electric and magnetic perturbation fields can be identified: Alfvén waves and quasi-static, field-aligned currents (FACs) that close in the ionosphere or at altitudes below a satellite. Both sources have magnetic and electric field perturbations with the same polarization and are associated with Poynting flux propagation along magnetic field lines.

Additionally, there are two contributions to the Poynting flux associated with Alfvén waves. One contribution represents the convective transport of the flux perpendicular to the background magnetic field, proportional to $\delta\mathbf{E} \times \mathbf{B}_0$, and is zero when averaged over many wave periods. The contribution, that accounts for the transport of energy along the background magnetic field, is entirely due to the perturbation electric ($\delta\mathbf{E}$) and magnetic ($\delta\mathbf{B}$) fields (see above). In the case of static fields the situation is similar; only $\delta\mathbf{E}$ and $\delta\mathbf{B}$ contribute to a physically meaningful Poynting flux. As shown by Kelley et al. (1991), the quantity $\delta\mathbf{E} \times \mathbf{B}_0$ does not contain any useful information concerning energy flow or dissipation. Hence, it is appropriate to filter out $\mathbf{B}_0$.

Both quasi-static field structures and Alfvén waves can be present simultaneously, and can be superposed in the measured signal. At times, it can be challenging to separate the two contributions. Either physical insight into the problem is needed to permit the separation of the two signals into Alfvénic and quasi-static structure, or one needs to apply an iterative approach for filtering different frequency bands. The filtering of different frequency bands should be checked at each step to determine whether or not any of the Alfvén wave criteria, as described in Sect. 1.4, have been fulfilled.

2 Alfvén Waves in the Central Plasma Sheet

The central plasma sheet (CPS), bounded by the plasma sheet boundary layer (PSBL) and the low-latitude boundary layer (LLBL), contains hot plasma, and is the site of the field

reversal region and the current sheet. The CPS is known to be the site of many phenomena, such as bursty bulk flows (BBF), flapping motion, substorm current wedge initiation, braking of fast flows, instabilities leading to a cross-tail current disruption, adiabatic and non-adiabatic heating, and bouncing ion clusters, etc. The CPS is also rich in phenomena associated with MHD waves, both fast and Alfvén mode, covering a range of frequencies spanning Pc5 (1–7 mHz) to Pi1 (22 mHz–1 Hz) pulsations. The reader is reminded that only Alfvén wave observations are reviewed here in an attempt to focus on their roles. Also noted is that the focus here is on nightside observations for which there are far fewer observational reports compared with dayside.

An early example of Alfvén waves in the CPS is shown in Fig. 6 (Hughes and Grard 1984). The FLR was recorded for an L between six and nine in the postmidnight sector close to the inner boundary of the CPS. E and B were out of phase by 90°, the signature of standing Alfvén waves. The waves had a period of approximately 90 seconds and lasted for a few hours. Standing wave signatures are often associated with FLR, which require closed field lines (although not necessarily; see examples in Sects. 3 and 5). Two additional requirements for FLR are small ionospheric damping so that the wave energy can sufficiently be reflected, and small wave dissipation along the magnetic field line via, for example, electron acceleration (see Sect. 3). Well established is the fact that FLR in the CPS play important roles in the dynamics of the magnetotail. FLRs can be divided into those which have frequencies in the Pc5 range and those with frequencies in the Pi2 range, which occur in concert with ground Pi2s and substorm onset. Fewer space observations exist for the former type. I discuss both types separately in Sects. 2.1 and 2.2, respectively.

In the literature, special interest has been devoted to a class of auroral arcs that are driven by FLR in the CPS. Most of these studies have utilized ground-based optical and magnetic field measurements, which are not reviewed here because the focus is space observations. To date, only one study has reported simultaneous in-situ (CPS) and ground observations of arc-related FLR. The study is reviewed in Sect. 2.3. The contribution of energy input into the auroral region from Alfvén waves in the CPS during substorms and storms, and its association with the aurora is also briefly discussed in Sect. 2.3.

One Pi2 mechanism is intimately linked to transient Alfvén waves launched in the near-Earth CPS. The mechanism is called the transient response model (see review by Baumjohann and Glassmeier 1984). Although well established from ground data, there is very limited confirmation in space. In fact, no new observations have been reported in the main time period covered in this review (Sect. 2.4).

Section 2.5 summarizes the results of Alfvén wave observations in the CPS. Some readers may find it useful to look first at the block diagram in this sub-section, which graphically links all reviewed phenomena, so as to better follow the logical flow of Sect. 2.

2.1 Pc 5 Pulsations

Ample ground-based evidence of nightside FLR activity in the 1–7 mHz band (i.e., the Pc5 band) on field lines that map from the CPS is available (e.g., Samson et al. 1991a, 1991b, 1992a, 1992b, 1996; Ruohoniemi et al. 1991; Ziesolleck and McDiarmid 1994; Rankin et al. 1999a, 1999b, 2000, 2005; Wanliss and Rankin 2002). However, few studies have correlated ground-based observations with low-altitude spacecraft (<4000 km) observations (e.g., Lotko et al. 1998; and Samson et al. 2003). These two studies provided direct evidence that electron acceleration inside the FLR leads to auroral arcs. For a brief review of ground-based and low-altitude FLR observations, see the recent monograph on ULF waves (Takahashi et al. 2006). In the CPS proper, FLR activity has been recorded near the inner

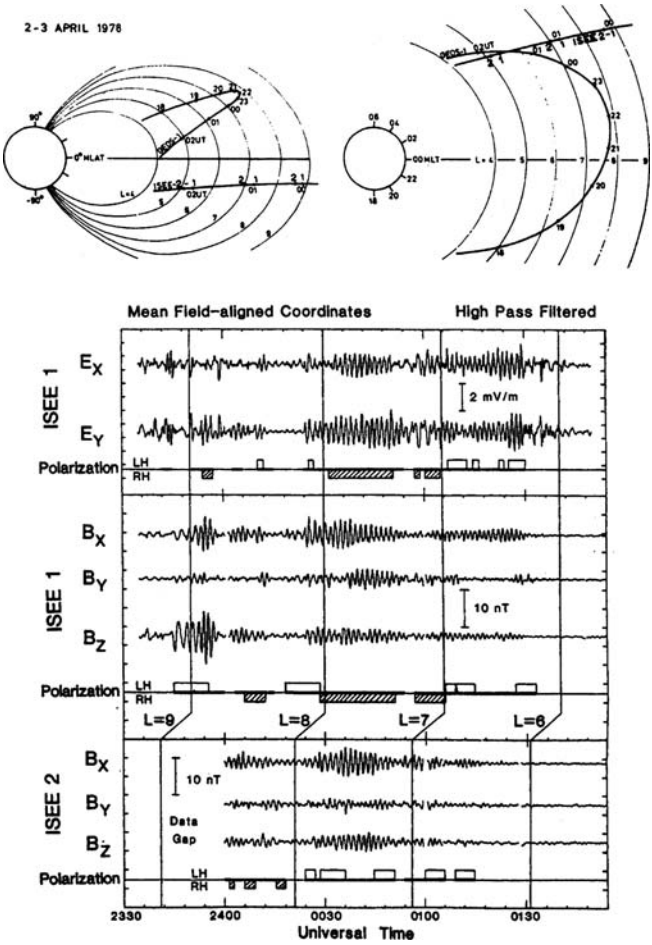

Fig. 6 (from Hughes and Grard 1984) (*Top*) Orbits of GEOS 1, ISEE 1, and ISEE 2 shown in the magnetic meridian plane, and projected into the magnetic equatorial plane. (*Bottom*) Electric and magnetic field data from ISEE 1, and magnetic field data from ISEE 2. The data were band-pass filtered to remove trends with periods longer than 300 s and shorter than 12 s

edge of the CPS (e.g., Hughes and Grard 1984, and Samson et al. 2003), Fig. 7. Very few new observations exist for Pc5 Alfvén waves since 1999.

The first coordinated CPS-ground based study of FLR was performed by Lessard et al. (1999), using ground magnetometers and scanning auroral photometers from CANOPUS (the Canadian Auroral Network for the Open Unified Study) and in-situ electromagnetic field data from CRRES (the Combined Release and Radiation Effects Satellite), Fig. 8. All data sets showed a spectral peak at 2.1 mHz while recorded at approximately the same invariant latitude. The phase relation between *in situ* electric and magnetic fields confirmed the standing nature of Alfvén waves. Optical data indicated that the FLR modulated the auroral luminosity in the ionosphere (see Sect. 2.3 for further discussion). Peaks were also present at 1.4 and 1.7 mHz in the ground-based magnetometer data and CRRES data at a slightly higher latitude. The anti-sunward phase velocity of the ground oscillations indicated that the source of the FLR excitation was located in the dayside magnetosphere. The authors

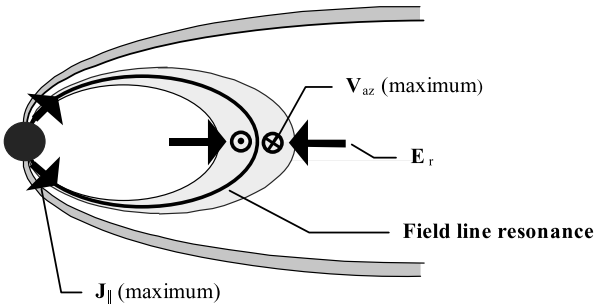

Fig. 7 A schematic of FLR in the near-Earth magnetotail. The outer shaded region is the plasma sheet boundary layer. The inner shaded region is the earthward edge of the plasma sheet (from Samson et al. 2003)

concluded from this finding that the substorm onset, which occurred before the observation of the FLR, was not the cause of the resonance. but that a solar wind source was more probable. Simultaneous data from the geosynchronous satellites, GOES 6 and 7, did not show spectral peaks similar to the FLR. Therefore, the authors ruled out a cavity-type mode resonance and suggested a waveguide structure, consistent with the anti-sunward phase velocity of the FLR.

With an increased number of spacecraft simultaneously in space, Mann et al. (2002) and Rae et al. (2005) studied nightside Pc5 with 2–2.5 mHz and 1.4–1.6 mHz, respectively. In these studies, the authors were able to track the solar wind energy from the magnetopause down to the Earth's surface using a comprehensive set of data sources including different satellites, ground-based magnetometers, radar, and optical instruments. Both studies concluded that the most likely explanation for the Pc5 was that magnetopause oscillations at the flanks coupled energy to field lines inside the magnetosphere. These oscillations resulted in the generation of standing Alfvén waves along resonant field lines, which were then also observed on the ground. In the absence of monochromatic dynamic pressure variations in the solar wind, the authors have also suggested that the discrete frequency pulsations in the magnetosphere resulted from the excitation of a magnetospheric waveguide mode, perhaps excited via the shear flow Kelvin-Helmholtz instability (KHI) (e.g., Southwood 1974; and Chen and Hasegawa 1974) at the duskside magnetopause. The narrow-band Pc5 pulsations presented by Rae et al. (2005) lasted many hours and occurred during the recovery phase of a large geomagnetic storm (Fig. 9). The large wide-spread distribution of Pc5 activity at the frequency of 1.4–1.6 mHz, except in the solar wind dynamic pressure (see the power spectra in Fig. 9 on the right), clearly demonstrated the global nature of the pulsations. Alfvén waves were identified as an intermediate energy carrier in a longer sequence of events. Furthermore, Poynting flux calculations for the Pc5 FLR (Fig. 9 left, bottom three panels) showed that in addition to an oscillating field-aligned component due to the FLR, a significant component was directed downtail. An additional component is consistent with a solar wind energy source rather than an energy source in the distant tail, and shows that some coupling of fast modes was present locally.

The study by Zheng et al. (2006) reported both a discrete Pc5 and an L-dependent Pc5 during the same time interval. The Cluster spacecraft, being the farthest away, and ground stations near Cluster's footpoint, recorded Pc5 pulsations (1.1 mHz), Fig. 10. Cluster electric and magnetic field measurements directly confirmed their standing wave nature. Simultaneously, quasi-periodic oscillations at different frequencies were observed in the post-midnight/early morning sector by GOES 12 (2.5 mHz at $L = 8.7$), Polar (1.4 and 1.9 mHz at $L = 11$ and 14, respectively), and Geotail (2.5 mHz at $L = 9.8$). While GOES 12 and Geotail observed similar waveforms, all the satellites observed different waveforms and onset times,

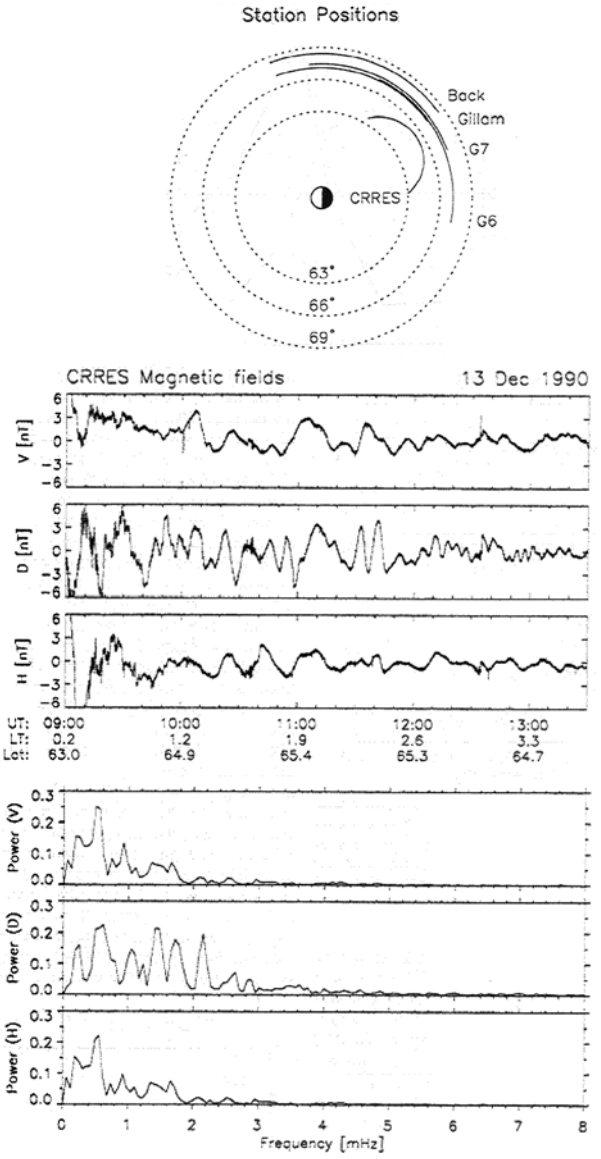

Fig. 8 (from Lessard et al. 1999) (*Top*) The locations of CANOPUS ground stations and various satellites (CRRES, GOES 6 and 7) during a Pc5 event. Magnetic invariant latitude is represented as the radial component, and magnetic local time as the angular component. The *solid lines* represent the path of each station and each satellite. (*Bottom*) Magnetic fields observed by CRRES, presented in a VDH (rectangular) coordinate system. Spectra for all components were calculated using the entire interval and are shown in the *lower panels*

when compared to Cluster's Pc5. Also noted was that the ground 1.1-mHz pulsations propagated westward, consistent with the tailward streaming high-speed solar wind observed by the ACE (Advanced Composition Explorer) spacecraft. Therefore, Zheng et al. (2006) proposed that Cluster's Pc5 was due to a waveguide oscillation excited by solar wind interaction (via KHI) at the flanks, while the lower L-value Pc5 was due to a broad-band source coupling to FLR, consistent with the L-dependent frequency variations. L-dependent variations of Pc5 FLR had been reported previously by Laakso et al. (1998). More commonly, L-dependent behavior occurs for FLRs associated with substorms, as discussed in Sect. 2.2.

Many studies have commented on unexpected low frequencies (1–4 mHz) for Pc5 FLR in the CPS, since they are not consistent with dipole field lines (e.g., Warner and Orr 1979;

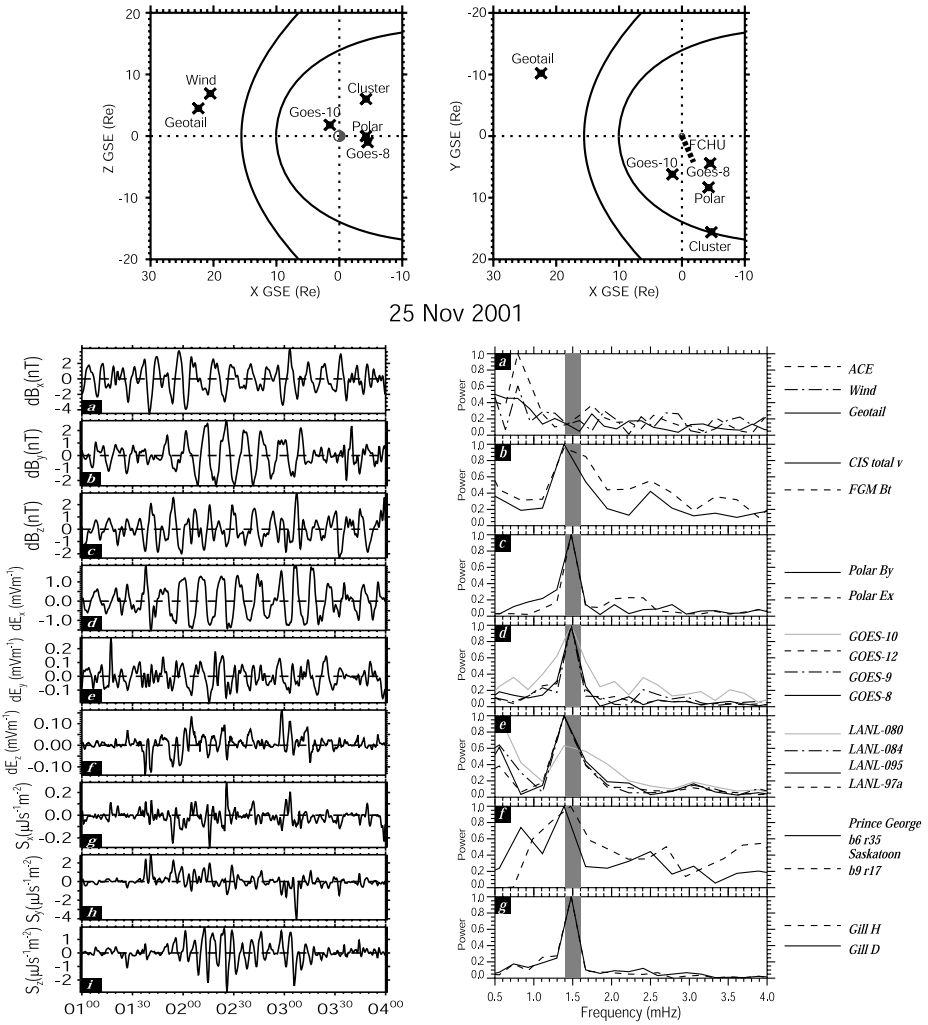

Fig. 9 (from Rae et al. 2005) (*Top*) The positions of the relevant spacecraft (ACE and LANL satellites not shown) at 0200 UT on November 25, 2001. (*Bottom, left*) (**a–i**) Magnetic and electric field data from Polar transformed into field-aligned coordinates and components of the wave Poynting vector. (*Bottom, right*) Normalized FFT power spectra of (**a**) time-lagged (24 min) solar wind dynamic pressure, (**b**) Cluster-3 total magnetic field and total ion velocity, (**c**) Polar E_x and B_y measurements in field-aligned coordinates, (**d**) GOES azimuthal magnetic fields, (**e**) LANL electron energy flux in the 225–315 keV range, (**f**) SuperDARN line-of-sight velocity data from Prince George and Saskatoon radars, and (**g**) H- and D-component magnetic fields from the Gillam magnetometer, all between 0145 and 0315 UT on 25 November 2001. The *gray shaded area* denotes the 1.4–1.6 mHz band

Singer et al. 1981; Walker et al. 1992; Waters et al. 1995; Lotko et al. 1998; Rankin et al. 1999a, 1999b; Streltsov and Lotko 1999; Rankin et al. 2000; Wanliss et al. 2002; and Bekhor 2006). The most common explanations are a stretched magnetic field topology and an increased mass density along field lines. The work by Zheng et al. (2006), showed that the ground station Gillam (located at 66.4°) and Cluster were on field lines that mapped to $R > 20R_E$ in the equatorial plane (Fig. 11 on the top and left). For comparison, Fig. 11

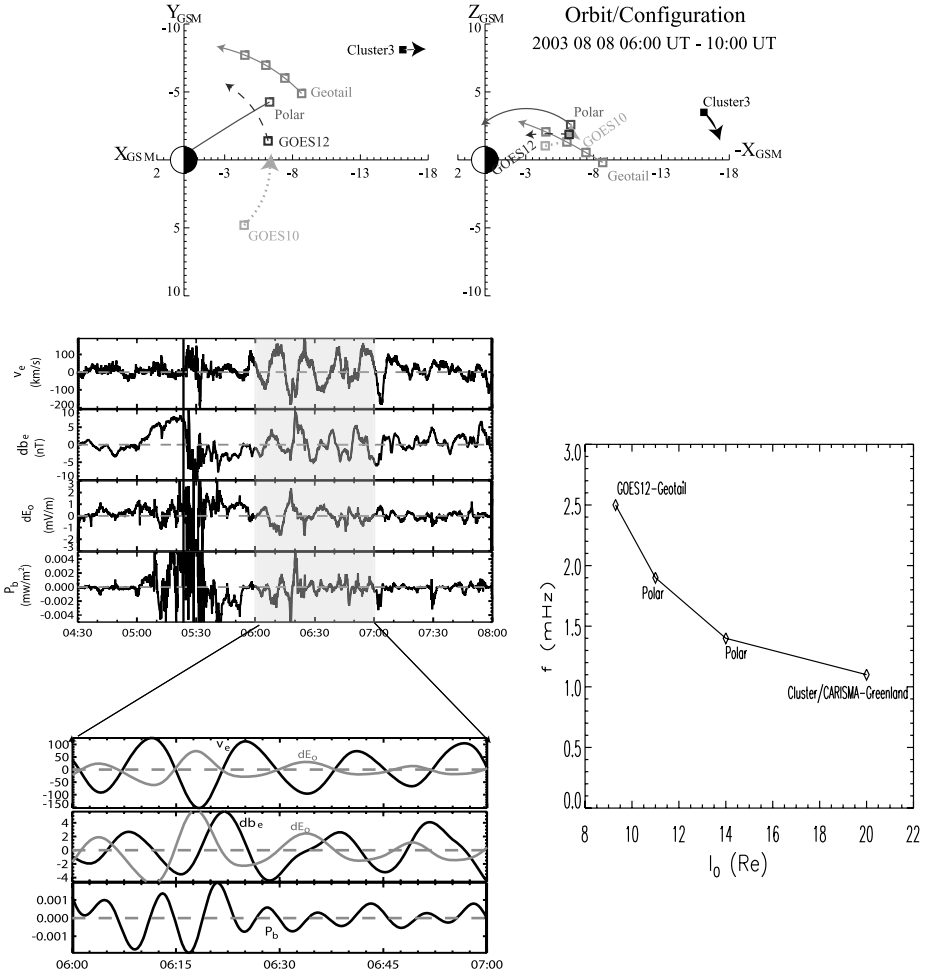

Fig. 10 (from Zheng et al. 2006) (*Top*) The orbit configuration of the satellites used in this study, with arrows indicating the direction of motion. (*Bottom, left*) Parameters of oscillation recorded by Cluster and an expanded view of band-pass filtered data. (*Bottom, right*) Frequency versus L shell for different satellites and ground data. L values were estimated using the Tsyganenko 96 model

on the top and right, illustrates the stretching of a field line that originated at a latitude of 68° on the Earth's surface for four different *Kp* inputs using the T89c field model (Lui and Cheng 2001). In stretched magnetic field topologies of a self-consistent equilibrium magnetosphere, numerical calculations yielded values between 0.77 and 7.06 mHz for equatorial crossing distances of 8 to 20 R_E, see the bottom of Fig. 11, which is similar to typical observations.

2.2 Substorm/Pi2-Associated FLR

A different class of FLR in the CPS shows higher frequency oscillations (10–40 mHz) when compared with those described in Sect. 2.1. These FLRs occur at substorm onset together with ground Pi2 pulsations (e.g., Sakurai and McPherron 1983; Takahashi et al. 1988; Taka-

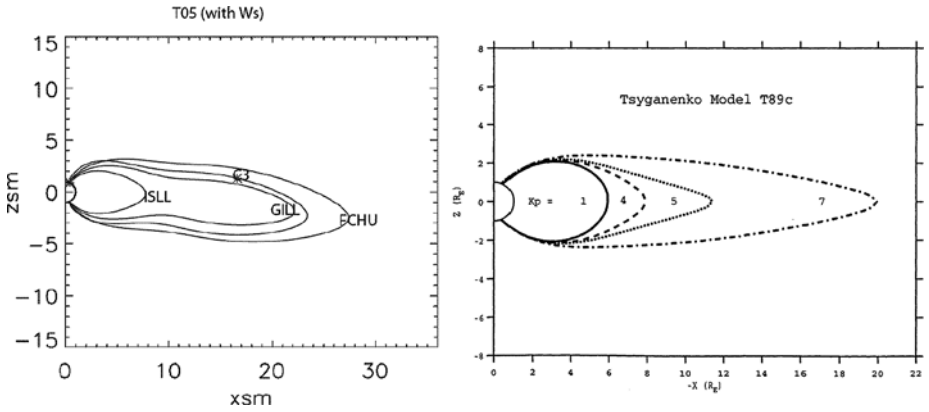

Kp	X_0, R_E	B_0, nT	β_0	f_{s_A-even}	f_{s_A-odd}	f_{s_M-even}	f_{s_M-odd}
1	5.9	119	0.166	33.6	86.3	0.17	2.17
4	7.9	11.7	17.2	7.06	16.2	0.031	2.04
5	11.4	1.7	815	1.25	3.10	0.0024	0.69
7	19.9	3.3	212	0.77	2.46	0.0054	0.37

Fig. 11 (*Top, left*) (from Zheng et al. 2006) Modeled magnetic field lines in the x–y plane from the T05 model for the event shown in Fig. 10. (*Top, right*) (from Lui and Cheng 2001) The diagram illustrates the stretching of a field line originating from 68° latitude on the Earth's surface for four different *Kp* inputs using the T89c field model. (*Bottom*) (from Lui and Cheng 2001) Frequencies in mHz of FLR based on an ideal MHD equilibrium model. X_0 is the equatorial crossing distance, B_0 is the magnetic field at the equator, and β_0 is the plasma beta. Subscripts for frequency s_A and s_M stand for shear Alfvén and slow mode, respectively

hashi et al. 1996; Saka et al. 1996; and Nose et al. 1998), although they have also been reported during pseudo-breakups (Takahashi et al. 1996). A comprehensive study on this type of FLR was done by Takahashi et al. (1996) who reported a dominant occurrence in the post-midnight sector on L shells with $4 < L < 8$. Using multiple spacecraft, monitoring several L shells simultaneously, it was also shown that the frequency of these FLRs decreased for larger L values. The L-dependent variation is consistent with a scenario that indicates that field lines independently oscillate at their eigenfrequency. A broad-band frequency source, such as a sudden compressional impulse at substorm onset, is thought to provide the energy for L-dependent FLR (e.g., Takahashi et al. 1996; and Nose et al. 1998). Since the spectral content of simultaneous ground Pi2s at lower L values is different from the FLR, it was further proposed that the energy source might be the same for both, but that the mechanisms establishing the frequencies are different.

Only few new studies have appeared in the last seven years that reported substorm-associated FLR in the CPS. These studies reported: (a) differences of *in situ* observations in the inner versus outer magnetosphere, (b) L-dependent variation of FLR frequencies along a single meridian, and (c) coupling of fast and Alfvén modes. These studies are discussed below.

Kim et al. (2001) analyzed Pi2 pulsations simultaneously recorded *in situ*, in the inner magnetosphere ($L < 5$, nightside) using AMPTE CCE (Active Magnetospheric Particle Tracer Explorers/Charge Composition Explorer) data, and low-latitude ($L < 2$, dayside) measurements from the ground (Kakioka and Hermanus ground stations), in concert

with magnetic field oscillations in the CPS recorded at geosynchronous orbit (by GOES 5 and 6) (Fig. 12). AMPTE CCE recorded compressional Pi2s, which were not correlated with the compressional waves from the GOES satellites. In addition, at the onset of the compressional Pi2s from AMPTE CCE, strong transverse oscillations from both GOES satellites were nearly simultaneously excited with slightly different frequencies (11 and 12 mHz). Although not explicitly shown, no electric field measurements were available, it was assumed that these oscillations were FLR similar to those reported by Takahashi et al. (1996). The observations suggest that Pi2 events in the inner magnetosphere (plasmasphere) and the FLR at geosynchronous orbit (i.e., CPS) were energized by a common source with a broad frequency spectrum, associated with substorm onset; but that their generation mechanisms may be different, possibly a trapped fast mode for the compressional oscillations, and a field line resonance for the transverse oscillations (Kim et al. 2001). The authors also discussed, but ruled out, alternative scenarios. In general, there are several competing mechanisms for the Pi2 generation mechanism. The interested reader is referred to Olson (1999) for a review of this topic.

Keiling et al. (2003a) compared Polar data of FLR in the CPS (~0330 MLT) and magnetometer data (SAMNET—the Sub-Auroral Magnetometer Network) of ground Pi2 at low to mid-latitudes ($2.6 < L < 4.5$, around midnight MLT). As seen in Fig. 13, the data indicate

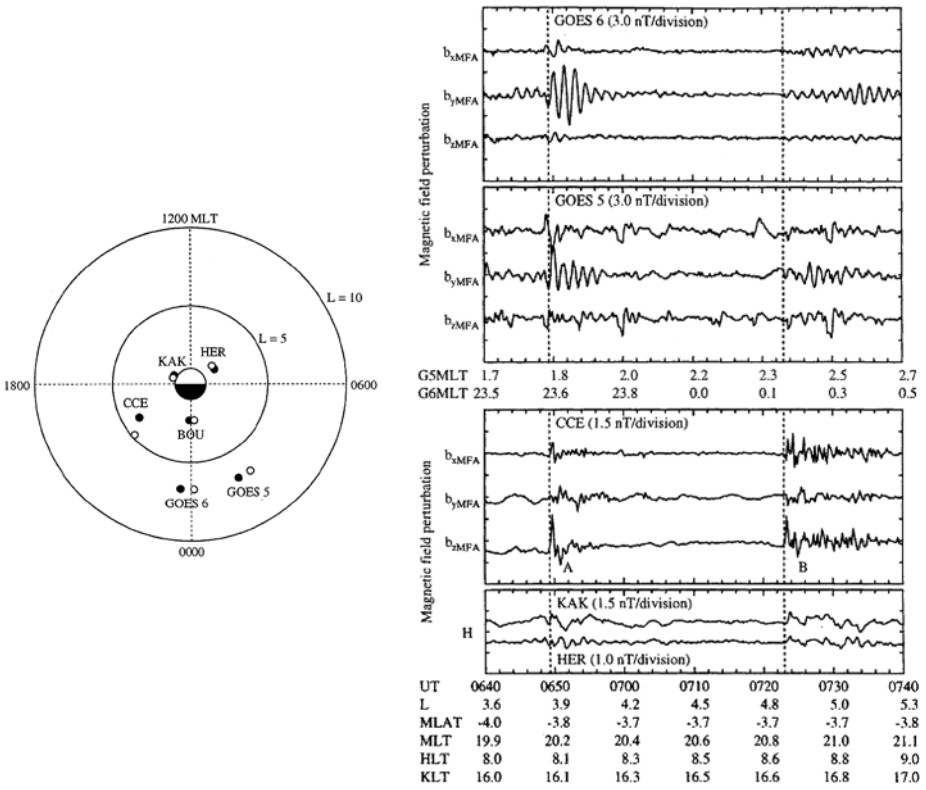

Fig. 12 (from Kim et al. 2001) (*Left*) Locations of satellites and ground stations during the FLR events. (*Right*) Magnetic field data from GOES 5 and 6, AMPTE CCE, the Kakioka ground station (KAK), and the Hermanus ground station (HER). Fields are given in the local mean-field-aligned (MFA) coordinates for GOES and AMPTE CCE. Presented data from KAK and HER were filtered

that on the ground the Pi2 frequency remained nearly constant with time and was similar for all stations with different L values, whereas the frequency of the *in situ* FLR ($L > 4$) decreased from 35 to 15 mHz as the satellite crossed field lines on a nearly constant meridian with increasing L value ($L = 4$ to 5.3) inside the CPS. In spite of the azimuthally large, separated observation sites, the onset of the space oscillations coincided with the onset of the ground Pi2 suggesting that the space FLR and ground Pi2 resulted from the same initial magnetospheric disturbance. Therefore, the observations are in agreement with the scenario of one impulsive source but different excitation mechanisms for the low to mid-latitude Pi2 pulsations and the higher-latitude FLR in the CPS (cf. Kim et al. 2001). Also noted was that no compressional component with the same frequency variation accompanied the FLR, which can be explained by assuming that the mode-coupling region was located away from the satellite observation points. The reported L-dependent frequency variation of FLR along a fixed meridian complements the results of Takahashi et al. (1996), who showed the L-dependence by using more than one satellite at different locations.

A one-year visual survey of nightside Polar passes yielded 24 FLR events (Fig. 13 at the top). A concentration of FLR events in the postmidnight sector can be seen, in agreement with the earlier survey by Takahashi et al. (1996). For each event, electric and magnetic fields and plasma density data were investigated, and it was found that for all events, E_x (radial) and B_y (azimuthal) were out of phase by 90°, indicating standing waves. The azimuthal magnetic field component (B_y) dominated over the compressional component (B_z). Furthermore, density data indicated that FLR events occurred outside the plasmasphere, and inside the plasma sheet whenever a plasmapause could clearly be identified in the data. Events were found both very close to the inner edge of the plasma sheet and deeper inside the CPS, suggesting that FLR can occur throughout the CPS. Also likely, is the possibility that FLR can simultaneously occupy extended regions of the CPS.

In contrast to substorm-associated FLR, excited by a non-monochromatic, possibly broadband, source, Keiling et al. (2001b) reported substorm-associated FLR at 2300 MLT in the CPS, excited by a monochromatic source. The FLR did not show any L-dependent frequency variations as the Polar spacecraft crossed L shells from 4.1 to 3.7 (Fig. 14). Although the FLR occurred on magnetic field lines with very low L values, usually associated with the plasmasphere, particle data confirmed that the FLR occurred inside the CPS. The geomagnetic activity was high ($Kp > 5$) prior to and during this event, which may explain the closer inner edge of the CPS. The FLR was triggered at substorm onset (dashed line) and was accompanied by a significant compressional (fast mode) component with identical frequency to the FLR (Fig. 15). Hence, the FLR was mode-coupled to the fast mode wave, which shifted from standing to traveling. The largest Poynting flux component was field-aligned, with little indication of ionospheric damping. In addition, a net energy flow was present that pointed radially outward. The FLR had the same wave packet-like form and nearly the same monochromatic frequency as the ground Pi2 pulsations, which occurred over a range of L values ($L = 1.83$–3.75). Practically conjugate to the space FLR ($L \sim 3.9$), ground stations recorded between $L = 3.4$ and 3.75 an amplitude maximum and a phase reversal in the H component of the Pi2 event, both of which are ground signatures of FLR (e.g., Samson et al. 1971; and Lanzerotti et al. 1974). As a result, it was suggested that the space FLR caused the conjugate ground Pi2. This amplitude maximum has been coined "secondary amplitude maximum" because it occurs at latitudes below the larger auroral Pi2 maximum ($L > 5$). This secondary maximum has been much debated in the Pi2 community, and beside the FLR scenario other scenarios have been proposed to explain it, including a surface wave on the plasmapause (Sutcliffe 1975) and a cavity mode (e.g., Yeoman and Orr 1989).

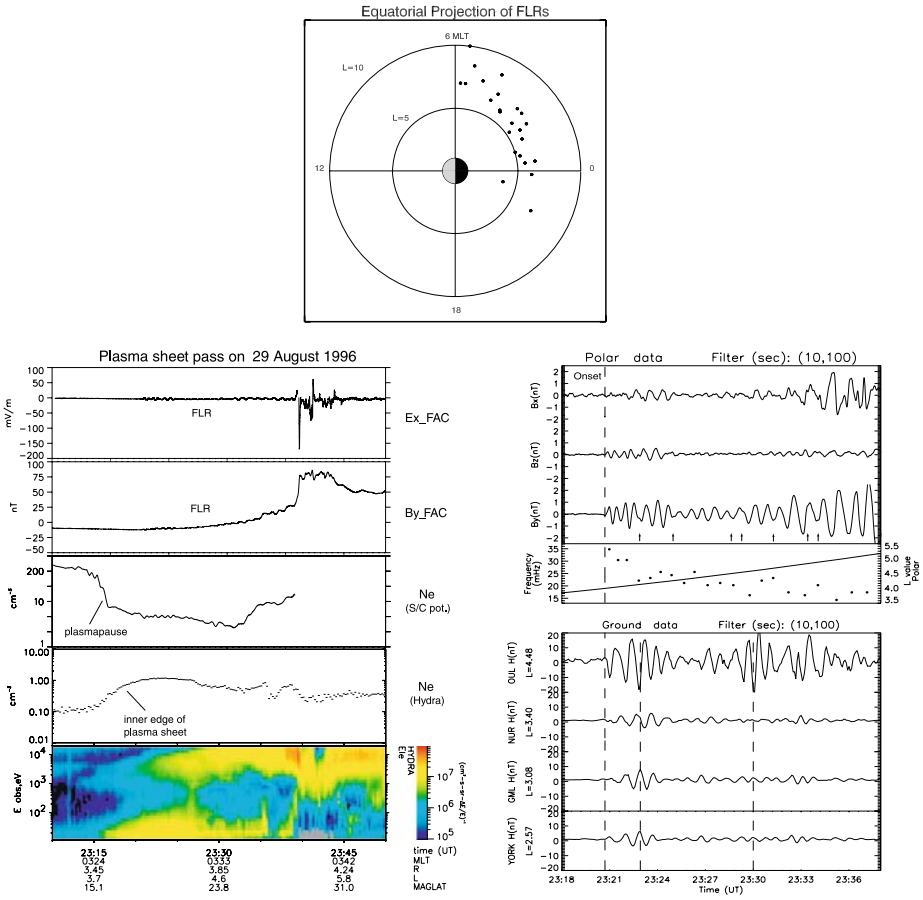

Fig. 13 (from Keiling et al. 2003a) (*Top*) Equatorial projection of FLR events recorded by Polar during 1997. Note that only the nightside (1800–0600 MLT) was surveyed. (*Bottom, left*) Field and particle data from one selected FLR event during a plasma sheet crossing, recorded by Polar. (*Bottom, right*) A comparison of waveforms in space and on the ground, band-pass filtered data. The *fourth panel* shows the L value (*solid line*) crossed by Polar, together with the frequency variation of the azimuthal magnetic field component (*dots*), throughout the crossing of the plasma sheet

2.3 Discrete Aurorae

Much of the aurora that is caused by Alfvén-wave-accelerated electrons is associated with the poleward region of the auroral oval which maps to the PSBL (see Sect. 3 for more details). Some discrete auroral arcs occur near the inner edge of the auroral oval, which presumably map to the inner region of the CPS. Ground-based observations provide evidence, supported by numerical work, that latitudinally narrow FLR in the 1–4 mHz band, Sect. 2.1, cause these auroral arcs (e.g., Samson et al. 1991a, 1991b, 1996, 2003; Xu et al. 1993; Trondsen et al. 1997; Rankin et al. 1999a, 1999b, 2000, 2005; Milan et al. 2001; and Wanliss and Rankin 2002). Direct observations of FLR in the CPS and their association with auroral structures are however very sparse. The first, and to my knowledge, only high-altitude observation of FLR in the CPS and its association with auroral structures, was reported by Lessard et al. (1999). This study was already partially reviewed in Sect. 2.1, where it was

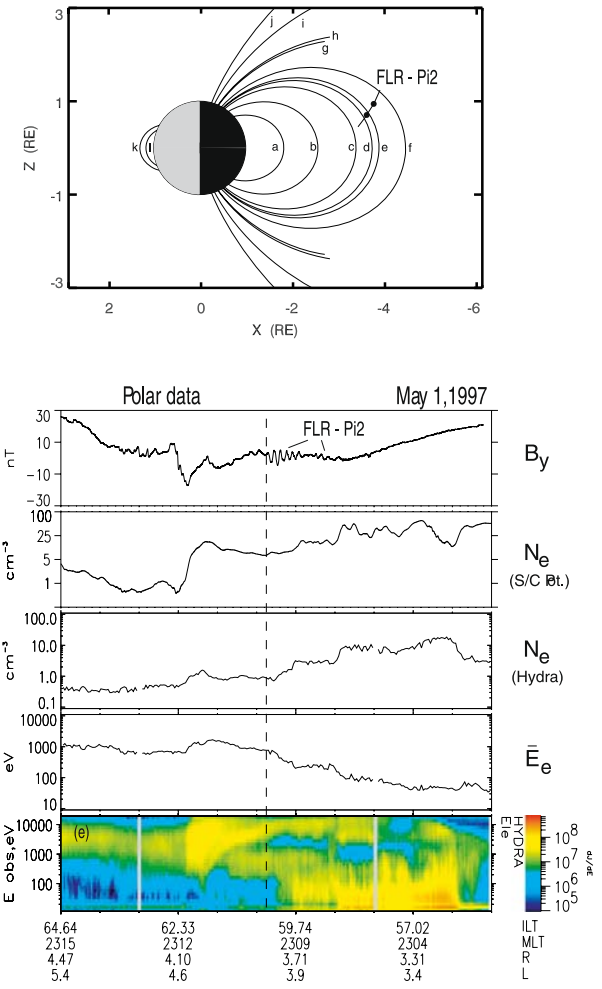

Fig. 14 (from Keiling et al. 2001b) (*Top*) Meridional projection of magnetic field lines connected to several ground stations labeled '*a*' through '*j*'. (*Bottom*) Polar-spacecraft based observations of a FLR triggered at substorm onset, *dashed line*

shown that the FLR had a spectral peak at 2.1 mHz. Figure 16 shows additional scanning photometer data recorded by three stations, and the auroral intensity at 5577 Å observed at Gillam, with its frequency spectrum. Gillam, located approximately on the same invariant latitude as CRRES, recorded a peak at 2.1 mHz, strongly suggesting that the auroral luminosity was modulated by the FLR observed in the CPS. Observations of FLR at low-altitude near the equatorward boundary of the auroral oval, in association with conjugate auroral arcs, have also been reported (Lotko et al. 1998), and are reviewed in Sect. 7.3. In addition to auroral arcs associated with FLR in the CPS, it was recently demonstrated by Mende et al. (2003a) that Alfvén waves in the auroral zone, located on field lines that presumably map to the CPS, can cause a different type of aurora, namely the substorm break-up arc. Since the observations were also made in the auroral zone at low altitude (<4000 km), I also review this event in more detail in Sect. 7.3.

Intense Alfvénic Poynting flux has been demonstrated as a common occurrence in the PSBL during the substorm expansion phase, as is further discussed in Sect. 3.2. In contrast, few reports of intense Earthward Poynting flux in the CPS during substorms exist (Maynard

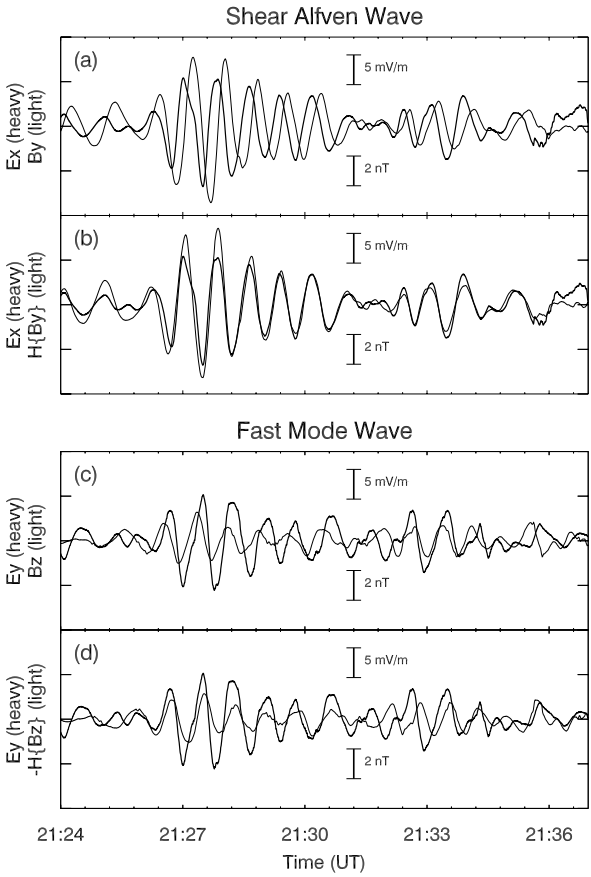

Fig. 15 (from Keiling et al. 2001b) Comparison of waveforms for the electric and magnetic components on May 1, 1997, associated with the shear Alfvén wave and the fast mode wave, center Fig. 14. A phase shift between E and B of 90° indicates a standing wave. The result of the Hilbert transform, H{}, is described in Sect. 1.4. Presented data were band-pass filtered (10 s, 80 s)

et al. 1996; Keiling et al. 2001a; and Toivanen et al. 2001). The Poynting fluxes carried by Alfvén waves can take on values in the order of 1 mW/m^2 (or several hundreds of mW/m^2 when mapped to ionospheric altitudes), up to two orders of magnitude larger than for FLR. The most intense Alfvén waves, with Poynting fluxes of ∼1000 mW/m^2, mapped to the ionosphere, were recorded inside the CPS during the main phase of a major geomagnetic storm (Dombeck et al. 2006). The waves were recorded by Polar at ∼5.5 R_E geocentric distance and ∼2300 MLT. Although not verified by optical data, it is likely that these Alfvén waves provide the power necessary for aurora deep inside the CPS. A conjugate FAST pass, during the same time interval, provided additional evidence for Alfvénic Poynting flux powering auroral acceleration at low latitude during storms. Therefore, Alfvén waves are capable of bringing significant amounts of energy into the inner magnetosphere during both substorm and storms. Also important is that Polar simultaneously recorded strong compressional waves which could be the source for the intense Alfvén waves.

2.4 Substorm Current Wedge and Onset

The substorm current wedge (SCW) is a current system that is believed to be initiated at substorm onset in the CPS. At first, it launches Alfvén waves towards the ionosphere. A few early studies had reported *in situ* observations of these Alfvén waves. Sakurai and McPherron (1983) attributed azimuthally polarized transient field line oscillations to an oscillating

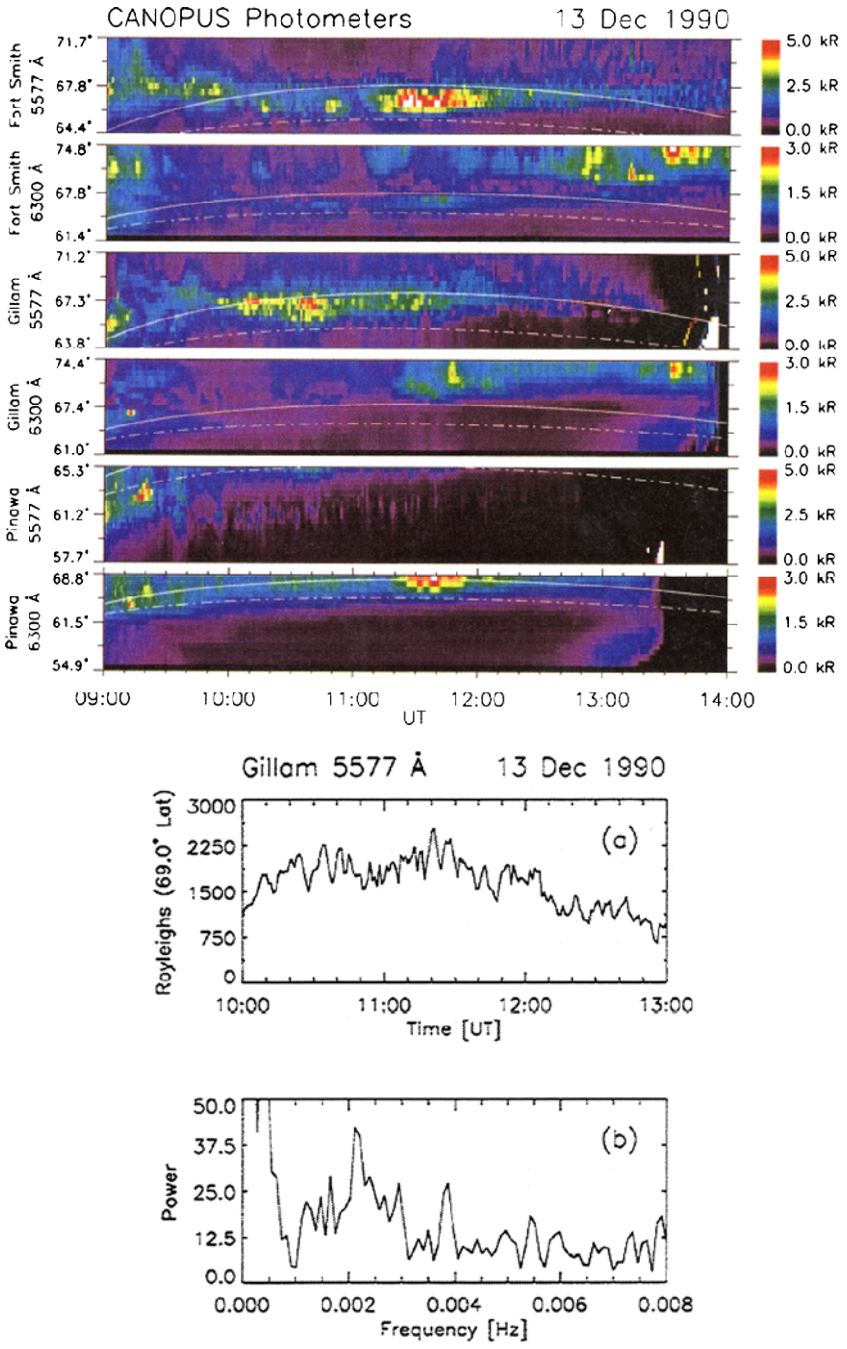

Fig. 16 (from Lessard et al. 1999) (*Top*) Meridian scanning photometer observations from three ground stations, plotted as a function of magnetic invariant latitude versus time. The *solid white line* and the *dashed line* represent the mapping of CRRES using different magnetic field models. (*Bottom*) Auroral intensity observed at Gillam (68.5° invariant latitude), and the spectral power of the auroral intensity. A 2.1-mHz peak was present which was also present in ground magnetometer and CRRES data (not shown)

component of the substorm current wedge. Bauer et al. (1995) reported neutral sheet oscillations at about 12 R_E, also believed to be associated with the SCW at substorm onset, while launching Alfvén waves toward the ionosphere (Fig. 17). Maynard et al. (1996) reported a Poynting flux associated with Alfvén waves at the inner edge of the CPS during a substorm, and attributed the waves to the SCW. These transient Alfvén waves showed variations in the Pi2 frequency range.

The launching of Alfvén waves in association with the SCW, and their subsequent bouncing between the auroral ionosphere and the neutral sheet, is called the transient response model (see review by Baumjohann and Glassmeier 1984). These Alfvén waves are thought to cause the high-latitude Pi2 pulsations which are the largest Pi2 pulsations and have distinct properties from those occurring at lower latitudes. The wave period is determined by the Alfvén travel time between the auroral ionosphere and the neutral sheet. The onset of the SCW presumably occurs where dipole-like and tail-lobe-like field lines meet; the onset mechanism is still under investigation.

No further reports for SCW-associated Alfvén waves in the CPS have been reported since 2000. Although Erickson et al. (2000) reported field-aligned Poynting fluxes associated with substorms at or near the inner edge of the plasma sheet, similar to Maynard et al. (1996), they did not comment on a possible Alfvénic nature for these fluxes. On the other hand, low-altitude (<4000 km) auroral zone observations of Alfvén waves, on field lines mapping to the CPS at substorm onset, have been reported (Mende et al. 2003a; and Lessard et al. 2006), and it is possible that these waves are associated with the SCW, or with a process associated with substorm onset. As mentioned in Sect. 2.3, Mende et al. provided evidence of a relationship to the auroral surge, and more details can be found in Sect. 7.3. Lessard et al. (2006) reported conjugate Pi1B pulsations on the ground, from GOES 9 (geosynchronous orbit) and from FAST (Fig. 18). The pulsations started with the onset of an intense substorm (AE > 1000 nT) at about 7:30 UT. At GOES 9, the waves were largely compressional but were Alfvénic at FAST. Therefore, it was suggested that somewhere inside the CPS, be-

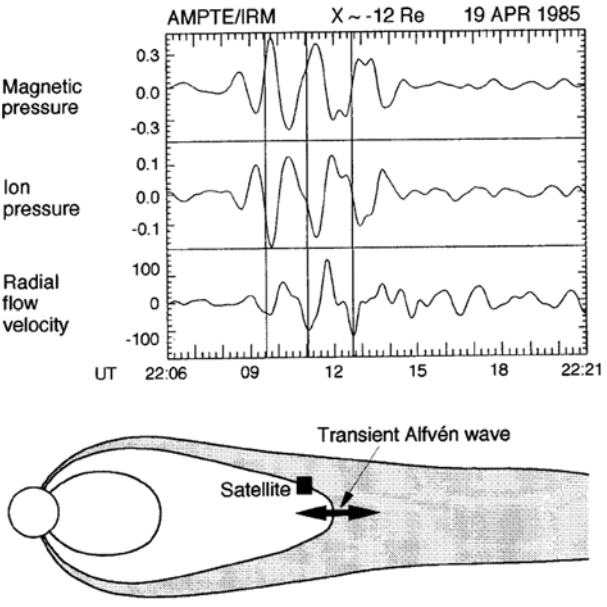

Fig. 17 (from Takahashi 1998 who adapted the figure from Bauer et al. 1995) An example of Pi2-band oscillations observed in the magnetotail by the AMPTE IRM satellite. The location of the satellite (*solid square*) relative to the plasma sheet (*shaded region*) is schematically illustrated at the bottom. Note that these observations do not directly show the wave fields of Alfvén waves. The Alfvén waves are believed to be excited by these neutral sheet oscillations

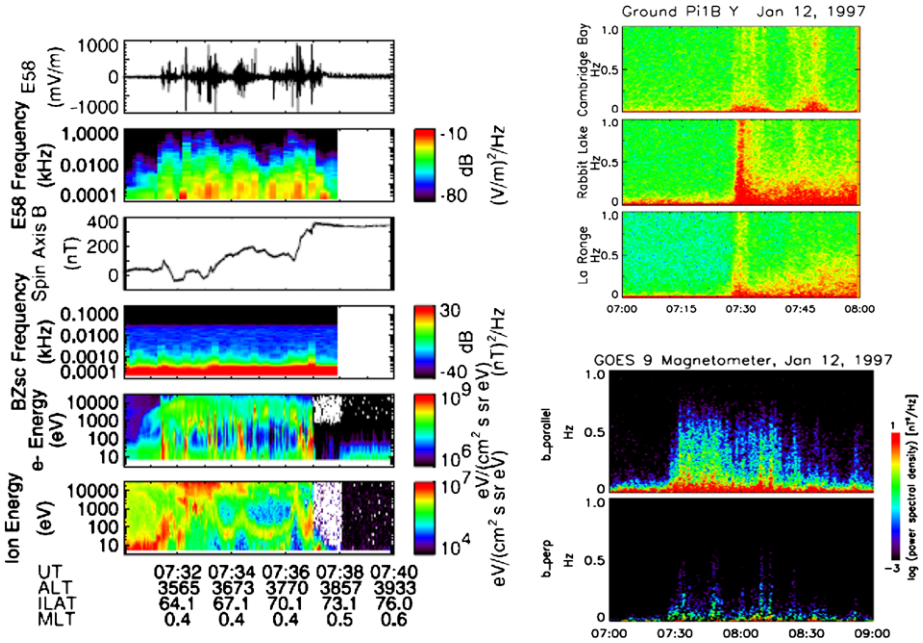

Fig. 18 (from Lessard et al. 2006) (*Left*) Data from the FAST satellite. The *first and second panels* show the electric field and its spectra. The *third and fourth panels* show the magnetic field and its spectra. The *fifth panel* shows electron energies, and the *sixth panel* shows ion energies. (*Right, top*) Dynamic spectra calculated using induction coil data from three ground stations. (*Right, bottom*) Parallel and perpendicular spectra of GOES 9 magnetic field data

low the altitude of GOES 9, the compressional waves underwent mode conversion to shear Alfvén waves.

2.5 Summary—Central Plasma Sheet

Based on literature published in the last eight years concerning Alfvén waves in the CPS, a diagram is constructed connecting the established and speculated relationships among various phenomena causally connected to Alfvén waves in the CPS (Fig. 19). The diagram will, no doubt, be refined in the coming years. The occurrence of Alfvén waves inside the CPS along various paths is emphasized by shading the relevant boxes. Note that each path only represents a possible path, from top to bottom, and that all paths are not necessarily followed at the same time. One path or several paths can occur at any given time. At the very top lies the solar wind, which provides energy for almost all magnetospheric phenomena. The solar wind energy follows three paths (i.e., three branches in the diagram) which are tentatively connected further down by dashed lines indicating a possible connection that has not yet been firmly established (see below). On the left, the solar wind is the driver of KHI on the flanks of the magnetosphere. The KHI-associated boundary motion of the magnetopause couples to a waveguide mode in the magnetosphere. Under the right conditions (e.g., the pre-existence of a stretched magnetotail which lowers the eigenfrequencies of stretched field lines) the compressional waves of the waveguide resonantly couple to the field lines with the matching eigenfrequency, eventually leading to discrete standing Alfvén waves (FLR) in the Pc5 frequency band. Alternatively, compressional waves with a range of frequencies (i.e.,

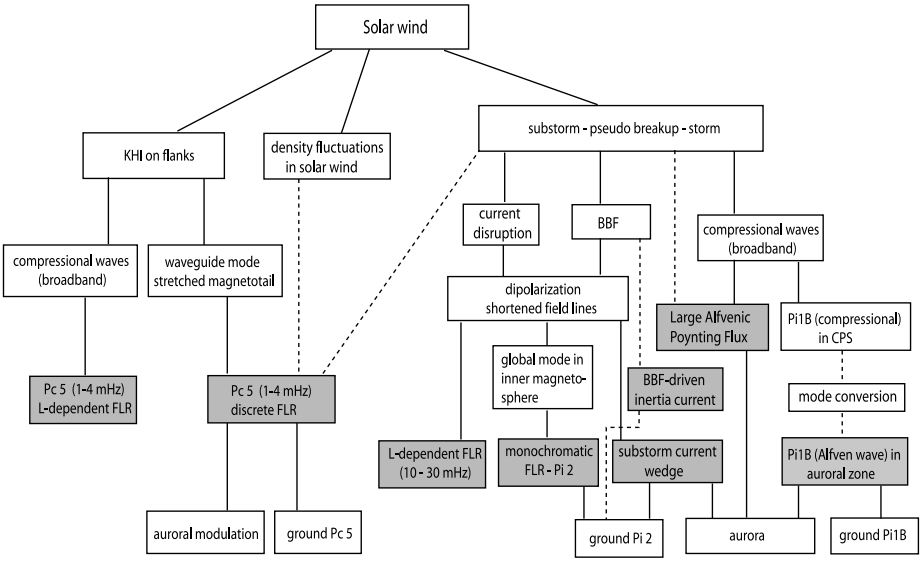

Fig. 19 Diagram indicating the various paths for energy to flow from the solar wind into the creation of Alfvén waves in the CPS, and the effect of these Alfvén waves on other phenomena. *Dashed lines* indicate speculative paths

broadband) may be excited in the magnetotail and couple to L-dependent Pc5 FLR. Such stretched field lines occur during very active geomagnetic times; mostly during growth and recovery phases. The discrete Pc5 FLR interacts with precipitating electrons, and can be observed in ground magnetometer and optical data. Most studies using coordinated ground-space data have proposed this path. Whether substorm/storm activity itself can lead to Pc5 pulsations in the tail, is still open for investigation. It has been suggested that ground Pc5 FLR have preferentially discrete frequencies of 1.3, 1.9, 2.6, and 4.2 mHz (Samson et al. 1991a, 1991b; and Walker et al. 1992). However, the space observations of Pc5 reviewed here did not report these frequencies. Additionally, it has been proposed that Pc5 FLR might play a role in the triggering of substorms. No spacecraft evidence has been found for this conjecture, but it should be investigated further. The dashed line leading from the Pc5 box and the substorm box, in Fig. 19, indicates this uncertainty.

The second branch starting with the solar wind is also speculative. Some evidence has been reported that discrete Pc5 in the dayside can sometimes be directly driven by density oscillations in the solar wind (Kepko et al. 2002). Whether this is also the case for Pc5s occurring in the nightside CPS is not yet known, as indicated by the dashed line in Fig. 19.

The third branch, beginning with the solar wind, is more complicated. Solar wind energy provides the energy for substorms, pseudo-breakups, and storms. How the substorm/pseudo-breakup is initiated and its exact relationship to BBF and current disruption, is still studied intensely, and is not part of this review. Regardless of the initiation mechanism, the substorm leads to a dipolarization of the magnetotail that is accompanied by the development of the SCW. The SCW initially launches Alfvén waves towards the ionosphere. This transient response leads to auroral zone Pi2 on the ground and to the auroral surge. Dipolarization also leads to the formation of FLR in the CPS with a range of frequencies between 10–40 mHz, depending on the L shell; field lines are not as stretched, as they are in the other two main branches on the left, when Pc5s develop, and can be explained with a re-

laxation/shortening of the field lines during the dipolarization process. A higher frequency range is consistent with this view. In one event studied, a non-L-dependent, monochromatic FLR was observed at substorm onset in the CPS. Simultaneously, on the ground, a mid-latitude FLR was recorded which caused the second amplitude maximum of ground Pi2, and it was shown that this FLR was likely coupled to a global compressional cavity mode. Whether the plasmasphere overlapped with the CPS, or whether monochromatic compressional waves leaked from the plasmasphere, via the virtual resonance mode, into the CPS, could not be determined.

In addition to the BBFs, broadband compressional waves in the magnetotail move radially inward towards Earth. These waves likely couple to shear Alfvén waves in the inner magnetosphere. Two branches are included in the diagram. First, during storms the most energetic Alfvén waves occur deep inside the CPS, supplying significant energy to the inner magnetosphere. During substorms, energetic Alfvén waves are mostly confined to the PSBL (see Sect. 3). The origin of these intense Alfvén waves has not yet been confirmed, and the reconnection site and mode conversion from compressional to shear mode, either at the outer boundary of the plasma sheet, see Sect. 3, or deeper inside the CPS, are scenarios considered in the literature. This uncertainty is expressed by the dashed line in Fig. 19. Second, compressional and Alfvénic waves in the Pi1B range have been reported to occur simultaneously in the CPS and at low altitudes (<4000 km); and it has been proposed that the compressional Pi1Bs mode converts to the Alfvén mode. The location, for where in the CPS this conversion occurs, is an outstanding question, illustrated with a dashed line in Fig. 19. Alfvén waves on these two branches do not form FLR; and are mainly dissipated via electron acceleration and Joule heating, leading/contributing to the aurora.

Proposed, but not observationally confirmed in space, is the idea that periodic BBFs can lead to periodic inertia currents in the region where tail- and dipole-like field lines meet. These inertia currents would initially travel as Alfvén waves down to the ionosphere, causing ground Pi2. Thus, this branch is still somewhat speculative, as illustrated with a dashed line in Fig. 19.

Finally, the diagram illustrates that Alfvén waves in the CPS play a significant role as intermediate energy carriers in many paths from the solar wind to the ionosphere. Many of the Alfvén waves in the CPS appear in the form of FLR. The mechanisms for generating Alfvén waves in the CPS are only partially understood and confirmed; hence it remains an active area of research. More conjugate studies are required to better characterize the energy transfer processes and the energy paths in Fig. 19. For example, currently the mode where conversion occurs for Pi1B from the compressional to the transverse mode is not known, and there are still no direct space confirmations for the transient response model for ground Pi2—which would require direct observations and information on the oscillating behavior in space, together with ground observations. Although strong evidence exists that FLR play a role in the formation of some auroral arcs, additional coordinated ground-space observations are required to determine the exact nature of energy transfer. The intriguing proposal that FLR trigger substorms lacks direct observational evidence from space, and should be investigated further. Investigation regarding the role of Alfvén waves in the CPS during intense storms has just begun, and more results are expected in the near future.

3 Alfvén Waves in the Plasma Sheet Boundary Layer

The PSBL forms the outer part of the plasma sheet with its low and high-altitude ends, mapping into the auroral zone and the reconnection region, respectively. The lobe-PSBL

interface is the division between open and closed field lines in the magnetotail. Such characteristics give the PSBL a special significance in all magnetospheric regions, and make it the site of diverse phenomena. Exact mapping of the PSBL in relation to other regions, during active geomagnetic conditions, in particular, is still an outstanding problem that has not reached consensus in the field.

The PSBL is a region of great importance for auroral substorm physics. For example, it has been demonstrated that energy carried in various forms inside the PSBL contributes to the creation of the aurora. The energy transport was largely thought to rely on kinetic energy carried by ion beams, and electromagnetic energy carried by quasi-static FAC. Recently, this view has been revised by new studies reporting large-amplitude Alfvén waves in the PSBL that carry significant Poynting flux towards the auroral acceleration region. Additionally, evidence for energetic field-aligned electron acceleration inside the PSBL also adds to the number of energy carriers possibly contributing to the aurora.

Many observations of electric fields in the PSBL were initially, and still are, interpreted as electrostatic structures (e.g., Mozer 1981; Cattell et al. 1982, 1994; Levin et al. 1983; Gurnett et al. 1984; Weimer and Gurnett 1993; Streed et al. 2001; and Johansson et al. 2004). In addition, there was also early evidence for Alfvén waves in the PSBL, derived from three different sources. First, in-situ identification of Alfvén waves in the PSBL using ISEE 1/2 relied on magnetic field measurements only, Fig. 20 (Hayward and Dungey 1983), and must have been regarded as speculative because the most unambiguous identification requires both **E** and **B** measurements (see Sect. 1.4). Second, from low-altitude rocket and satellite observations of Alfvén waves in the auroral zone, it was hypothesized that these waves more than likely came from larger distances in the tail (e.g., Nagatsuma et al. 1996). Finally, ground-based observations in the auroral zone showed that Alfvén wave activity is present at the poleward boundaries of the auroral oval (e.g., Samson et al. 1991a, 1991b), a region that maps into the magnetotail.

An unambiguous identification of Alfvén waves in the PSBL used full 3-d measurements of **E** and **B** from the Polar spacecraft above the auroral acceleration region at 4–7 R_E

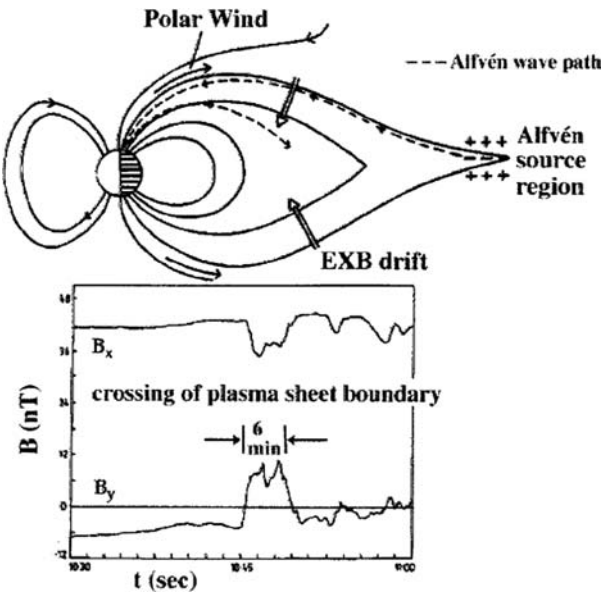

Fig. 20 (from Gekelman 1999, who adapted the figure from Hayward and Dungey 1983) The *top* shows a schematic of the plasma sheet, and a hypothesized source of Alfvén waves in the far tail. The *bottom* shows the magnetic field during a crossing of the plasma sheet boundary layer by the ISEE 1 satellite. The hodograms, not shown, of the 6-min interval indicate that only the direction of **B** changes, not its magnitude. The authors, therefore, interpreted the signal as due to shear Alfvén waves associated with the boundary layer current

(Wygant et al. 2000; and Keiling et al. 2000). The E/B ratio was $\sim$10,000 km/s, comparable to the local Alfvén speed, and was evidence for the Alfvénic interpretation. Furthermore, it was demonstrated that Alfvén waves carried significant Poynting flux towards Earth. These observations provided a link between the magnetotail and the auroral zone, where much Alfvén wave activity had been reported (e.g., Boehm et al. 1990; Dubinin et al. 1990; Knudsen et al. 1992; Louarn et al. 1994; Wahlund et al. 1994; Volwerk et al. 1996; Stasiewicz et al. 1997; Gary et al. 1998; Chaston et al. 2000; Kletzing and Hu 2001; and Mende et al. 2003a). Recently using Geotail at further distances (>15 R_E), Alfvén waves, having peak Poynting fluxes larger than the Polar results, have been reported (Angelopoulos et al. 2002). Observations such as these demonstrate that the PSBL plays an important role as a region containing significant Alfvénic energy flux. These results and other observations are described below.

3.1 Aurorae

A series of Polar-spacecraft-based studies (Wygant et al. 2000; and Keiling et al., 2002, 2003b) used *in situ* Alfvénic Poynting flux measurements at 4–7 R_E in the PSBL to document a connection with auroras. Wygant et al. (2000) reported two PSBL crossings showing large-amplitude Alfvén waves ($\delta E \sim 100$ mV/m, $\delta B \sim 20$ nT) that carried a Poynting flux of approximately 1 mW/m^2 towards Earth (Fig. 21). When mapped to ionospheric altitudes along converging magnetic field lines, the Poynting flux corresponded to values above 100 mW/m^2. These enhanced Poynting fluxes were magnetically conjugate to intense auroral structures, as detected from UVI images (Fig. 21 at the top), and were sufficient to power the auroral luminosity. Note that the LBH-long filter used in the UVI images provides an estimate of the total energy deposited into the ionosphere by precipitating electrons (Torr et al. 1995).

Using the same experimental setup, bottom left of Fig. 21, Keiling et al. (2002) compared in-situ Poynting flux, between 4 and 7 R_E, with the luminosity of magnetically conjugate auroral structures during 40 PSBL crossings. In this comparison, cases with large *in situ* values of Poynting flux ($\sim$1 mW/m^2), and cases with low values ($\sim$0.1 mW/m^2) were included. During this comparison, it was found that the high-altitude Poynting flux was correlated with auroral luminosity which can be converted into energy deposition due to precipitating electron beams (bottom right of Fig. 21). The ionospheric precipitating electron energy flux during times of intense Poynting flux in the plasma sheet exceeded 20 mW/m^2. In the absence of a strong Poynting flux in the plasma sheet, electron precipitation was small (<5 mW/m^2). For almost all events, the mapped Poynting flux was larger than the ionospheric electron energy flux by a factor of one to ten, allowing for the possibility that Alfvén waves were energizing the precipitating electrons. This view is further supported by conjugate studies of satellites located above and in, or below, the auroral acceleration region (see Sect. 3.3). Moreover, much theoretical/simulation work supports this acceleration scenario (e.g., Hasegawa 1976; Goertz 1984; Kletzing and Hu 2001; Watt et al. 2005; Chaston et al. 2006b, and references therein). Also, Keiling et al. (2002) reported that the Alfvénic Poynting flux events observed at the outer edge of the plasma sheet were conjugate to the poleward border of active auroral regions, giving further evidence that at least some portion

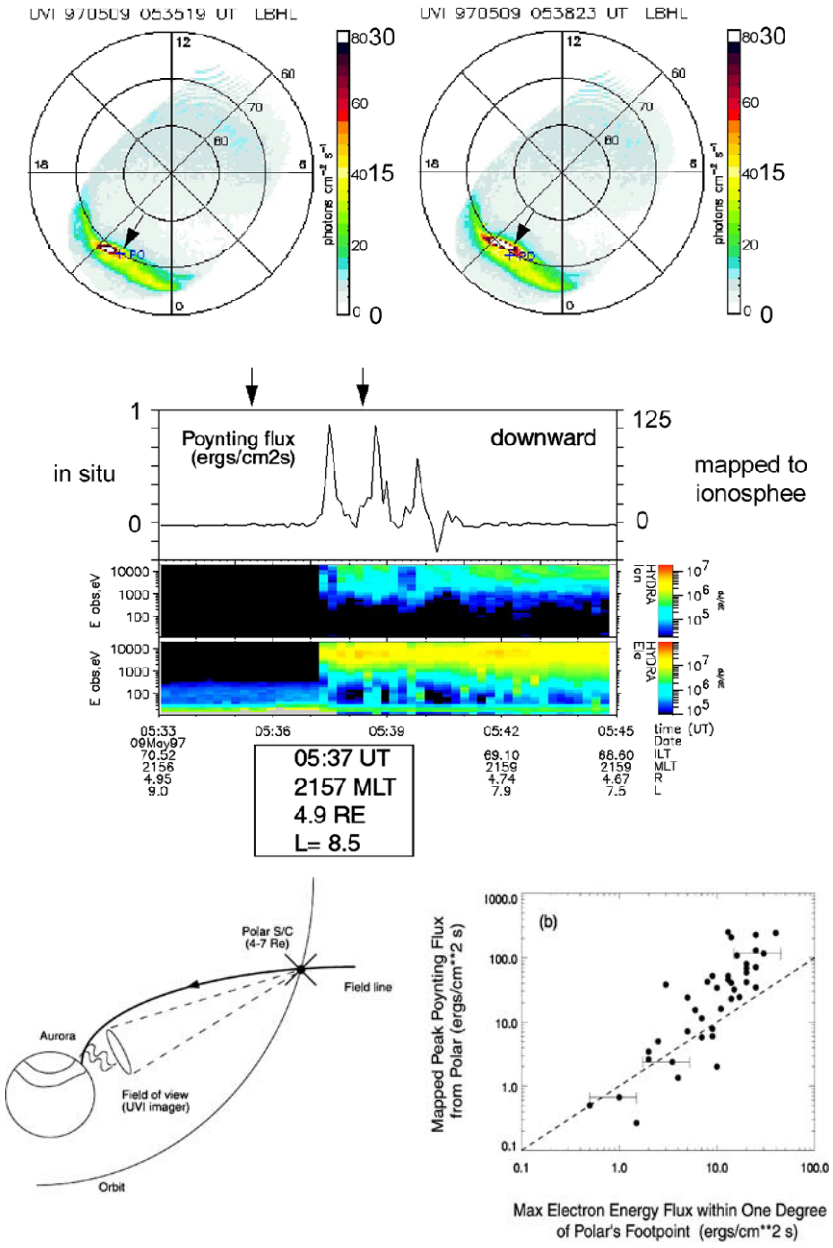

Fig. 21 (*Top*) Measurements from the Polar spacecraft crossing the PSBL on May 9, 1997. The top shows ultraviolet images of an active auroral region. The energy scale shows both photons $\mathrm{cm}^{-2}\ \mathrm{s}^{-1}$ and $\mathrm{mW/m}^2$. The latter is the energy flux of precipitating electrons. The *arrows* point to Polar's footprint. The panels show the in-situ component of the Poynting flux along the magnetic field, and the energy flux-time spectrograms of electrons and ions, modified from Wygant et al. (2000). The *two arrows above the first panel* mark the times of the two UVI images. (*Bottom, left*) Illustration of the setup used in the studies of Wygant et al. (2000) and Keiling et al. (2002) (from Keiling et al. 2002). (*Bottom, right*) Energy flux comparison for 40 PSBL crossings using the setup shown to the left (from Keiling et al. 2002). The dashed line corresponds to cases where mapped Poynting flux and inferred energy flux of precipitating electrons are equal

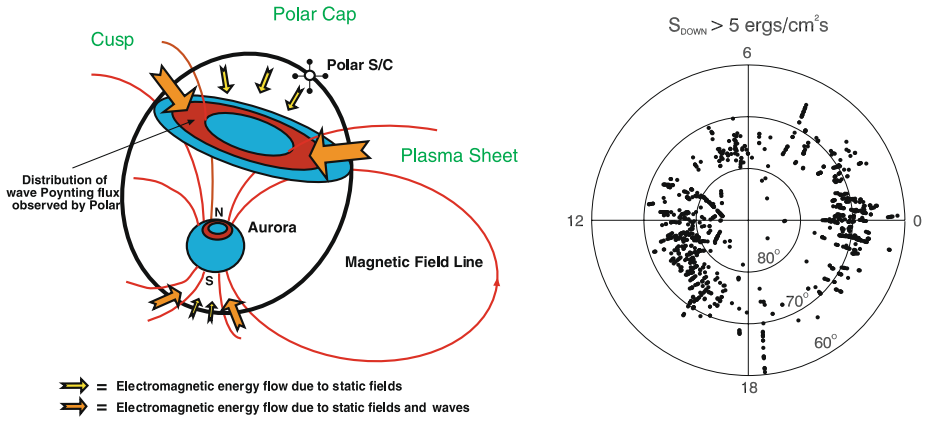

Fig. 22 (From Keiling et al. 2003b) (*Left*) Sketch of Polar's orbit and the two contributions of Poynting flux flowing along magnetic field lines into the polar region. The Poynting flux is carried by static fields (i.e., convection electric fields and magnetic fields associated with quasi-static FACs) and Alfvén waves. (*Right*) Distribution of events with Poynting fluxes larger than 5 $\mathrm{mW/m^2}$ (mapped along converging magnetic field lines into the ionosphere, ∼100 km), recorded by Polar, given versus latitude and local time. E and B were band-pass filtered (6 s, 180 s) before calculating the Poynting flux. The events approximately delineate the statistical location of auroras

of the discrete aurora maps to the PSBL—a finding that is in agreement with observations in the auroral zone where Alfvén waves are often, but not exclusively, recorded near the polar cap boundary (e.g., Chaston et al., 2003, and Sect. 3.3).

During the course of one year, the orbital plane of Polar precesses by 360°, making it possible to survey the distribution of Alfvén wave events over the entire northern hemisphere at distances between 4–7 R_E. Figure 22 shows the distribution of events with downward Poynting flux larger than 5 $\mathrm{mW/m^2}$ (mapped along converging magnetic field lines into the ionosphere, ∼100 km) recorded by Polar, versus latitude and local time (Keiling et al. 2003b). The threshold of 5 $\mathrm{mW/m^2}$ is sufficient to cause visible aurora. **E** and **B** were band-pass filtered (6 s, 180 s) before calculating the Poynting flux. The events approximately delineate the statistical location of auroras. The PSBL approximately maps to 70° latitude in the nightside, although the angle varies depending on geomagnetic activity. Most likely, not all of the events in Fig. 22 occurred inside the PSBL, but recall that most of the large Poynting flux events do indeed occur inside the PSBL, as inferred from individual case studies, see above and Sect. 3.2 for additional examples. Examples of large Poynting flux events inside the CPS can be found in Toivanen et al. (2001), Keiling et al. (2001a) and Dombeck et al. (2005). Note the two long traces of large Poynting flux events (at ∼18 : 20 and ∼04 : 30 local time on the right side of Fig. 22) which occurred on January 10, 1997 and August 3, 1997. During both of these orbits, geomagnetic storms prevailed. Geomagnetic storms are periods of enhanced energy transfer over an extended period of time, from one to many days, when compared with auroral substorms, lasting 30 minutes to 3 hours. The Polar satellite recorded enhanced Poynting fluxes throughout the plasma sheet on these days, accounting for the long traces seen in Fig. 22 (also see Sect. 2.3).

In Sect. 7.2, I will review how much of the energy causing the aurora is actually contributed by high-altitude Alfvén waves in comparison with other magnetotail drivers.

3.2 Substorms

The optical aurora occurs during all phases of a substorm, with the most intense aurora occurring during auroral break-up. Instead of comparing the large Alfvénic Poynting flux in the PSBL with conjugate aurora, as discussed in Sect. 3.1, Keiling et al. (2000) compared Alfvénic Poynting flux with substorm phases. They found that the largest Alfvén wave events, which were dominantly propagating Earthward, occurred during times of rapid changes in the H (or X) component of ground magnetometer data. These times corresponded to the expansion phase of substorms (or pseudo-breakups). The black lines, to the left in Fig. 23, show H and X bays recorded by ground magnetometer stations for different events. Red lines show the Alfvénic Poynting flux simultaneously measured by Polar in the PSBL at 4–7 R_E. A Poynting flux of 1 mW/m^2 maps to ~125 mW/m^2 in the ionosphere. In the right side of Fig. 23, the distribution of the Alfvén wave events as a function of invariant latitude (ILAT) and magnetic local time (MLT) is shown. These observations demonstrate the existence of Alfvén wave power in the PSBL as a means of energy transport from the

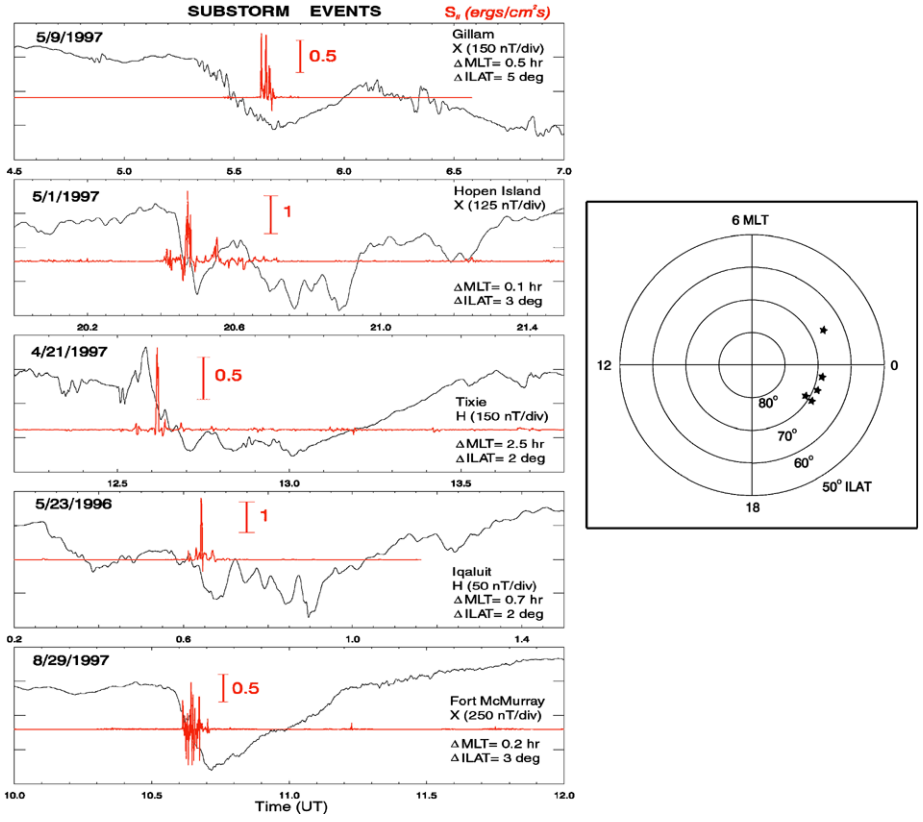

Fig. 23 (from Keiling et al. 2000) (*Left*) Temporal comparison of in-situ magnetic-field-aligned Alfvénic Poynting flux, *red lines*, as measured by Polar in the PSBL; and ground signatures of H and X bays, *black lines*. Positive Poynting flux values indicate directions towards the nearest ionosphere. (*Right*) Distribution of the Alfvén wave events, from the left, as a function of invariant latitude (ILAT) and magnetic local time (MLT)

magnetotail to the auroral acceleration region during the most dynamic phase of magnetospheric substorms.

The global nature of ULF wave activity, including Alfvén waves, during substorms was demonstrated by Toivanen et al. (2003) who investigated an isolated substorm using the following data sources: Polar in the PSBL at 7 R_E, GOES 8 at geosynchronous orbit (inner plasma sheet), and ground magnetometer data (Fig. 24). All regions recorded time-delayed pulsations in different modes with a frequency of ∼6 mHz. The Polar satellite recorded large-amplitude Alfvén waves upon which higher frequency Alfvén waves were superposed. GOES 8 recorded compressional waves approximately 2 minutes after the Alfvén waves were recorded at Polar. Using these wave data and additional particle data, Toivanen et al. (2003) suggested a development of events consistent with the near-Earth neutral line model (NENL). They further proposed that the Alfvén waves were initiated near the plasma sheet boundary and were associated with reconnection.

3.3 Alfvénic Electron Acceleration

Alfvén-wave-induced acceleration of electrons occurs in the auroral acceleration region where Alfvén waves are dispersive and can acquire significant electric fields parallel to the magnetic field (e.g., Stasiewicz et al. 2000, and references therein). A recent and brief review regarding some of the theory/simulation work for electron acceleration on auroral field lines was given by Chaston et al. (2006b).

The most likely energy sources of small-scale auroral zone Alfvén waves are the Alfvén waves observed in the PSBL, see Sects. 3.1 and 3.2. As pointed out, the Poynting flux of large-amplitude Alfvén waves in the PSBL at 4–7 R_E is one order of magnitude larger than that measured in or below the auroral acceleration region (Wygant et al. 2000; and Keiling et al. 2002). In addition, little reflected Alfvén wave energy has been recorded at Polar's altitude (Keiling et al. 2005; Dombeck et al. 2005; and see Sect. 3.6). These observations imply that much of the Alfvén wave energy is dissipated at lower altitudes. Electron acceleration is one dissipation mechanism for which there is ample observational evidence. Recent observations of electron acceleration are reviewed below, while at the same time, the question regarding where the bulk of electron acceleration occurs along auroral field lines, is addressed.

Figure 25 combines statistical observations obtained at 4–7 R_E from Polar, and at 1.05–1.65 R_E geocentric from FAST (Chaston et al. 2006b). The Polar results were discussed in Sect. 3.1, and show Poynting fluxes mapped to ionospheric altitudes at 100 km, with the assumption of no dissipation, plotted versus the energy flux of magnetically conjugate precipitating electrons, as inferred from UVI images of auroral luminosity (Keiling et al. 2002). The FAST results show *in situ* values of both Poynting flux and electron energy flux mapped to the same reference altitude of 100 km (Chaston et al. 2003). The comparison shows that for Polar, the Poynting flux is almost always larger than the ionospheric electron energy flux, by as much as ten times larger, but for FAST the energy balance is reversed—there is more energy flux in electrons than in the Poynting flux. The difference provides supportive evidence that the dissipation of Alfvén wave energy occurs via, at least partial, parallel acceleration of electrons over the altitude range separating the two satellites.

A more direct verification of this result uses two or more satellites located along the same flux tube at different geocentric distances, in so-called conjunction studies, allowing one to follow the evolution of Alfvén waves between two points. Perfect conjunctions (i.e., measurements on the same field line by both satellites) are impossible to achieve. All conjunction studies suffer from various problems/difficulties such as field line mapping, different

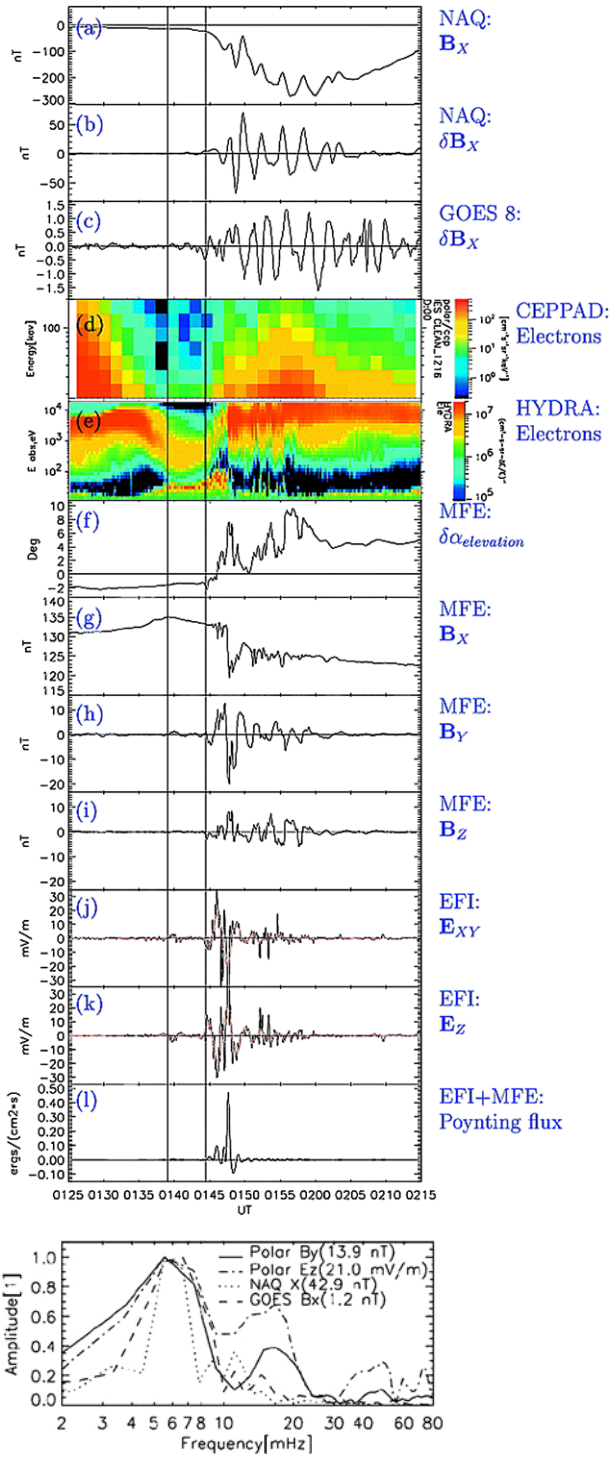

Fig. 24 (from Toivanen et al. 2003) (*Top*) (**a**) The northward component at NAQ ground station; (**b**) the 180-s detrended northward component at NAQ; (**c**) the 180-s detrended magnetic field at GOES 8; (**d**) CEPPAD (Comprehensive Energetic Particle Pitch Angle Distribution) electrons (17–200 keV); (**e**) Hydra electrons (0.1–20 keV); (**f**) measured magnetic field elevation angle with respect to the elevation angle of the T89 model; (**g–i**) the magnetic field at Polar; (**j**) XY_{GSE} and (**k**) Z_{GSE} components of the electric field at Polar; and (**l**) Parallel Poynting flux (positive towards the ionosphere). The *vertical lines* indicate the onset time (01:44:23 UT) and a transient signature at 01:39:00 UT as determined from the EFI instrument. (*Bottom*) Amplitude spectra of various quantities given in the *upper corner*; each spectrum is normalized to the maximum amplitude

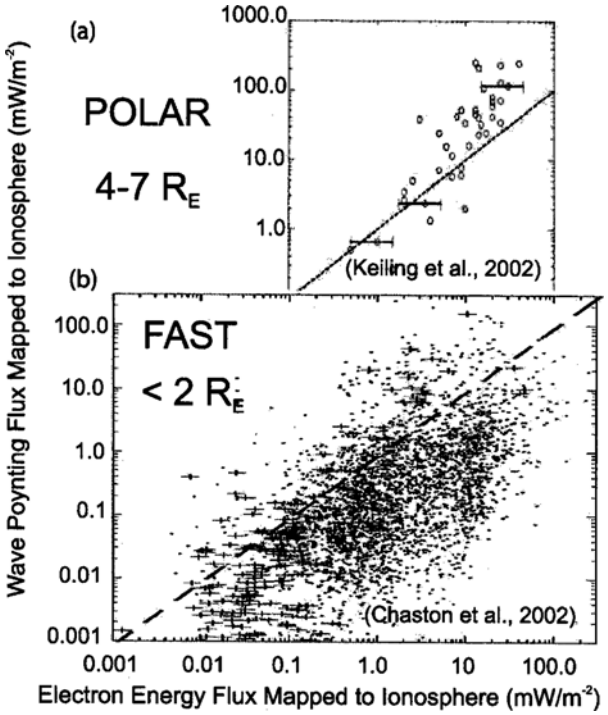

Fig. 25 (from Chaston et al. 2006b) Comparison of Alfvénic Poynting flux and electron energy flux from measurements taken at two different locations

motions of the field lines at the satellite locations, different orbital speeds of the satellites, and time delays in signal propagation along the field lines. Therefore, each conjunction study defines more or less stringent criteria to be met for a conjunction. Nevertheless, conjunction studies are a powerful method for helping us understand the dissipation processes of Alfvén waves along magnetic field lines.

Several conjunction studies on auroral field lines, including the PSBL, in the last eight years have utilized FAST, DMSP, Polar, Geotail and Cluster. For example, Schriver et al. (2003) reported seven events during conjunctions of FAST and Polar in the nightside. Two of the events were storm-related, one was substorm-related, and the other four events occurred during quiet times with little discernible magnetic activity. Only during geomagnetically active times were large-amplitude Alfvén waves recorded at Polar's altitude, at or near the lobe-PSBL boundary. Conjugate to the Alfvén waves, FAST recorded field-aligned electron acceleration events, and the UVI imager onboard Polar recorded strong auroral luminosity in the ionosphere. Figure 26 shows one such conjunction event. In this study it was concluded that Alfvén waves are drivers of auroral acceleration in addition to quasistatic, parallel potential drops caused by quasistatic FACs and the earthward flow of energetic plasma beams from the magnetotail.

In another Polar-FAST conjunction, Dombeck et al. (2005) reported one Alfvén wave event during a conjunction of Polar at 7 R_E and FAST at 3500 km, both at ~23 MLT, during the main phase of a geomagnetic storm. Both Alfvénic Poynting flux and the electron energy flux were compared at the two spacecraft locations, and a mean net loss of ~2.1 mW/m^2 in earthward Poynting flux and a mean net increase in earthward electron energy flux of up to ~1.2 mW/m^2 over the altitude region between Polar and FAST were found, directly confirming the statistical results shown in Fig. 25. Based on these data, reflectivity and

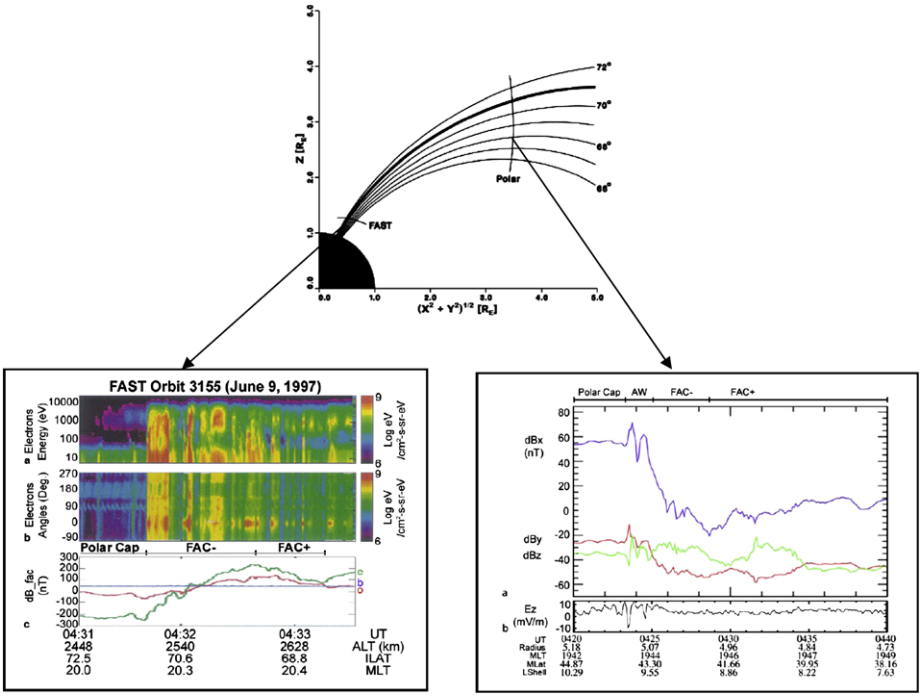

Fig. 26 (from Schriver et al. 2003) (*Top*) Schematic diagram showing the relative positions of the FAST and Polar satellites. (*Bottom, left*) FAST data showing electron energy and pitch angle and the magnetic field with the field-aligned component in *blue*, the east–west component in *green*, and the component transverse to these two components in *red*. FAST crosses from the polar cap into the auroral region at approximately 0431:30 UT as seen by the sudden appearance of high-energy electrons. Bursts of field-aligned energized electrons occur intermittently inside the auroral zone. (*Bottom, right*) Model-subtracted magnetic field and electric field data from Polar are shown in GSM and GSE coordinates, respectively. Polar crosses from the polar cap into the PSBL at approximately 0423 UT, recording large fluctuations in both the magnetic and electric fields associated with a large-amplitude Alfvén wave (labeled *AW*)

dissipation coefficients were calculated, shown in Sect. 3.6, and it was further suggested that some high-frequency kinetic Alfvén wave were generated between Polar and FAST.

Conjugate studies confirm and strengthen the statistical results on Alfvén wave dissipation via electron acceleration along magnetic field lines. These studies also indicate that the energy exchange often occurs near the poleward boundary of the auroral region. However, the studies can not address questions relating to the position of acceleration along the field line, except to point out that acceleration must have occurred somewhere between Polar and FAST. This question was addressed in a series of statistical studies covering the altitude range from 1 to 6 R_E (Janhunen et al., 2004, 2005, 2006). As seen in the left section of Fig. 27, Janhunen et al. (2006) showed that a statistical decrease in Poynting flux for data collected during five years in the 18–06 MLT sector and at 65–74° ILAT, approximately corresponding to auroral field lines, was largest in the altitude range from 4–5 R_E. The authors attributed the change to wave dissipation via electron acceleration, and argued that the acceleration was due to Landau damping since v_e, the electron thermal speed, and v_A, the Alfvén speed, are comparable in this region. The result not only suggests that Alfvén-wave acceleration occurs above the nominal auroral acceleration region, but also suggests that most of it occurs above the nominal auroral acceleration region. Although Janhunen et al.

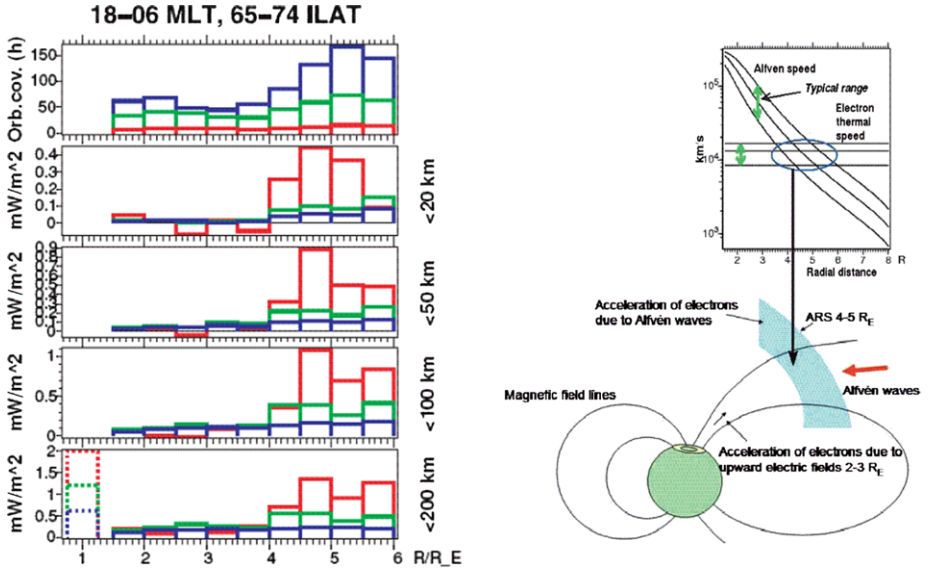

Fig. 27 (from Janhunen et al. 2006) (*Left*) Downward parallel Poynting vector, mapped to ionospheric altitudes, plotted against geocentric distance, R, in the nightside auroral zone (18–06 MLT, 65–74° ILAT). The *top panel* is the orbital coverage in hours for each bin. *Other panels* show the downward component of the Poynting vector in $\mathrm{mW/m^2}$ for different frequency ranges, corresponding to spatial scales of 20 to 200 km. $Kp \leq 2$ is given in *blue*; $2 < Kp \leq 4$ is given in *green*; and $Kp > 4$ is given in *red*. The *bottom panel* also shows, with *dotted lines*, the electron precipitation power from the statistical model of Hardy et al. (1987). (*Right*) Schematic diagram showing the enhanced Alfvénic electron acceleration region at 4–5 R_E radial distance, as proposed in this study. At the *top of this diagram*, the typical range of the Alfvén wave speed and electron thermal speeds is plotted vs. radial distance

did not separate between PSBL and CPS, it is reasonable to relate this result to the PSBL, in agreement with other event studies (see above) indicating that the most energetic Alfvén waves do, in fact, occur inside the PSBL. By considering the *Kp* index, it was further shown that Alfvén-wave-induced electron acceleration depends on the magnetic disturbance level.

Observational evidence for the parallel acceleration of electrons by kinetic Alfvén waves has recently been reported at ∼5 R_E in the PSBL (Wygant et al. 2002). In a case study it was shown that small-scale kinetic Alfvén waves, 0.25–1 second in duration, were superposed on large-amplitude shear Alfvén waves, 20–60 seconds in duration (see bottom of Fig. 28). The E/B ratio for small-scale waves was two to five times the local Alfvén speed, as expected for kinetic Alfvén waves. It was proposed that the small-scale kinetic Alfvén waves were generated from the simultaneously occurring larger-scale shear Alfvén waves. The interval spanning the kinetic Alfvén waves showed signatures of parallel electron heating and earthward electron beams, seen in Fig. 28 at the top. The parallel energy of the electrons (∼1 keV) is consistent with theoretical estimates of field-aligned potential drops in kinetic Alfvén waves, suggesting that Alfvén wave-induced electron acceleration had occurred.

Angelopoulos et al. (2002) showed evidence that Alfvén wave-induced electron acceleration occurs at distances greater than 5 R_E. In a near-conjugate study of Polar at 5 R_E and Geotail at 18 R_E, it was shown that the Alfvénic Poynting flux at Geotail was one order of magnitude larger possibly suggesting its dissipation before reaching Polar (Fig. 29). The authors proposed that kinetic Alfvén waves dissipate via parallel electron acceleration along

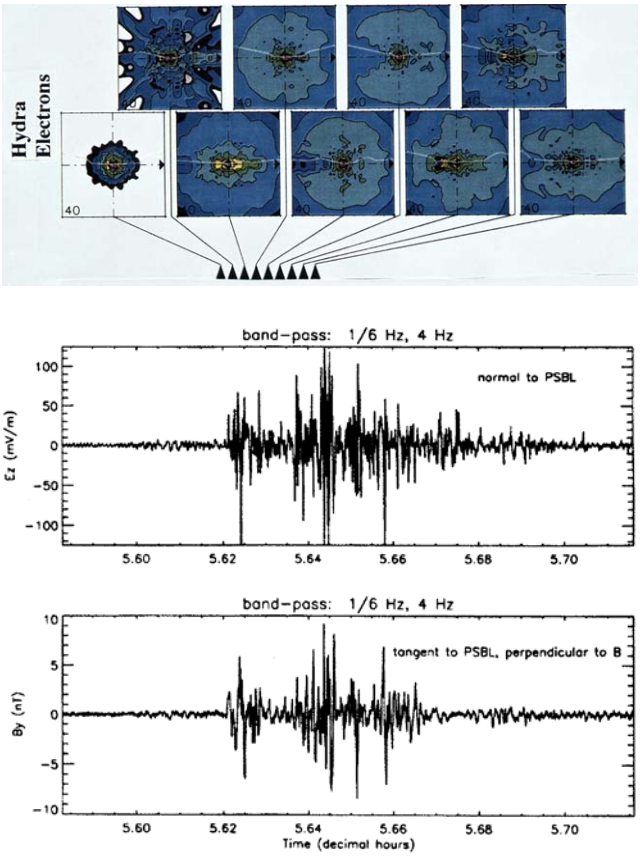

Fig. 28 (from Wygant et al. 2002) Electron and electric field data during a PSBL crossing (May 9, 1997) by Polar at 5 R_E. (*Top*) Hydra electron two-dimensional velocity space distribution functions, parallel and perpendicular to the magnetic field, obtained during a period of intense kinetic Alfvén waves. The maximum electron velocities displayed are 40,000 km/s. Velocities toward the Earth along the magnetic field line can be seen along the horizontal axis to the right. (*Bottom*) E_z and B_y filtered between 1/6 and 4 Hz

the PSBL. The presence of increased field-aligned electron fluxes near the times of peak Poynting flux, at both spacecraft, reinforced this conjecture.

The studies that have been reviewed here reported Alfvén waves in the PSBL that were conjugate to the nightside auroral region. Observations of Alfvén wave-induced electron acceleration by the four Cluster spacecraft at 6 R_E, in the flank-side plasma sheet boundary above the dusk-side auroral region, were reported by Morooka et al. (2004). Both Alfvén waves and upward electron beams showed a quasi-periodicity of approximately two minutes, and the downward Alfvénic Poynting flux was large enough to power the upward electron beams (Fig. 30). Although a one-to-one correlation was not observed, electron beams and Alfvén waves occurred within quasi-stationary flux tubes of a 0.5° latitudinal extent, as determined using Cluster's multipoint capability. It was proposed that the Alfvén waves were generated in the LLBL. In Sect. 3.1, it was statistically shown that Alfvén wave activity occurs along the entire auroral oval which is consistent with the observations of Morooka et al. (2004) for Alfvén waves in the dusk-side auroral region.

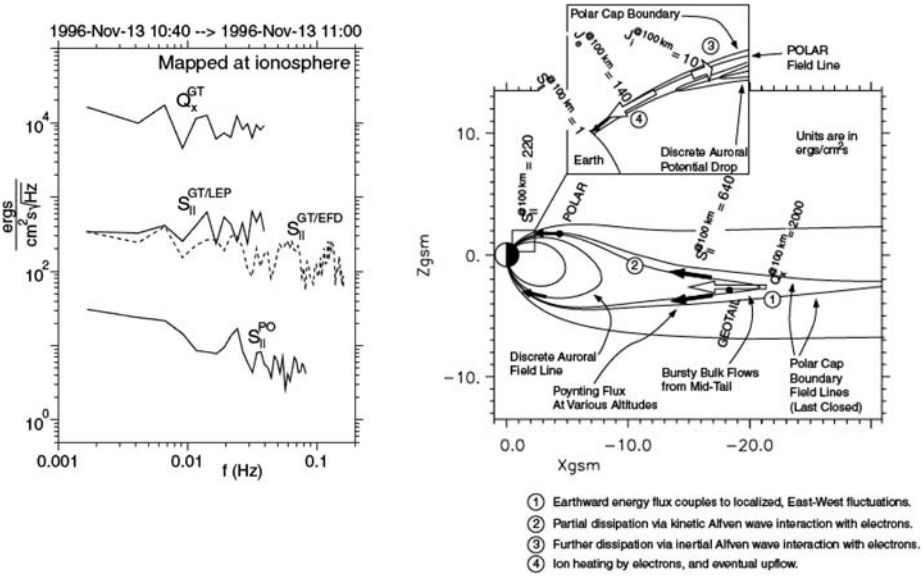

Fig. 29 (from Angelopoulos et al. 2002) (*Left*) Spectral density of the Poynting flux at Polar and Geotail, and energy flux at Geotail mapped at 100 km altitude. (*Right*) Schematic representation of energy generation and dissipation along field lines. Peak energy fluxes measured and particle fluxes expected, at low altitudes, are also shown. All energy flux values are in units of $\mathrm{mW/m^2}$ and have been mapped to an altitude of 100 km

3.4 Alfvénic Generator Region

Electromagnetic energy is generated in the outer magnetosphere and transmitted as the Poynting flux to the auroral acceleration region, and the ionosphere where it is dissipated (e.g., see review by Lysak 1990). Both Alfvén waves and large-scale quasi-static FAC are carriers of electromagnetic energy, and thus provide links between the low-altitude region and the distant tail. Two companion papers, Hamrin et al. (2006) and Marghitu et al. (2006), calculated the power density, $\mathbf{E} \cdot \mathbf{J}$, in the magnetotail at 18 R_E, using four-point Cluster measurements. Approximately conjugate FAST observations were used to assess the low-altitude response. The events investigated occurred in the PSBL during a geomagnetically quiet interval. Both studies reported a negative power density, $\mathbf{E} \cdot \mathbf{J} < 0$, at Cluster's location, which corresponded to the generator region (Fig. 31), and simultaneous electron precipitation at FAST. This result is consistent with the scenario that some Poynting flux is converted into particle energy flux, $\mathbf{E} \cdot \mathbf{J} > 0$. Whereas Hamrin et al. (2006) attributed the Poynting flux to the quasi-static FAC, Marghitu et al. (2006) suggested that part of the Poynting flux was carried by Alfvén waves.

3.5 Association with Ion Beams

The PSBL is the site of both Alfvén waves and ions beams. Whether or not there is a causal relationship between both has not been conclusively determined. Three opposing possibilities exist: (1) Alfvén waves are generated by instabilities caused by ion beams, (2) ion beams are generated by Alfvén waves, and/or (3) both are generated by other sources. No direct observations exist that can confirm any of these possibilities. Reported observations are, at most, suggestive but not conclusive.

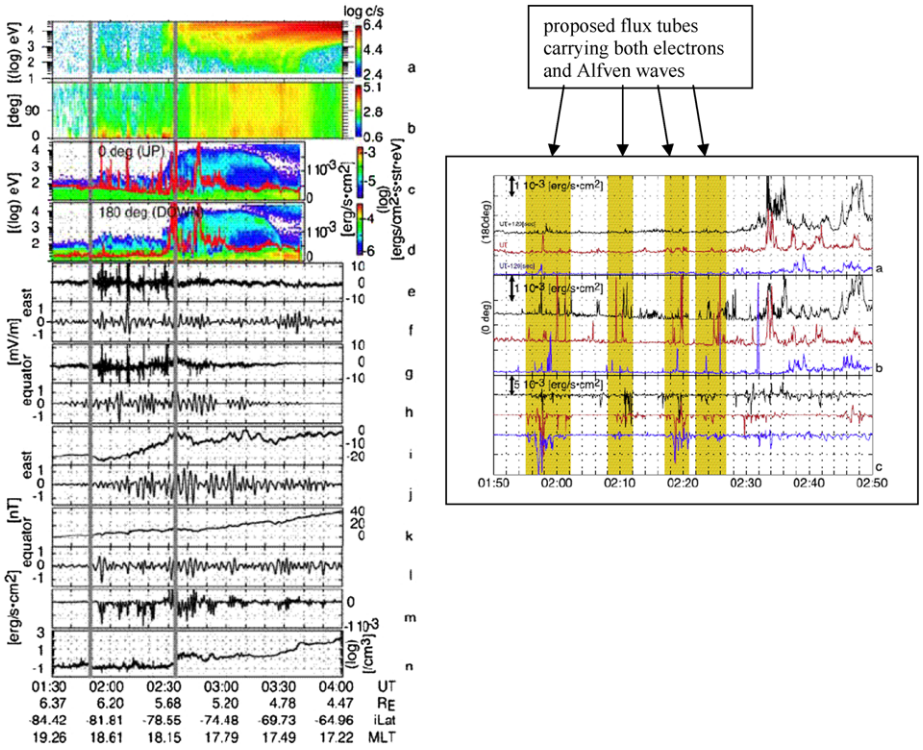

Fig. 30 (from Morooka et al. 2004) (*Left*) (**a**) A summary plot of event 2001–06–20 obtained by Cluster 1, in the southern hemisphere, showing: (**a**) Energy spectrogram; (**b**) pitch angle spectrogram of the low energy (10–1000 eV) component of H+; (**c**, **d**) energy flux of electrons, where the red line indicates the integrated energy flux; (**e**–**h**) perpendicular component of electric field data (**e** and **f** are raw data, **g** and **h** are band-passed with [5–10 mHz]); (**i**–**l**) perpendicular component of magnetic field data (**i** and **k** are deviations from the IGRF01 model, **j** and **l** are band-passed with [5–10 mHz]); (**m**) Poynting flux derived from **f**, **h**, **j**, and **l**. *Minus signs* indicate the earthward direction; and (**n**) density derived from the spacecraft potential. (*Right*) Energy flux of downward and upward electrons (panels **a** and **b**), and the Poynting flux of the ULF waves (panel **c**) for S/C-1, 2, and 4, during 01:50–02:50 UT. Cluster 1 and 4 are time shifted by +120 sec and −120 sec, respectively

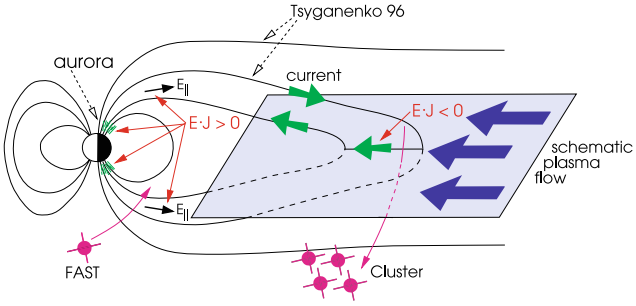

Fig. 31 (from Hamrin et al. 2006) A schematic sketch of the auroral current circuit. The generator region ($E \cdot J < 0$) in the magnetosphere powers the loads ($E \cdot J > 0$) in the acceleration region, and in the auroral ionosphere. The FAST and Cluster trajectories are shown for the event occurring between 22:00 UT (September 19, 2001) and 01:30 UT (September 20, 2001)

An association between Alfvén waves and ion flow in the lobe-PSBL region using Cluster was proposed by Zelenyi et al. (2004) who investigated properties of dispersionless ions found on fluctuating magnetic field lines, identified as Alfvénic. It was suggested that ion structures injected from the current sheet excite Alfvén waves on the same flux tube via the tail firehose instability. The conditions for the firehose instability need to be met near the source region in the distant tail, and could not be directly verified; but as argued in Zelenyi et al. (2004), the conditions can be met in the current sheet. Such a scenario is illustrated at the bottom of Fig. 32. Keiling et al. (2006) reported several well-separated ion beamlets with pronounced energy dispersion signatures at 4.5 R_E using Cluster. The region of these beamlets was threaded by low-frequency Alfvén waves which showed both traveling and standing signatures. In the study, the energy fluxes of beamlets and Alfvén waves were

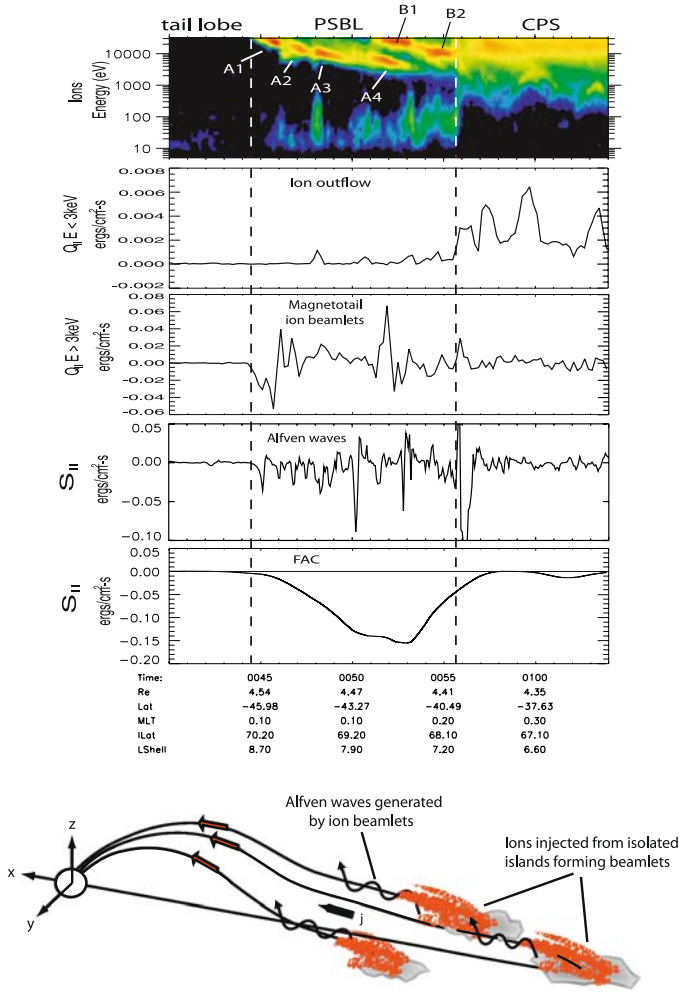

Fig. 32 (from Keiling et al. 2006) (*Top*) Energy flux comparison: (**a**) E–t spectrogram of ions, (**b**) ion outflow with energies <3 keV, (**c**) magnetotail ions with energies >3 keV, (**d**) Alfvén waves, and (**e**) static FAC. The *vertical dashed lines* bracket the PSBL. (*Bottom*) Simplified cartoon showing the injection of ion beamlets, and the generation of Alfvén waves at the site of ion injections

comparable, and it was noted that the observations were consistent with the proposal by Zelenyi et al. (2004) for a causal relationship between ion beams and Alfvén waves. The event occurred during the recovery phase; therefore, the amplitude of the Alfvén waves was significantly lower than is typical during the substorm expansion phase. For example, the Alfvén wave electric field amplitude was on the order of a few mV/m, which is one to two orders of magnitude smaller when compared to Alfvén waves in the PSBL during the substorm expansion phase (Keiling et al. 2000). Thus, it is uncertain as to whether the firehose instability can also explain the larger amplitudes of Alfvén waves observed during the substorm expansion phase.

Takada et al. (2005a, 2005b) also reported the simultaneous occurrence of Alfvén waves and ion flows in the PSBL. The left portion of Fig. 33, shows a Geotail pass entering and leaving the PSBL several times. Concurrent with the ion beams, the wave activity increased. Using five years of Geotail data at $X < -15\ R_E$ (GSM) in the PSBL, Takada et al. (2005b) investigated possible relationships between Alfvén waves (0.01–0.1 Hz) and ion distribution functions. The estimated Poynting flux of the waves was in the range of 10^{-6} to 5.6×10^{-2} mW/m^2, which is comparable, when mapped to the same location, to the Poynting flux of large-amplitude Alfvén waves reported in Polar spacecraft-based studies for altitudes between 4–7 R_E (e.g., Wygant et al. 2000; and Keiling et al. 2000). This similarity suggests that the Alfvén waves at both locations, Geotail and Polar, were caused by the

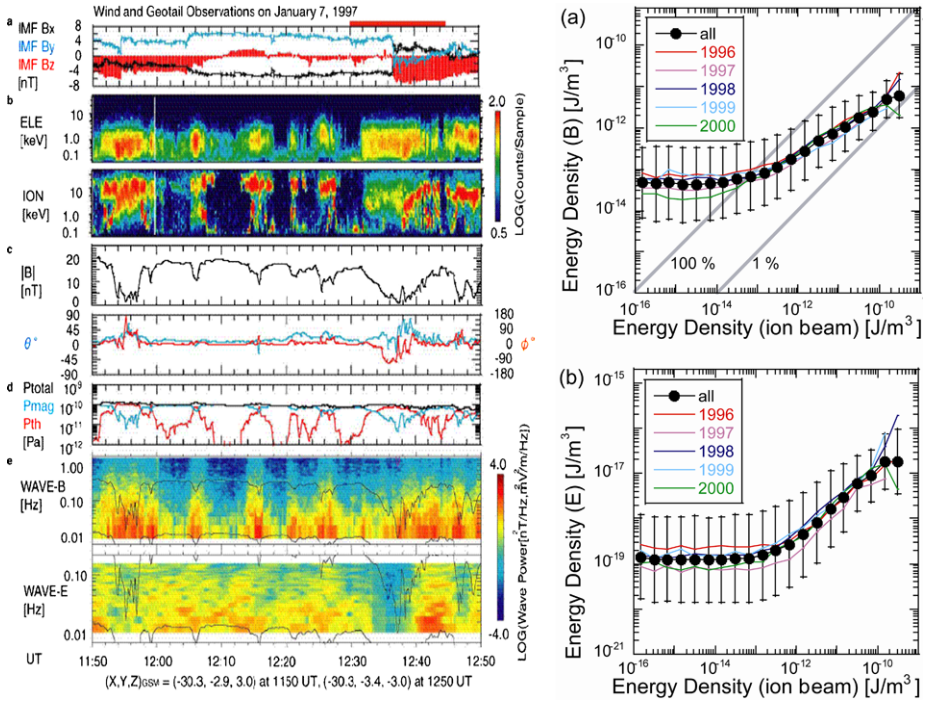

Fig. 33 (*Left*) (from Takada et al. 2005a) Wind and Geotail observations during the course of substorm activity on January 7, 1997. (*Right*) (modified from Takada et al. 2005b, personal communication, T. Takada) (**a**) Energy density of the wave magnetic field, and (**b**) the electric field plotted against the energy density of ion flows parallel to the magnetic field. *Solid circles* with 1-second error *bars* show the average in each bin. *Color lines* show the average value of each year. *Gray solid lines* in (**a**) show the levels at which the wave energy density becomes 1% and 100% of the beam energy density

same phenomenon. Further noted was that the wave energy density of δB and δE correlated with the energy density (printed as 'energy flux' in Takada et al. 2005b and corrected here, personal communication, T. Takada) of ion flows parallel to the magnetic field, and that the wave energy density (corrected, same as above) was less than 10% of the ion energy density for much of the time, allowing for the possibility that the ion beams provided the free energy for Alfvén wave generation, as seen in the right in Fig. 33. Ion distribution functions often showed several ion components and a strong temperature anisotropy. The comparison with linear theory led the authors to suggest the importance of the ion cyclotron anisotropy instability for Alfvén wave excitation.

3.6 Traveling and Standing Alfvén Waves

Dombeck et al. (2005) and Keiling et al. (2005) investigated properties of large-amplitude PSBL Alfvén waves for various spectral bands covering the range from 0.25 to 300 seconds (3.3 mHz to 4 Hz). It was found that large-amplitude Alfvén waves in the PSBL consist of a mixture of traveling and standing waves for different frequency ranges, with low-frequency waves predominantly Earthward-traveling and higher-frequency waves that travel bidirectionally. Furthermore, E/B ratios tend to increase with frequency, consistent with the ratios expected for kinetic Alfvén waves. Low-frequency components carry most of the Poynting flux, while the reflected Poynting flux is less, by two orders of magnitude, than the largest earthward directed Poynting flux. To illustrate these results, Fig. 34 shows a spectral analysis for one large-amplitude Alfvén wave event, occurring during a substorm (Keiling et al. 2005). Note that panels e through h, in Fig. 34, show the signature of a standing wave in the period range of 40 to 67 seconds.

Using simultaneous Poynting flux measurements from both Polar ($\sim$7 R_E geocentric distance) and FAST ($\sim$2 R_E geocentric distance) during the period of a decreasing AE index during the main phase of a major geomagnetic storm in the pre-midnight region (seen left in Fig. 35 as frequency band analysis), Dombeck et al. (2005) inferred average reflection (R) and dissipation (D) coefficients (seen in the right bottom of Fig. 35). They found that waves in the low-frequency bands, $<$0.1 Hz, are generally consistent with the frequency response predicted by the model of Streltsov and Lotko (2003), except for the lowest frequency band. Interestingly, as seen in the left portion of Fig. 35, it was also inferred that high-frequency, $>$1 Hz, kinetic Alfvén waves were possibly generated between Polar and FAST.

Much theoretical/numerical work exists on the topic of Alfvén waves with various temporal and spatial scales, and how they are modified by their interaction with the ionosphere and regions of parallel electric fields. The reader is referred to, for example, Mallinckrodt and Carlson (1978), Lysak and Dum (1983), Knudsen et al. (1992), Vogt and Haerendel (1998), Streltsov and Lotko (2003, 2004), and Sect. 7.1 of this review for additional discussion.

3.7 Summary—Plasma Sheet Boundary Layer

It is now well established that Alfvén waves are a common occurrence in the PSBL. In recent years, significant advances have been made in establishing their roles in the PSBL. During geomagnetically active conditions such as substorms, the PSBL is a region that carries significant energy, released in the magnetotail, in the form of Alfvén waves in addition to other energy carriers. These are the largest Alfvén waves, in terms of Poynting flux, in the magnetosphere during substorms. During storms, very large Alfvén waves are also observed deeper into the plasma sheet (see Sect. 2.3). Figure 36 shows several energy carriers in the

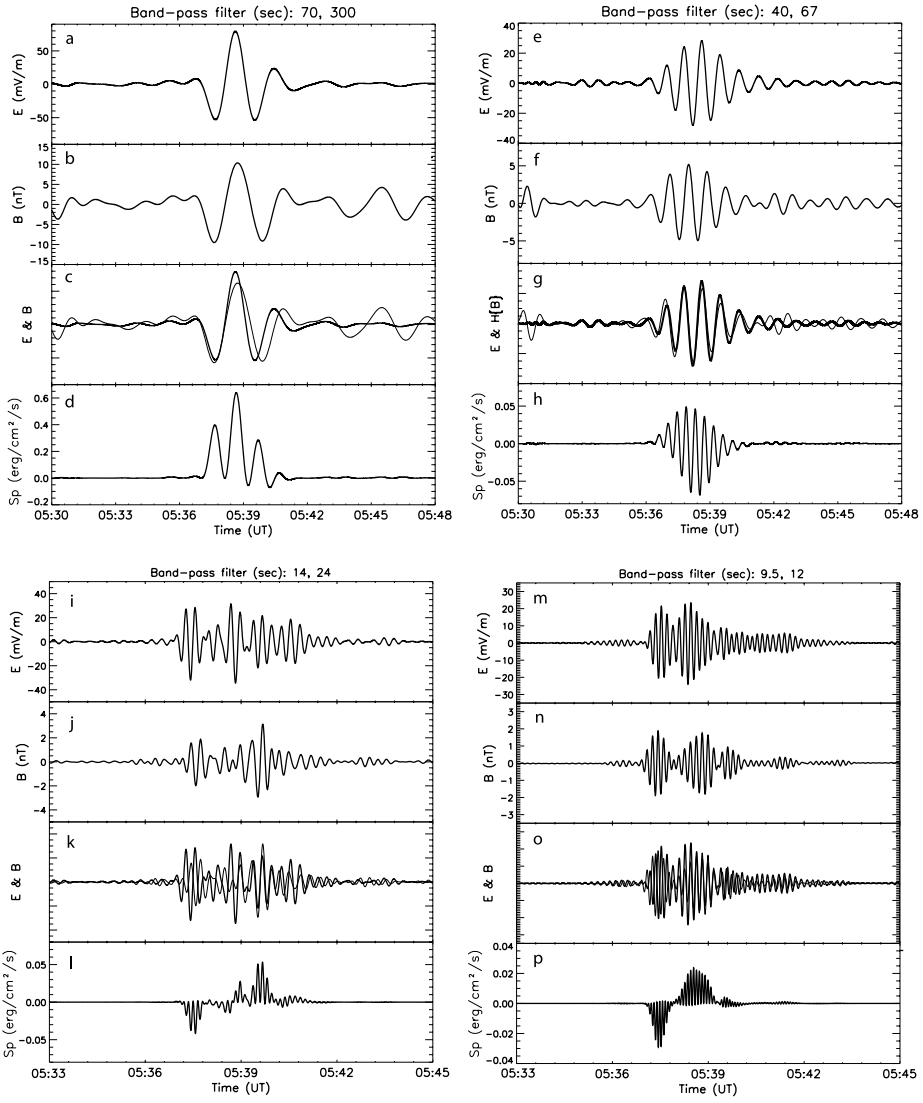

Fig. 34 (from Keiling et al. 2005) Four spectral components of a large-amplitude Alfvén wave event during a PSBL crossing by Polar. For each frequency components, the electric field, E_z, the magnetic field, B_y, the overlaid electric and magnetic field (or Hilbert-transformed magnetic field), and the Poynting flux calculated from the two field components are shown, see Sect. 1.4 for the effect of the Hilbert transform. The first (**a**–**d**), third (**i**–**l**), and fourth (**m**–**p**) spectral components show traveling waves, whereas the second (**e**–**h**) spectral component shows a standing wave signature, since E_z and $H(B_y)$ are in phase or, equivalently, E_z and B_y are in phase quadrature

magnetotail, participating in the transport of energy during substorms which was the consensus for some time (Fairfield et al. 1999). The reader should note that Alfvén waves were not part of the consensus. However, it should also be noted that a comparison of Alfvénic Poynting flux and particle energy flux, associated with BBFs during one substorm event at $\sim$18 R_E, indicates that the former was only 10% and less than the latter (Angelopoulos et

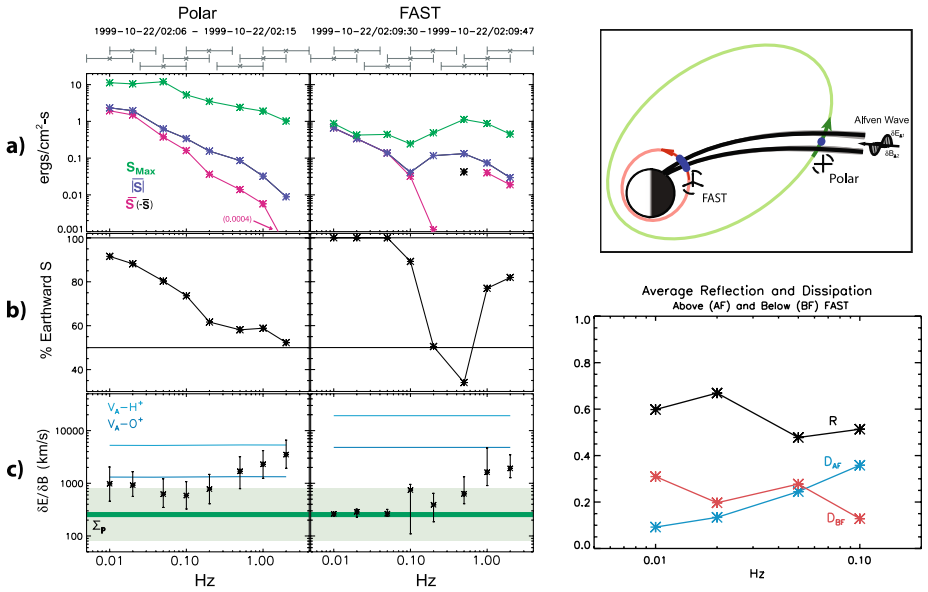

Fig. 35 (from Dombeck et al. 2005) (*Left*) Summary of frequency band analysis of Polar and FAST Poynting fluxes (S) and dE/dB ratios. (**a**) The mean total, $|S|$; the net earthward Poynting flux, S; and the peak Poynting flux, S_{Max}; in each band mapped to the ionosphere. (**b**) The percentage of S directed earthward for each band. (**c**) The dE/dB ratio in each band with the Alfvén velocity, V_A, for 100% H^+ (O^+) shown as a *light (dark) blue line*. The *light green box* shows the dE/dB ratio expected for ionospheric closure, and the *dark green line* shows the value for such closure if the lowest-frequency FAST waves are ionospherically coupled. (*Right, top*) Polar and FAST orbit during the analyzed event. (*Right, bottom*) The coefficients of reflection (R), the dissipation above FAST (D_{AF}) and the dissipation below FAST (D_{BF}) for the observed Polar waves in the lowest four frequency bands

al. 2002). In contrast, a comparison of various energy carriers at 5 R_E in the PSBL showed that Alfvén waves dominated during the substorm expansion phase (Wygant et al. 2002), whereas during the recovery phase the quasi-static FAC carried the largest amount of energy flux (Keiling et al. 2006). None of these comparative studies, however, were able to assess the entire energy flow through an extended cross-section, and therefore must be taken with caution. Clearly, additional work is required to quantify the energy transport via Alfvén waves in comparison to other energy carriers in the magnetotail.

It is widely assumed that the PSBL maps into the auroral acceleration region. From low-altitude satellites, <10,000 km, it is known that Alfvén wave-accelerated electrons and ion outflows occur, but not exclusively, near the polar cap boundary of the auroral oval during active geomagnetic times (see Sect. 7.3 for further information). Individual case studies and statistical studies also show that sufficient energy flux is carried by PSBL Alfvén waves to account for a significant fraction of the auroral luminosity, and that the Alfvénic Poynting flux is substantially absorbed at low altitude (see Sect. 7.2 for more discussion on this topic). Hence it has been established that PSBL Alfvén waves are important energy suppliers for low-altitude acceleration processes leading, among other things, to the aurora (Fig. 37).

Another important recent result is that electron acceleration due to Alfvén waves also occurs in the PSBL above the auroral acceleration region. Some evidence even suggests that a large fraction of Alfvén wave acceleration occurs above the auroral acceleration region. It was further demonstrated that the Alfvén waves in the PSBL cover a broad range of fre-

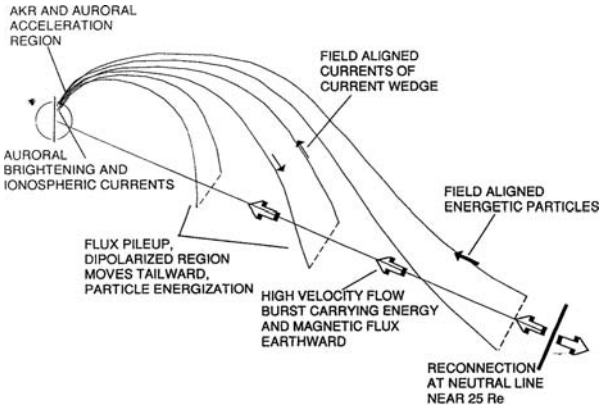

Fig. 36 (from Fairfield et al. 1999) Different energy carriers in the magnetotail. Note that Alfvén waves were not included in this earlier understanding of energy transport in the magnetotail

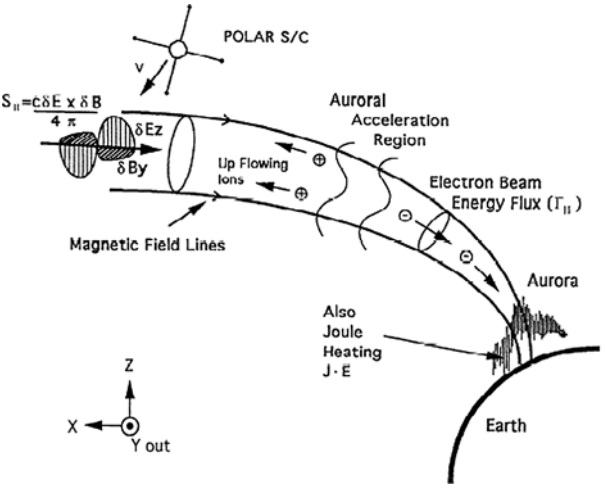

Fig. 37 Alfvén waves from the PSBL provide electromagnetic energy for acceleration processes in the auroral acceleration region (from Wygant et al. 2000)

quencies all the way into the kinetic regime. These smaller-scale waves provide the magnetic field-aligned electric field necessary for electron acceleration. Pronounced density gradients are observed in the PSBL in conjunction with kinetic Alfvén waves. This is also the case in the auroral acceleration region and, as shown later, in the reconnection region (see Sect. 6), suggesting that density gradients play an important role in the cascading of Alfvén wave energy to smaller scales (Genot et al. 2004).

Finally, the source of PSBL Alfvén waves has not been identified. At least four different scenarios have been discussed in the literature. Mode-coupling of fast mode and Alfvén waves is well established in other regions of the magnetosphere, see Sect. 2.2 for examples, and has also been suggested for PSBL Alfvén waves. In such a scenario, compressional energy from substorm processes near the radial axis of the magnetotail couples to shear Alfvén waves in the region of strong Alfvén velocity gradients (or density gradients) in the PSBL (e.g., Liu et al. 1995; and Allan and Wright 2000). Some observations have been reported that suggest that an ion-beam related instability generates Alfvén waves on PSBL field lines. At both low and high altitude, Alfvén waves are superimposed on large-scale upward currents (e.g., Nagatsuma et al. 1996), which allows for the possibility that the currents drive the waves. Recent observations of Alfvén waves in the dayside reconnection region, see

Sect. 6, support the view that reconnection is a viable source for Alfvén waves in the PSBL since these Alfvén waves travel on field lines closest to the open-closed field line boundary, presumably mapping into the reconnection region. The source or possible sources for Alfvén waves in the PSBL can ultimately only be determined through a combination of theory/simulation and observations.

4 Alfvén Waves in the Plasmasphere

The plasmasphere contains dense and cold plasma that corotates with the Earth. The plasmaspheric magnetic field is largely dipolar and approximately includes field lines with $L < 5$, depending on geomagnetic activity and local time (Chappell 1972). This L range is referred to here as low and mid-latitude. The plasmasphere interacts via compressional ULF waves with the CPS and the auroral zone, and is thought to resonantly oscillate via an excitation that is external to the plasmasphere. The oscillations are standing fast mode waves which efficiently mode-convert to shear Alfvén waves wherever the eigenfrequency of the global cavity matches the eigenfrequency of the field lines (e.g., Kivelson and Southwood 1986). An assessment of the Poynting flux is important for understanding this coupling.

Alfvén waves in the plasmasphere have been reported in connection with ULF pulsations. Most observations of ULF pulsations have come from ground-based instruments (e.g., Fukunishi 1975), and have relied on indirect measurements of the Alfvénic signature, see Sect. 1.4. Very few space observations for Alfvén waves exist in the plasmasphere (Osaki et al. 1998; and Collier et al. 2006). Important types of pulsations are Pi2 pulsations with periods between 40 and 150 seconds. Pi2s occur at substorm onset, and therefore have been used as onset indicators (Saito 1969). Although mostly observed by ground magnetometers, they also occur in space. Pi2s determined on the ground and in space can either be due to fast mode waves or shear Alfvén waves. Alfvén waves are commonly associated with high-latitude, auroral zone Pi2s, and these Pi2s show the largest amplitudes. At mid to low latitudes, $L < 5$, both types of Pi2s exist, although the compressional type is more common (e.g., Yeoman et al. 1991). Finding the origin of these pulsations has been proven to be difficult, largely because of the filtering effect of the ionosphere (Hughes 1974). Several models have been proposed to explain the multitude of Pi2 observations (see review by Olson 1999, and additional models by Kepko et al. 2001, and Keiling et al. 2006).

The plasmasphere should be a prime candidate for FLR because of the closed field lines at both ends in the ionosphere and less turbulent fields. Indeed, FLR have been reported on plasmaspheric field lines using ground-based measurements (see Waters et al. 1994, and references therein). However, they have only recently been confirmed in space (Collier et al. 2006).

4.1 Pi2 Pulsations—Traveling Alfvén Waves

A satellite-based confirmation of Alfvén waves in the plasmasphere was reported by Osaki et al. (1998). At the same time, it was confirmation that plasmaspheric Alfvén waves contribute to the Pi2 phenomenon. The Alfvénic oscillations had a period of ∼90 seconds, and started simultaneously with an identical ground Pi2 covering a range of low to mid-latitudes in the nightside. Either ground and space Pi2 had the same source, or the space Pi2 was the source of the ground Pi2. Using both magnetic and electric field measurements from the Akebono satellite, it was found that the space pulsations were traveling Alfvén waves. Figure 38 shows the phase relation between corresponding orthogonal components. Additionally, the

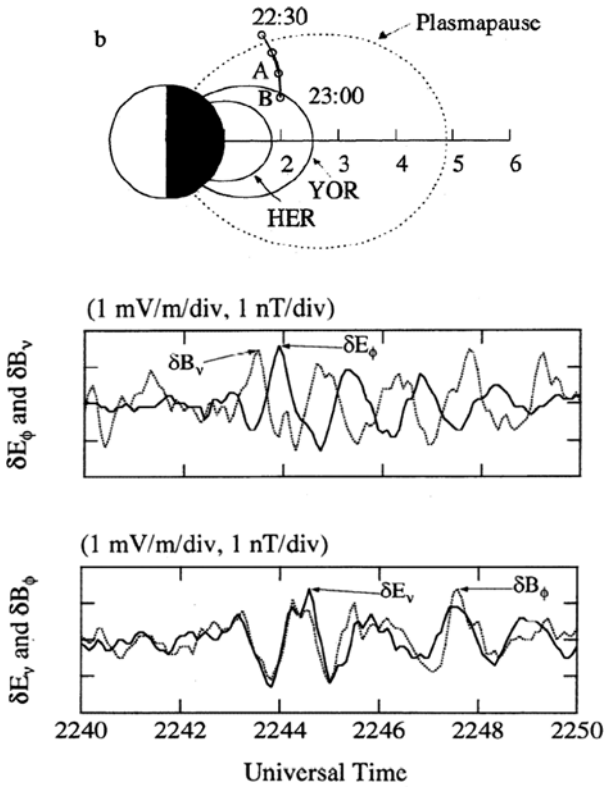

Fig. 38 (from Osaki et al. 1998) (*Top*) Partial orbit of the Akebono satellite on February 13, 1990, including the Pi2 event. The plasmapause ($L \sim 4.9$) is indicated with a *dashed line*. (*Bottom*) Comparison of the phase between the orthogonal components of the electric and magnetic fields of the Pi2 event

E/B ratio was consistent with the local Alfvén speed, and no compressional component was present. This study clearly demonstrated the advantage of space measurements over ground measurements in identifying the wave mode of Pi2s.

The traveling Alfvén waves were recorded for 400 seconds, that is, for roughly four cycles. No indication of reflected waves, seen in the Poynting flux calculations for the pulsations (Fig. 39), was seen. Osaki et al. (1998) calculated a strong ionospheric damping rate for Alfvén waves, consistent with the lack of reflected wave power. Due to this strong damping (i.e., energy leakage), it was suggested that a plasmaspheric cavity resonance would have been damped in a much shorter time than the 400 second duration of the oscillations. Therefore, the authors concluded that a driver, external to the plasmasphere, was the most likely explanation for the long duration of the Pi2. Here, we have an example of a continuous driving of Alfvén waves that does not necessarily lead to FLR which is in contrast to the event presented in Sect. 4.2. This study also illustrates how Alfvén waves act as an important energy sink in the plasmasphere, and how energy approaching from the tail is redirected into the ionosphere.

4.2 Pi2 Pulsations—Standing Alfvén Waves

The requirement of closed magnetic field lines on both ends is a necessary but not a sufficient requirement for the formation of FLR. As shown above, Sect. 4.1, strong ionospheric damping prevented FLR formation. In contrast, Collier et al. (2006) reported standing Alfvén waves, identified by a phase shift of 90° in **E** and **B** (Fig. 40). While three spacecraft were

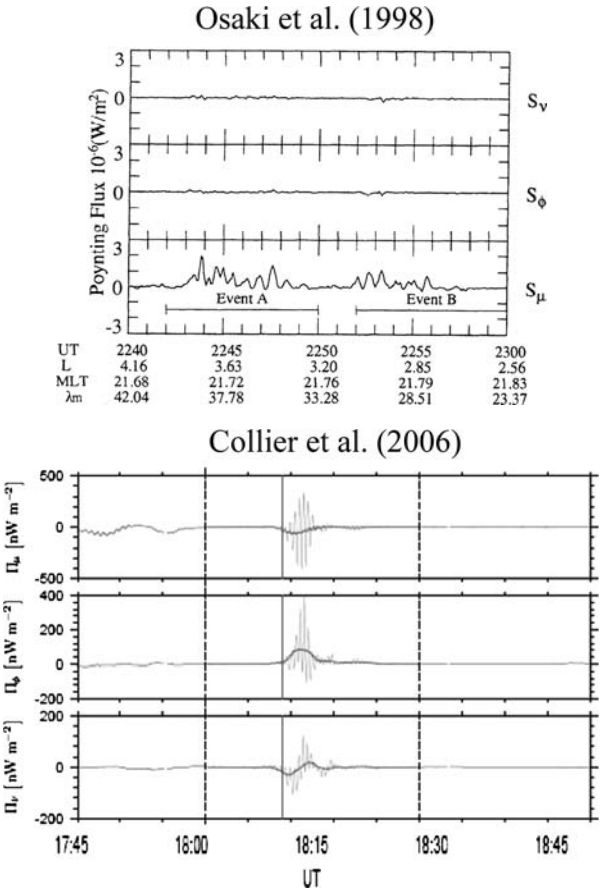

Fig. 39 Poynting flux (filtered) comparison for two Pi2 events reported by (*top*) Osaki et al. (1998) and (*bottom*) Collier et al. (2006). S_μ is the Poynting flux parallel to the mean background field, S_Φ is azimuthally eastward, and S_ν completes the right-handed orthogonal triplet

inside the plasmasphere, $L = 4.7, 4.5, 4.6$, one was located at or just outside the plasmapause ($L = 6.6$). Interestingly, the event was only clearly observed on those spacecraft that were inside the plasmasphere. The study also provided evidence for the coupling of standing fast mode waves and FLR inside the plasmasphere. These observations are suggestive of a cavity resonance within the plasmasphere, and the relative phase between satellites located on either side of the geomagnetic equator indicates that the FLR was an odd harmonic (Collier et al. 2006). Poynting flux calculations of the FLR indicated that only a little energy was dissipated in the ionosphere during the Pi2 event.

Figure 39 shows a comparison of the Poynting flux observations of Osaki et al. (1998) and Collier et al. (2006). The third panel of Osaki et al. (1998) and the first panel of Collier et al. (2006) show the field-aligned Poynting flux which is associated with Alfvén waves, and is only considered here. Whereas one panel shows unidirectional Poynting flux, the other panel shows bidirectional Poynting flux, indicating the presence of FLR. In the previous section, it was mentioned that due to low ionospheric conductivity, Alfvén waves were strongly dissipated in the ionosphere, causing the uni-directional flux at the spacecraft location (Osaki et al. 1998). The observations of bi-directional flux occurred on higher L values (i.e., closer to the auroral zone), and, therefore, on field lines mapping to significantly higher ionospheric conductivity which may explain the existence of FLR (Collier et al. 2006).

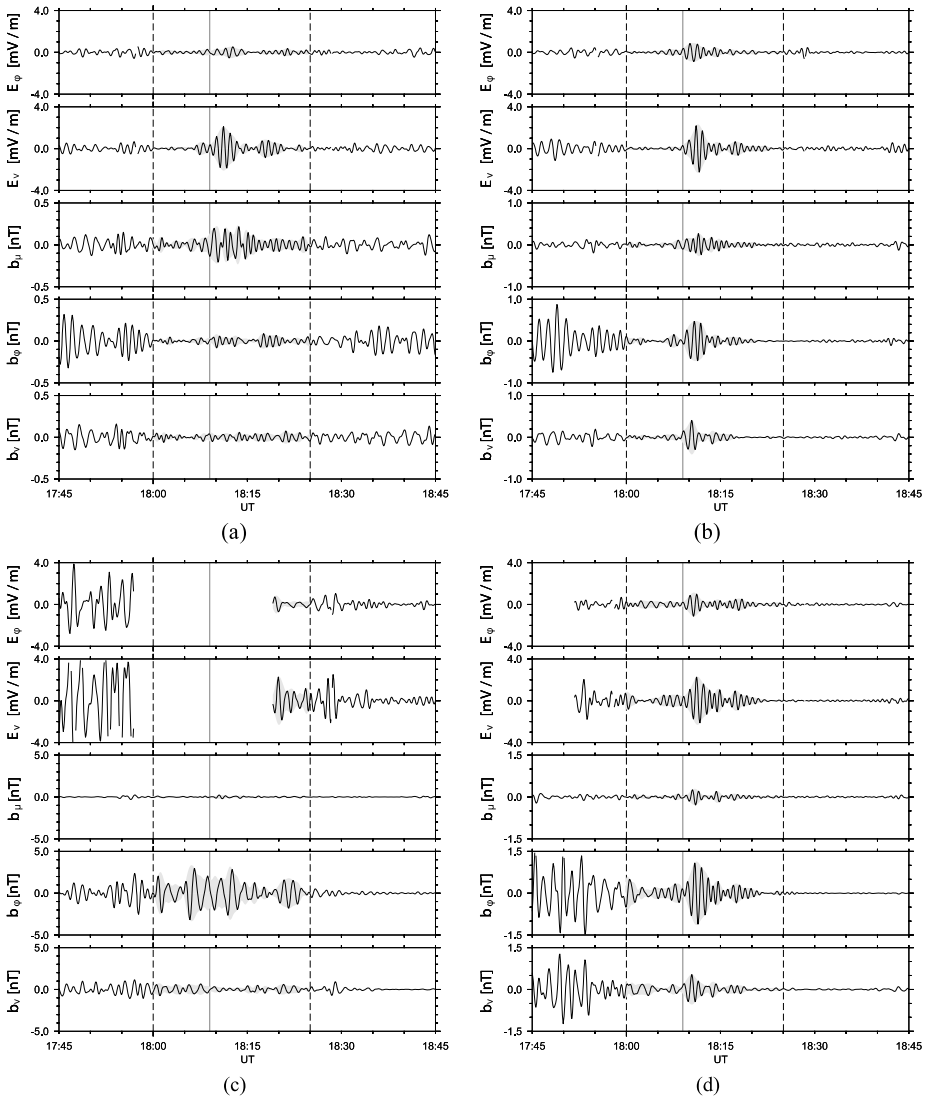

Fig. 40 (from Collier et al. 2006) Electric and magnetic waveforms, in mean field-aligned coordinates, for the four Cluster spacecraft. The signals were band-pass filtered (40 s, 150 s). Panels **a**, **b**, **c**, and **d** show data from spacecraft Cluster 1, 2, 3, and 4, respectively. All spacecraft except Cluster 3 show Pi2 pulsations starting at the time indicated by the *vertical solid line*

4.3 Summary—Plasmasphere

Somewhat surprisingly, Alfvén waves in the nightside plasmasphere have only been reported in two case studies thus far, both associated with ground Pi2 pulsations. One case was a traveling wave, and the other a standing wave (FLR). The difference can be explained by examining differences in the conductivity at the conjugate ionospheric footpoints for the two events. The traveling Alfvén wave was recorded at L shells from 2.4 to 3.8, whereas the FLR was recorded at $L = 4.5$, consistent with the view that the ionospheric conductivity

increases towards larger L values. Similarly, FLR associated with ground Pi2 occur inside the CPS where ionospheric conductivity is expected to be higher, Sect. 2.2. This increased conductivity leads to more wave reflection and therefore can lead to FLR.

Pi2-associated Alfvén waves in the plasmasphere are driven by compressional waves that can have different sources. This coupling provides a significant energy sink for compressional waves in the plasmasphere during substorm processes. The Alfvén waves do not play an active role in determining the characteristic Pi2 frequency; they are simply an intermediate energy carrier in the transport of Pi2 energy from the initial source to the ground. This is different for Alfvénic Pi2s in the auroral zone (see Sect. 2.4).

The rarity of Alfvén wave observations in the plasmasphere is not necessarily due to their rare occurrence, but rather due to their narrow extent latitudinally. Since Alfvén waves seem to appear only in conjunction with Pi2s, which are only short-lived, it is less likely to observe them, in contrast to frequently observed Pi2-associated compressional waves, which can span the entire plasmasphere or, at least, larger regions (Takahashi et al. 1995). The two contrasting observations of Alfvén waves in the plasmasphere reviewed here clearly indicate a need for future reports of Alfvén wave events in the plasmasphere.

5 Alfvén Waves in the Tail Lobes

The magnetotail lobes are threaded by field lines that connect to the Earth and the Sun which gives the lobes very different properties when compared to the neighboring PSBL. The lobe plasma density and the plasma energy are lower, and overall the dynamics of the lobe regions is much less. The lobes are generally considered to be passive regions during convective particle transport from the solar wind, through the magnetopause and into the plasma sheet. Both the solar wind and the ionosphere supply plasma to the lobes. Plasma sheet disturbances, such as reconnection and plasma fast flows, affect the lobes' dynamics via the transfer of ULF wave energy. In a recent brief review of high-latitude ULF waves on the ground, Engebretson et al. (2006) pointed out that in recent years it has been revealed that the ground signatures of ULF waves in the polar cap, the low-altitude extension of the lobe field lines, are surprisingly rich. In spite of many ULF wave studies using ground data in the polar cap, there are only few reports on *in situ* observations of ULF Alfvén waves in the lobes. These reports will be reviewed here.

An early ISEE 2 study reported ULF wave activity, periods of 3 to 64 minutes, including Alfvén wave activity in the tail lobe (Chen and Kivelson 1991). Using magnetic field data it was reported that the wave amplitudes of both compressional and transverse waves were weakly correlated with the AE index, which is a measure of substorm activity. In recent years, the tail lobes have received increasing attention. Several studies have reported Alfvén waves in the lobes and characterized some of their properties and associations with other phenomena. The first reports of Alfvén waves in the lobe using both electric and magnetic fields to unambiguously confirm their existence, appeared in Ober et al. (2001) and Keiling et al. (2001a). Keiling et al. (2005) and Takada et al. (2006) investigated tail lobe Alfvén waves in more detail, and compared them to the Alfvén waves found in the neighboring PSBL. These results are described in Sect. 5.1. Section 5.2 reviews two studies (Sauvaud et al. 2004; and Takada et al. 2006) that have investigated the relationship of outflowing oxygen and Alfvén waves in the lobes. In Sect. 5.3, I summarize the results.

5.1 Substorm and Storm

One of the sources of lobe Alfvén waves is substorm activity. Several recent studies have demonstrated this view very clearly. Ober et al. (2001) reported Alfvén waves with a period

of approximately 90 s at 4.4 R_E, using Polar spacecraft data, in the lobe during the expansion phase of a substorm (Fig. 41). Shortly thereafter, Polar entered the PSBL at about 0400 UT and encountered typical substorm-associated, large-amplitude Alfvén waves, Sect. 3. Pulsations on the ground, see the bottom panel in Fig. 41, with the same period as the lobe waves were observed near the magnetic footprint of Polar. Ober et al. (2001) proposed that Polar crossed a spatial boundary in the lobes at ∼0355 UT, the second dashed line Fig. 41, when it encountered Alfvén waves. It was suggested that the Alfvén waves were the result of DP 1 fringing fields, due to oscillations of the main electrojet in the ionosphere. The simultaneous occurrence of a downward current signature at Polar was taken as supportive evidence for this scenario.

In contrast, Keiling et al. (2001a, 2005) reported substorm-associated lobe Alfvén waves at 5–6 R_E, using Polar, that started at substorm onset as determined from ground magnetometer data (Fig. 42). The findings led the authors to propose that lobe Alfvén waves could be used as a new substorm indicator. Although Ober et al. (2001) reported a time delay of ∼3.5 minutes between the ground and space oscillation onset for their event, as seen in Fig. 41 with dashed lines, a reevaluation allows for the possibility that the *in situ* onset actually began earlier. Small oscillations, first panel in Fig. 41, that coincided with the ground onset, first dashed line from the left, are visible albeit with smaller amplitude than those pointed out by Ober et al. (2001). A new interpretation of this type is, however, not conclusive.

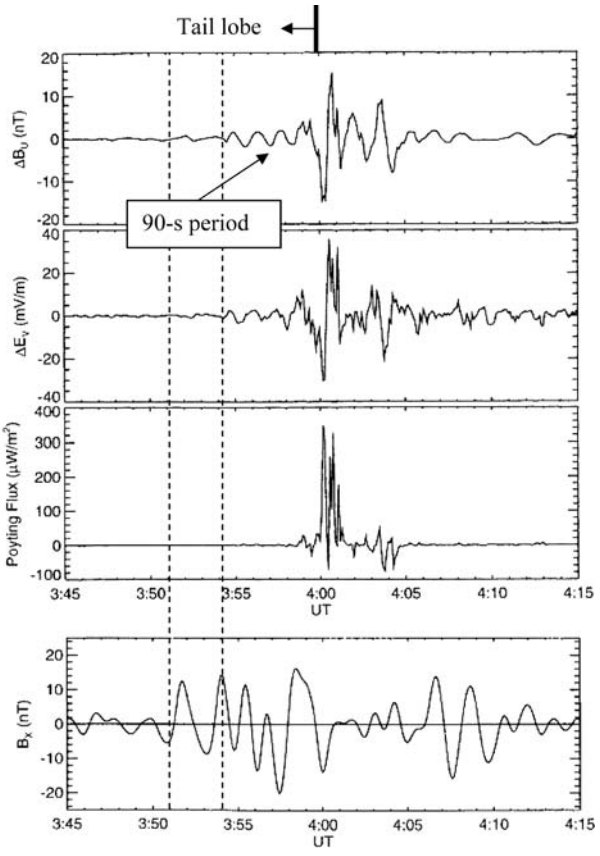

Fig. 41 (modified from Ober et al. 2001) Electric (radial) and magnetic (azimuthal) field perturbations observed by Polar on April 22, 1998 in a field-aligned coordinate system, and the parallel component of the Poynting flux, positive towards the nearest ionosphere. (*Bottom panel*) The high-frequency X component of the magnetic field at the ground station Cape Dorset

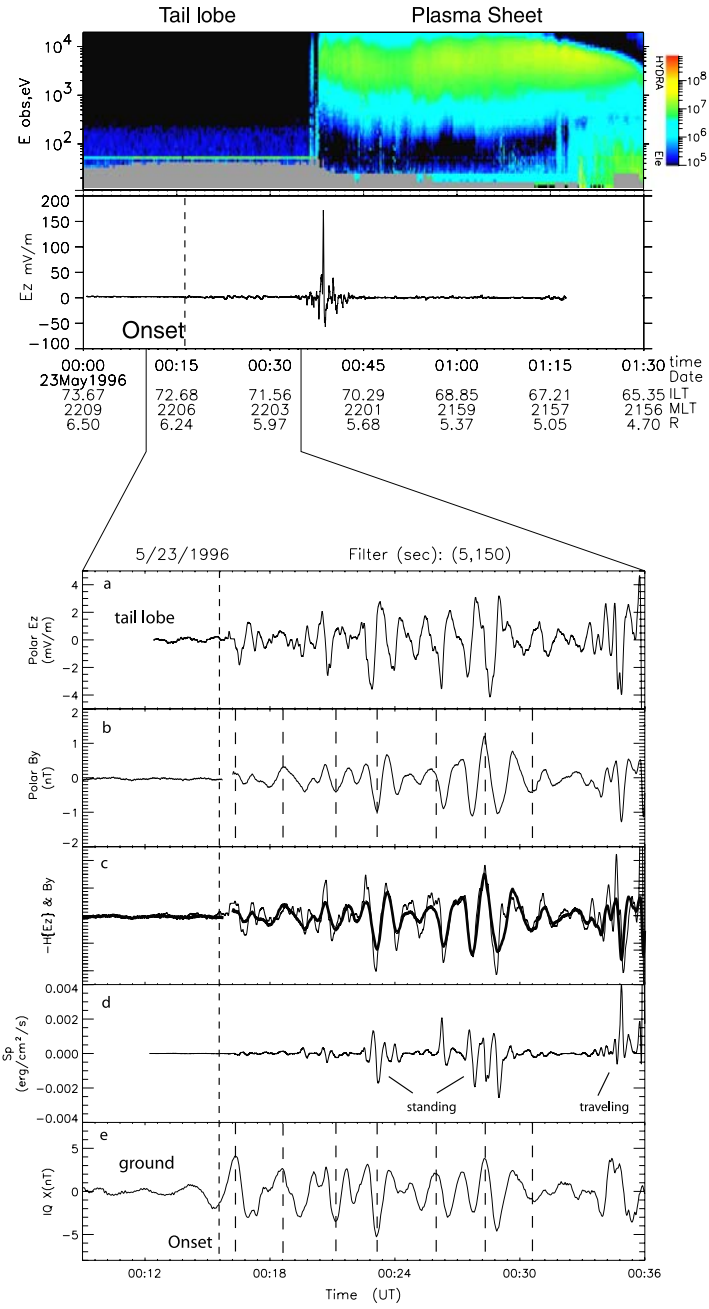

Fig. 42 (from Keiling et al. 2005) (*Top*) Electron energy–time spectrograms and electric field data on May 23, 1996 while Polar crossed the tail lobe and the plasma sheet. The time of substorm onset is indicated by the *dashed line*. (*Bottom*, **a–e**) Comparison of Polar and ground data on May 23, 1996, while Polar was in the tail lobe. The onset of the tail lobe Alfvén waves at Polar's location coincided with the onset of ground oscillations (*dashed lines*). The tail lobe Alfvén waves show clear standing wave signatures at Polar's location, as indicated by the 90° phase shift between E_z and B_y. The waveforms of the magnetic field oscillations recorded by Polar and the Iqaluit (IQ) ground station are very similar, see the *short vertical dashed lines*

At Polar's location, 5–6 R_E, the lobe Alfvén waves showed standing wave signatures with a large perpendicular scale size, inferred from the lack of Doppler-shift in the lobe waves in comparison with ground observations, and a near-zero net Poynting flux (Keiling et al. 2005). Since lobe field lines are open, the observed standing Alfvén waves in the lobe do not form FLR, i.e., they do not represent an eigenmode of the magnetic field line. Instead, it is possible that lobe Alfvén waves reflected off of the ionosphere leading to the superposition of incident and reflected waves, as was previously proposed by Wright et al. (1999) on purely theoretical grounds. Immediately poleward of the PSBL, the lobe Alfvén waves showed almost no sign of reflected waves, suggesting their dissipation in the ionosphere (second to the last panel in Fig. 42). The periods (frequencies) of the standing waves were in the range of 30 to 180 seconds (33 to 5.5 mHz). Nearly identical *in situ* oscillations were simultaneously recorded in ground magnetometer data without discernible time-delays, indicating that the lobe Alfvén waves propagated all the way to the ionosphere where they caused the ground oscillations. This is in contrast to the Alfvén waves in the PSBL that do not appear as ground oscillations but dissipated along the way (Keiling et al. 2005). Furthermore, the lobe waves were superimposed on the signature of a large-scale, field-aligned current (FAC) similar to the Ober et al. (2001) observation. Keiling et al. (2005) suggested that the remote magnetic effect of the SCW current, possibly accounted for the FAC signature in the tail lobe at Polar's location. The onset of this FAC was simultaneous with the onset of the magnetic substorm bay. It was further reported that substorm-related PSBL Alfvén waves, described in detail in Sect. 3, carried a two to three order magnitude larger Poynting flux than the lobe Alfvén waves.

Cluster observations at 6–19 R_E of Alfvén waves in the magnetotail lobe close to the PSBL were reported by Takada et al. (2006), see Fig. 43 in Sect. 5.2. In contrast to previous studies (Ober et al. 2001; and Keiling et al., 2001a, 2005) the lobe Alfvén waves transported on average their wave energy (Poynting flux) toward the Earth along magnetic field lines. It could be possible that the waves had not yet been reflected from the ionosphere, since Cluster observations occurred at larger distances, although it is surprising that not even one event was reported indicating a standing wave signature. Although Keiling et al. (2005) also reported Earthward traveling Alfvén waves, they occurred much closer, within one to two minutes, of the lobe-PSBL interface. Takada et al. (2006) reported a difference of two to three orders of magnitude in the Poynting flux between lobe and PSBL Alfvén waves, consistent with Keiling et al. (2005). In comparison, Sauvaud et al. (2004) reported lobe Alfvén waves during an intense storm with Poynting fluxes that were enhanced by one order of magnitude. The waves also propagated Earthward and were recorded by Cluster at 18 R_E. The study of Sauvaud et al. (2004) is further presented in Sect. 5.2 in association with ion outflows.

Takada et al. (2006) considered two excitation mechanisms for lobe waves. They concluded that the waves were mainly substorm-associated rather than KHI-associated, since the wave appearance correlated with auroral electrojet enhancements in their observations, in agreement with the studies mentioned above. A possible association with KHI was investigated by comparing solar wind speed data but could not be found.

5.2 Association with Oxygen

It is known that outflowing ionospheric plasma occupies lobe field lines (e.g., Vaisberg et al. 1996). Takada et al. (2006) reported that in all but one Alfvén wave event in the lobe, previous section, ionospheric oxygen, O^+, outflow with densities of $N_{O^+} > N_p$ were present,

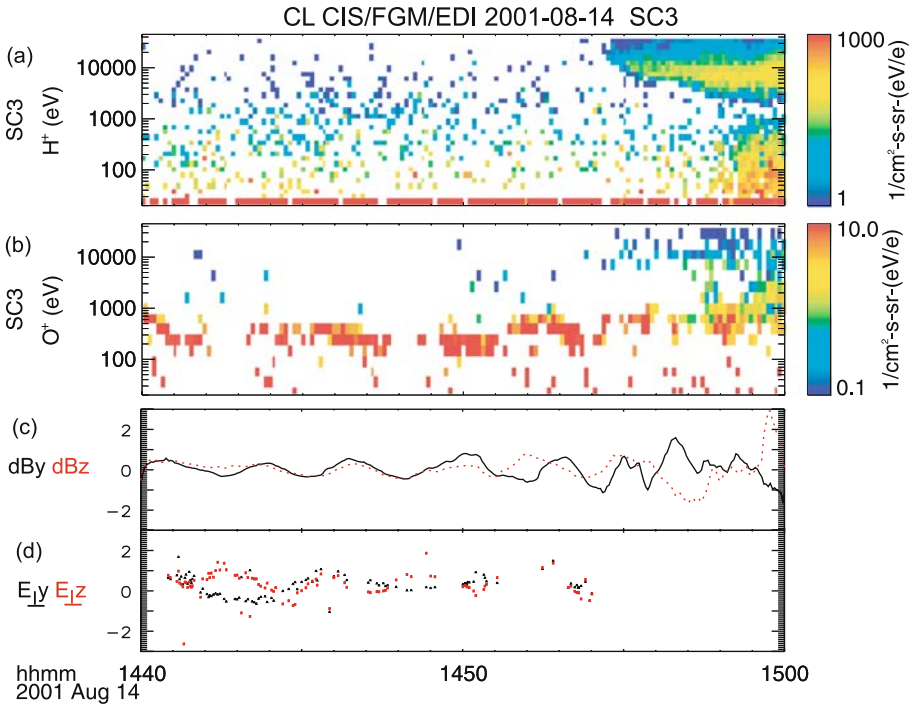

Fig. 43 (from Takada et al. 2006) Cluster 3 observations on August 14, 2001. The energy–time spectrograms of (**a**) protons and (**b**) O^+ are shown. (**c**) *dBy* (*black solid*) and *dBz* (*red dotted*) after subtraction of B_0, and (**d**) E_y (*black*) and E_z (*red*) are shown

Fig. 43. Therefore, an investigation as to whether O^+ was necessary for Alfvén wave appearance was undertaken. Since one counter example was reported (i.e., lobe Alfvén waves without oxygen on the same field lines) and storm-associated O^+ transport from the ionosphere into the tail was possible, the authors concluded that the presence of O^+ was not a necessary condition for lobe waves. Instead, they suggested that a rich O^+ plasma could serve to enhance magnetic field fluctuations, resulting in the greater likelihood of Alfvén wave observation.

Allan (1993) proposed that standing Alfvén waves on lobe field lines could generate a ponderomotive force strong enough to extract ionospheric O^+ into the tail lobes. However, this scenario requires that Alfvén waves interact with the ionosphere. Although several studies reported standing waves, Sect. 5.1, at lower altitudes, less than 6 R_E, Takada et al. (2006) only reported Earthward traveling waves, greater than 6 R_E. If the waves reported by Takada et al. (2006) become the lower-altitude standing waves, it would imply that no interaction with the ionosphere had taken place, thus ruling out the ponderomotive force as a driver for ionospheric outflow for their events. Instead, it is likely that ionospheric O^+ already occupied the lobe field lines, and was possibly associated with enhanced geomagnetic activity, as was pointed out by Takada et al. (2006).

An observable effect of lobe Alfvén waves on low-energetic lobe plasma, both hydrogen and oxygen, was demonstrated by Sauvaud et al. (2004). Figure 44 shows proton, oxygen, magnetic field, and electric field data from Cluster at ∼18 R_E in the tail lobe. Nearly monoenergetic oxygen ions were flowing tailward with energy modulations, due to a perpendic-

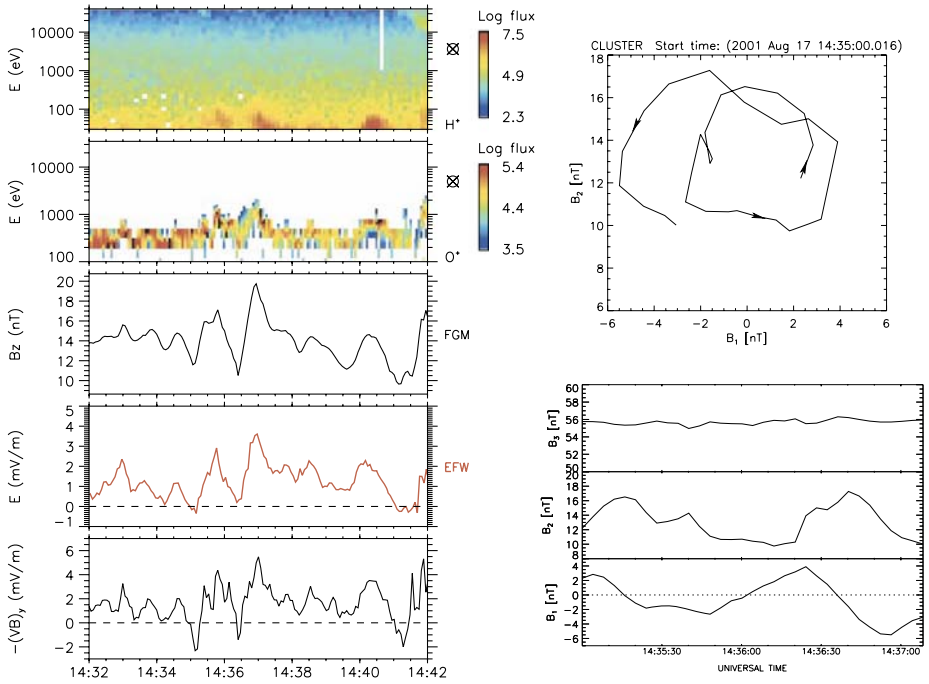

Fig. 44 (from Sauvaud et al. 2004) (*Left*) Cluster 1 observations on August 17, 2001, comparing the proton and oxygen energy–time spectrograms with the B_z component of the magnetic field, the E_y component of the electric field, and the $-(V\,B)_Y$ deduced from oxygen measurements. (*Right*) Hodogram of the magnetic field in a plane perpendicular to the main component, B3, and variations of the three components of the B field in a system deduced from minimum variance analysis

ular drift, which matched the fluctuations of both **E** and **B**. Sauvaud et al. (2004) suggested that the energy modulation was caused by the fluctuating electric field in the Alfvén wave field. Similarly, the energy of the protons was raised by the lobe Alfvén waves. Since δE and δB were in phase, this wave propagated Earthward with a phase velocity of ∼500 km/s, as computed from the E to B ratio, in agreement with the local Alfvén speed. The wave was left-hand circularly polarized, as seen in the right side of Fig. 44. The associated Poynting flux was $\sim 15 \times 10^{-6}$ W/m^2, or $\sim 15 \times 10^{-3}$ W/m^2 when mapped to the ionosphere. This value is one order of magnitude larger than that reported by Keiling et al. (2005) and Takada et al. (2006), likely due to the fact that this interval, August 17, 2001, occurred during a storm period.

5.3 Summary—Tail Lobes

The roles of lobe Alfvén waves that emerge in the dynamics of the magnetotail are largely one of an energy sink during substorm/storms, and one that provides an energy loss mechanism either to the solar wind or via some wave dissipation processes. Overall, lobe Alfvén waves are dynamically not as important to the magnetotail as PSBL Alfvén waves. The studies reviewed here associate Alfvén waves in the lobe with plasma sheet activities during substorms and storms, although the solar wind has also been considered as a direct driver of lobe ULF activity in the past, before 2000. Since the year 2000, studies reported properties

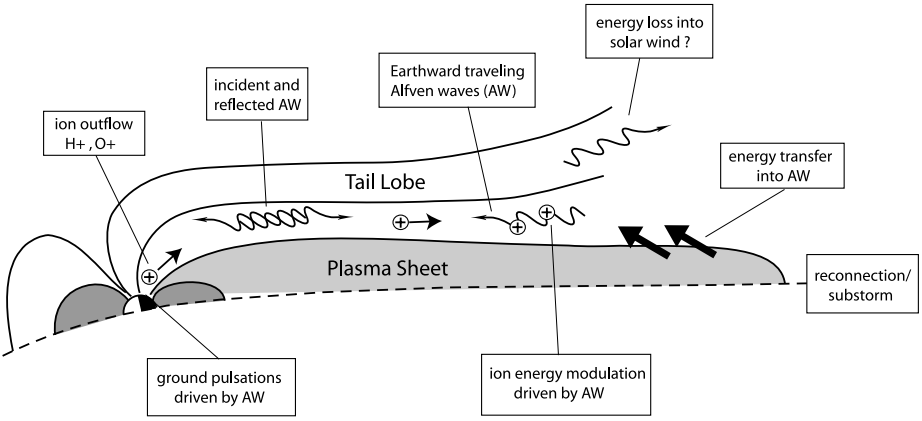

Fig. 45 Illustration of various phenomena associated with lobe Alfvén waves (labeled *AW*)

of Alfvén waves with periods less than ∼4 minutes. Studies conducted prior to 2000, on the other hand, reported waves with much longer periods, from three to 64 minutes (e.g., Chen and Kivelson 1991). The origin of these longer-period waves is somewhat uncertain. To clarify their roles, future work should revisit these longer-period Alfvén waves. Clearly, more Alfvén wave observations in the lobes are required to confirm or refine the conclusions of this review, which were only based on a few studies and which are summarized below.

5.3.1 Energy Sink

Alfvén wave events have been reported to occur exactly at substorm onset, and it has been proposed that these waves could be used as a substorm indicator. At distances of greater than 6 R_E, the reported lobe Alfvén waves were mostly traveling towards Earth, implying generation in the magnetotail as opposed to the ionosphere (Fig. 45). In order to gain an indication for the amount of energy transferred onto lobe Alfvén waves during substorms, the following estimate is proposed. The electric and magnetic field amplitudes of lobe Alfvén waves are on the order of 1 mV/m and 1 nT, which is much smaller than the amplitude of Alfvén waves occurring in the neighboring PSBL, at 100 mV/m and 20 nT, see Sect. 3. These smaller amplitudes also result in reduced Poynting fluxes. In general, the Alfvénic Poynting flux in the lobe is two to three orders of magnitude less intense than that in the PSBL, although during times of storms the Poynting flux in the lobe can increase by one order of magnitude. If one assumes a lobe thickness of 30 R_E, as compared to ∼1 R_E of the PSBL, and one assumes an entire lobe region threaded with Alfvén waves, the total wave energy traveling towards the ionosphere in the lobe is significantly less, by one to two orders of magnitude, than that in the PSBL. The estimate of ∼1 R_E thickness for the PSBL is an average thickness (Dandouras et al. 1986), and it is noted that the actual thickness of the Alfvén wave layer within the PSBL has not yet been determined.

5.3.2 Energy Loss

At distances less than 6 R_E, it was reported that lobe Alfvén waves showed standing wave signatures. This implies that at lower altitudes, in the ionosphere, Earthward traveling lobe Alfvén waves are reflected back so that most of the wave energy is not dissipated in the

ionosphere. Such a finding is a stark contrast to Alfvén waves in the PSBL, see Sect. 3. Traveling tailward, the lobe Alfvén waves eventually stream out of the magnetosphere along open field lines, as illustrated in Fig. 45, thus providing an energy loss mechanism for substorms. As estimated above, this loss is, however, at most 10% of the energy carried by substorm-associated PSBL waves. Furthermore, as the lobe Alfvén waves propagate towards and away from the Earth, lobe field lines reconnect in the tail during the substorm expansion phase—which has the effect of reducing the area through which lobe Alfvén waves can escape the magnetosphere. Therefore, some lobe Alfvén waves become trapped in the plasma sheet, which further reduces the total energy loss due to lobe Alfvén waves.

Two additional comments regarding this energy loss mechanism need to be made. First, the proposed scenario currently suffers from a discrepancy of observations at less than 6 R_E and greater than 6 R_E; strongly reflected wave power was observed closer to Earth, but not at distances farther away from Earth. However, so far only a small number of events have been reported, and this paradox needs to be solved before the energy loss mechanism can be accepted. Second, Pilipenko et al. (2005) proposed, on theoretical grounds, that Alfvén waves can be reflected on open lobe field lines in the distant tail, if the field lines have a pronounced curvature. Such a curvature may exist at the magnetopause. However, whether or not this effect is significant has not been observationally verified.

5.3.3 Energy Dissipation

Since most Alfvén wave energy appears to be reflected at the ionosphere back into the tail, lobe Alfvén waves appear to have very little effect on ionospheric and auroral activities. One reason for this reduced low-altitude impact is the fact that the lobe Alfvén waves have large perpendicular scales. Small perpendicular scales are required for the development of intense currents in Alfvén waves, which can be dissipated via parallel electron acceleration to power auroras. Such small scales can form at large density gradients via phase mixing (e.g., Allan and Wright 2000). However, such density gradients do not exist in the lobe; in fact, so far, there have been no observations of lobe Alfvén waves and magnetically conjugate auroral activity in the ionosphere.

Two effects that involve some wave dissipation were reported. First, it was confirmed that lobe Alfvén waves can cause ground pulsations, as proposed by previous studies (e.g., Uozumi et al., 2000, 2004). Second, it was demonstrated that lobe Alfvén waves can transversely accelerate ions in a "sloshing" fashion in the tail region, far away from the ionosphere. On the other hand, the proposed ponderomotive forcing of ionospheric ion outflow via standing lobe Alfvén waves has not been observationally confirmed.

6 Alfvén Waves in the Reconnection Region

The interaction of the solar wind and the Earth's magnetosphere creates so-called reconnection regions which occur in both the dayside and the nightside magnetosphere. Reconnection can occur at the boundary between open and closed field lines (e.g., the lobe-PSBL interface) and on closed field lines (e.g., the CPS). Because of their importance in magnetospheric physics, and indeed beyond, the reconnection region is separately reviewed here with regard to Alfvén wave observations. Semenov et al. (1992) and Vaivads et al. (2006) should be consulted for an in-depth look at the microphysical aspects of reconnection.

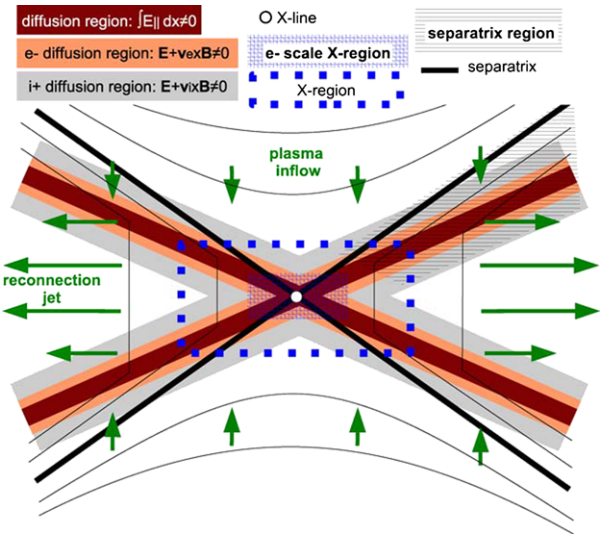

Fig. 46 (from Vaivads et al. 2006) Sketch of the main regions of reconnection

The reconnection region can be divided into an ion diffusion region and an electron diffusion region which are surrounded by inflow and outflow regions (Fig. 46). In the reconnection region the magnetic field topology is locally changed, but this change is mediated after some time to large parts of the entire magnetosphere. Reconnection is a transient process (e.g., Semenov et al. 1992, and references therein) which, at times, can last for several hours (e.g., Frey et al. 2003, who analyzed a dayside reconnection event). As such, it should be expected that Alfvén waves with a broad frequency range are launched from the reconnection region (e.g., Song and Lysak 1989; Song 1998). Recently, large-amplitude Alfvén waves have been recorded on PSBL field lines adjacent to the lobe-PSBL interface during times of substorm expansion, when the magnetotail undergoes large topological changes due to reconnection, see Sect. 3. Since the lobe-PSBL interface presumably maps either directly into the reconnection region or into its outflow region, this correlation is suggestive for the creation of Alfvén waves in the reconnection region. However, other generation scenarios have been proposed for PSBL Alfvén waves as well (e.g., Allan and Wright 2000). Furthermore, it has been argued that the field-aligned Hall currents resulting from reconnection, as shown in simulations (Yamade et al. 2000), and observed in the diffusion region (Vaivads et al. 2004), may be carried by Alfvén waves into the ionosphere (Yamade et al. 2000; and Fujimoto et al. 2001). However, so far there have been no reports of Alfvén waves inside the magnetotail reconnection region proper. Instead, one study recently reported Alfvén waves in the reconnection region in the dayside magnetopause (Chaston et al. 2005). Because of a lack of Alfvén wave observations in the nightside reconnection region, I review this study next, deviating from the general focus—the nightside magnetotail—of this review.

Chaston et al. (2005) determined wave properties inside the diffusion region of high-latitude lobe reconnection in the dayside magnetopause. The study took advantage of the multipoint measurement capability of Cluster. The left portion of Fig. 47 schematically shows the spacecraft trajectory through the magnetopause and the *X* line, followed by density, electric and magnetic field, and Poynting flux data. A comparison of the theoretical prediction of the dispersion relation of drift-kinetic Alfvén waves with observed values shows close agreement, as seen in the right side of Fig. 47, clearly indicating that fluctuations occur over many temporal and/or spatial scales. Furthermore, the Poynting flux panel

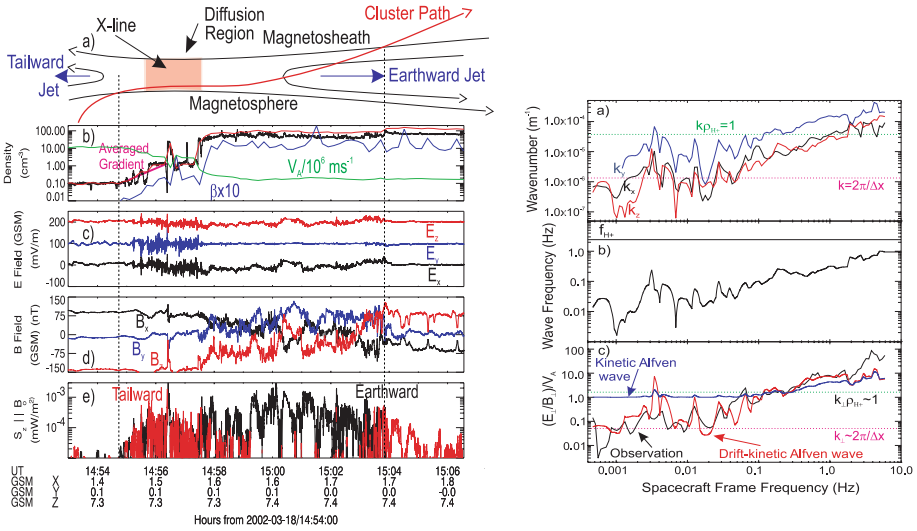

Fig. 47 (adapted from Chaston et al. 2005) (*Left*) (**a**) Schematic of *X* line crossing; (**b**) Plasma density from ion spectrometer (*red*), spacecraft potential (*black*), the local Alfvén speed (*green*) in m/s divided by 10^6, and plasma beta (*blue*) multiplied by 10 on the same scale; (**c**) Electric field in GSM coordinates with the assumption that $\mathbf{E} \cdot \mathbf{B}_0 = 0$ (y and z components have been shifted positive by 100 and 200 mV/m, respectively); (**d**) Magnetic field in GSM coordinates; (**e**) Field-aligned wave Poynting flux. (*Right*) Averaged results from 14:55–14:56:30 UT; (**a**) Wave vector from interferometry in field-aligned coordinates; (**b**) Theoretical wave frequency for the drift-kinetic wave; (**c**) Observed E to B ratio (*black*) in comparison with theoretical results for kinetic (*blue*) and drift-kinetic (*red*) Alfvén waves

shows that the waves radiated outward from the *X* line, suggesting that reconnection was the Alfvén wave source. Although these observations demonstrate that reconnection is a source of Alfvén waves, they have not yet explained the generation mechanism of these waves and their full impact on reconnection (Chaston et al. 2005).

An often identified signature of reconnection is an outflow of ion jets at the Alfvén speed which is, in the MHD picture, due to the magnetic tension in the reconnected field line. Essentially, in this scenario, it is an Alfvénic disturbance that accelerates the plasma up to the Alfvén speed in the perpendicular, to **B**, direction. In addition to this meso-scale Alfvén wave scenario, the observation by Chaston et al. (2005) demonstrates that Alfvén waves in the reconnection region are also present in the small-scale, kinetic regime covering a broad range of frequencies. Such waves have a parallel electric field which leads to the break-down of the ideal MHD regime, and that can provide anomalous resistivity. These observations support the theoretical view that kinetic Alfvén waves are one candidate, in addition to whistler waves, for mediating the reconnection process at small scales (e.g., Drake 1995; and Rogers et al. 2001). The parallel electric field might also provide a mechanism for field-aligned acceleration of particles inside the reconnection region, in addition to the perpendicular bulk flow.

In summary, reconnection is typically associated with energy conversion of magnetic field energy into kinetic energy in ion and electron streams. However, the recent Alfvén wave observations demonstrate that Alfvén waves at small scales are also an energy sink for reconnection. In addition, Alfvén waves may play an important role in reconnection dynamics by mediating the reconnection process at small scales. The full extent of their importance in all phases of reconnection (i.e., triggering, evolution, and dissipation) has

not yet been observationally demonstrated. Other outstanding questions are: How much of the Poynting flux associated with the magnetic flux, stored in the stretched magnetic field of the tail, converts into Alfvén waves during reconnection? How much converts into bulk kinetic energy of plasma flows? The recent observations clearly provide additional stimulus for investigations of the roles for Alfvén waves in the reconnection region.

7 Alfvénic Coupling with the Auroral Zone

The visible aurora which occurs inside the ionosphere is connected to remote regions in the magnetotail via magnetic field lines. The interaction between the collisional ionosphere and the collisionless magnetotail regions creates a complex transition region called the auroral zone. Inside the auroral zone, acceleration regions occur that are sites of a rich phenomenology of plasma processes, many of which are only partially understood. These acceleration regions play a key role in the acceleration of electrons via parallel electric fields, that precipitate into the ionosphere where they excite atoms and molecules leading to the aurora.

The auroral zone is also a region that is the focal point of many phenomena originating in the magnetotail. Guided by magnetic field lines, Alfvén waves launched in the magnetotail transport energy into the auroral zone, where they are dissipated through Joule heating in the ionosphere or through particle acceleration by collisionless wave-particle interactions above the ionosphere. Some of the Alfvén waves are not dissipated but are reflected back into the magnetotail. Waves coming from the outer magnetosphere encounter a vastly different environment at lower altitude, with gradients in density, pressure, parallel electric field, and magnetic field over a short distance in comparison to the Alfvén wave length. The ionosphere is also not homogenous vertically and horizontally, and can show strong variations in conductivity. This highly inhomogeneous environment creates complicated interactions between Alfvén waves and the plasma.

Observations of Alfvén waves from spacecraft and rocket flights are abundant in the auroral zone (e.g., Boehm et al. 1990; Dubinin et al. 1990; Knudsen et al. 1992; Louarn et al. 1994; Stasiewicz et al. 1997; Gary et al. 1998; and Wahlund et al. 1998). An excellent review describing some of these early observations and also providing the theory of dispersive Alfvén waves in this region was given by Stasiewicz et al. (2000). Since this review, many new auroral zone observations, in particular from FAST (e.g., Chaston et al., 2000, 2002, 2003; and Ergun et al. 2005) but also from Freja (e.g., Andersson et al. 2002), together with computer simulations necessary to overcome the analytical difficulties in describing this highly inhomogeneous and highly dynamic region, have conclusively established that Alfvén waves are accelerators of auroral electrons. In fact, electron acceleration leading to the aurora is now one of the most investigated effects of Alfvén waves in the auroral zone. Several scenarios have been proposed for Alfvénic acceleration mechanisms which are briefly reviewed by Chaston et al. (2006b).

It is emphasized that this section is not a comprehensive review of Alfvén wave observations in the auroral zone, nor is it a comprehensive review of magnetosphere–ionosphere (M-I) coupling. Both topics require their own review papers (e.g., Stasiewicz et al. 2000; and Lysak 1990, respectively) due to complexity. Another topic, not reviewed here, is the generation of Alfvén waves in the ionosphere, which is closely related to the topic of the ionospheric Alfvén resonator (e.g., Lysak 1988). The acceleration/heating of ions has been shown in connection with the ionospheric Alfvén resonator (e.g., Chaston et al. 2006a) and is also not reviewed here. Here, I will touch in a little more detail on the following three topics. First, it turns out that the interaction of Alfvén waves coming from the outer magnetosphere with the auroral zone modifies the structure and evolution of Alfvén waves in

the magnetotail, as well. This understanding has led to new interpretations for electric field structures that had previously been identified as pure electrostatic structures. Second, one of the main goals of space physics, and the origin of this field, was to explain the visible aurora. It is now established that Alfvén waves carry sufficient energy for auroral acceleration processes and contribute to the visible aurora. Since other energy carriers exist, an important question relates to the amount of energy contributed by Alfvén waves, or equivalently, how much of the aurora is Alfvénic? Another question that can be asked is, "Where in the auroral oval does the Alfvén wave-associated aurora occur?"

7.1 Electrostatic Versus Alfvénic Phenomenon

Since first observed by Mozer et al. (1977), a long debate has existed in auroral physics regarding the origin of large electric fields, perpendicular to the ambient magnetic field, on auroral field lines. The prevailing belief indicated that they are static structures that map equipotentially along magnetic field lines to higher altitudes. However, it had also been suggested, early on, that they may be associated with small-scale kinetic Alfvén waves (Goertz 1984). One of the early interests in these electric field structures was their association with auroral structures (e.g., Torbert and Mozer 1978; and Kletzing et al. 1983). Although there is now convincing observational evidence for the existence of both electrostatic and Alfvénic electric field structures, there is still a debate as to what extent either occurs and for which situations. Therefore, it is reasonable to ask, "What is the difference between a static electric field structure and a dynamic, Alfvénic structure?"

Lysak (1998) theoretically discussed this very topic. Expressions of the E/B ratio for an electrostatic model, a model of freely propagating Alfvén waves, and a model for which Alfvén waves reflect from the ionosphere were considered. As outlined in Sect. 1.4, the E/B ratio is an important indicator of Alfvén waves. In the electrostatic model an electric field along magnetic field lines was included, which introduced great variability into the ratio as a function of the perpendicular size of the electric structure. Thus, it is important to note that static structures do not necessarily show an E/B ratio of $1/(\mu_0 \Sigma_P)$ (Σ_P being the ionospheric Pedersen conductance). The scale size dependence on E/B is well known for purely traveling Alfvén waves if they are in the inertial or kinetic regime (Hasegawa 1976; and Goertz and Boswell 1979). Modified Alfvén wave dispersion relationships, accounting for the effects of small scales, increase the ratio of E/B from the Alfvénic ratio ($E/B = v_A$) up to ratios even exceeding the speed of light. In the third scenario, Alfvén waves were allowed to interfere with reflected waves. Lysak (1998) only considered wave reflection off the ionosphere but higher-altitude regions (e.g., an anomalous resistive layer) also contribute to reflected waves (Lysak and Dum 1983). This additional interaction significantly modifies the E/B ratio which then becomes a function of wave frequency, scale size, and altitude. Streltsov and Lotko (2003) showed that the reflection properties can also be a function of wave amplitude. For this combination, the ratio can take on nearly every value. Therefore, it turns out, that both electrostatic structures and Alfvén waves can take on the same ratio of E/B under certain conditions, depending on other parameters. It should be mentioned here, however, that because Σ_P is nearly always larger than Σ_A, values of E/B less than the Alfvén speed generally indicate at least some degree of connection to the ionosphere. In addition, the kinetic and inertial effects always increase the E/B ratios above the Alfvén speed. That being said, the standing wave structure of waves in FLR indicates that in any particular observation, the satellite could be at a node or antinode of the electric field structure, giving a ratio of zero or infinity. In addition, there is a parallel wavelength dependence of the E/B ratio. For example, if there is a FLR, say between 1–10 mHz, and

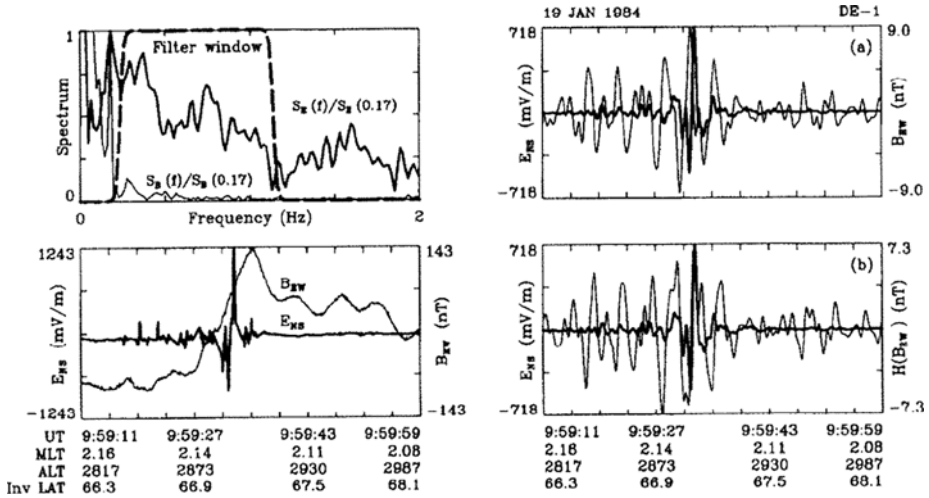

Fig. 48 (from Lotko and Streltsov 1997) Spectral analysis of satellite data: (*Lower left*) Electric (north–south) and magnetic (east–west) field from DE-1. (*Upper left*) Fourier spectra of E and B showing the bandpass filter. (*Upper right*) Bandpass-filtered E and B with peak values out of phase. (*Lower right*) Same as *upper right* with the Hilbert transform applied to B

a satellite at an altitude of $<$4000 km, it will record an ionospheric E/B, even though it is technically an Alfvén wave, since the wavelength is longer than the satellite-to-ionosphere separation. These theoretical/numerical considerations show that a simple interpretation of observed E/B ratios alone is not always sufficient for the identification of the nature of the field structure, and, in fact, might lead to misinterpretations (also see Aikio et al. 1996, who came to the same conclusion). As a result, additional information is sometimes required for an accurate interpretation and includes such things as perpendicular scale size, frequency, or observation altitude. Perpendicular scale sizes, however, are not easily obtainable with single spacecraft measurements, and in many cases are impossible to obtain. Similarly, wave frequencies can be modified by moving spacecraft and should be treated with caution.

An example of a small-scale, large-amplitude perpendicular electric field structure—sometimes interpreted as electrostatic field structures—that has been 'reinterpreted' in favor of an electromagnetic structure associated with FLR, is shown in Fig. 48. Both the electric and magnetic fields were recorded by DE-1 at low altitude, as seen in the lower left of Fig. 48. The bandpass-filtered time series are shown on the right side. The central peaks in E and B near 9:59:32 UT are not temporally coincident. The application of a Hilbert transform to the magnetic field, in the bottom right of Fig. 48, brings the central peaks into temporal coincidence while shifting the quasi-periodic oscillations to the left of the peak into phase quadrature. These features, together with impedance calculations, are consistent with the presence of a dispersive FLR at the location of DE-1 (Lotko and Streltsov 1997).

A second example of a seemingly electrostatic structure (i.e., a large perpendicular electric field, $E_\perp$, without any significant perturbation of $B_\perp$) that has been interpreted as an Alfvén wave was investigated in detail by three studies (Lotko et al. 1998; Streltsov and Lotko 1999; and Samson et al. 2003). Electromagnetic data from FAST at low altitude, see Sect. 7.3 for additional descriptions of this event, were compared with simulation results of a numerical model that describes shear Alfvén wave propagation including dispersion due to the finite ion gyroradius, electron inertia, and electron temperature (Fig. 49). The comparison indicates that the observations are well reproduced by the simulation. In particular,

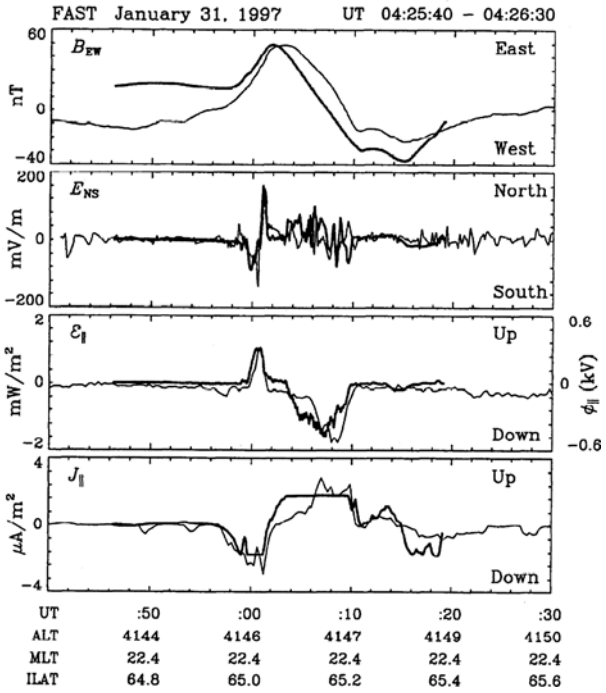

Fig. 49 (from Streltsov and Lotko 1999) FAST satellite data (*thin curves*) and simulation results (*thick curves*)

the simulation showed that the lack of $B_\perp$ was due to the wave reflection of a FLR at a micro-turbulent layer, produced by plasma anomalous resistivity, at low altitude.

Another reason for confusion in separating electrostatic and Alfvénic structures is a time-dependence aspect. For example, any static field-aligned current structure must have started out as a dynamic, Alfvénic, one and evolved into the static structure via an unknown sequence of processes. The idea is that a sudden dynamic change in convection or resistivity in some region of the magnetosphere launches an Alfvénic front (Goertz and Boswell 1979). The front propagates back and forth between the source and any potential boundary, like the ionosphere. Before steady state is achieved, this interaction changes the structure of Alfvén waves—sometimes to the point of disguising the Alfvénic nature of these fields. Eventually, a steady current will be set up, if one is generated at all. Any new change in the ionospheric conditions or the generator region will lead to additional Alfvén wave activity. The dynamics of this process were numerically modeled by Streltsov and Marklund (2006) and can be found in early works by Mallinckrodt and Carlson (1978) and Goertz and Boswell (1979), for example. Having the benefit of four spacecraft allows us to follow the temporal evolution of the electric field structure on auroral field lines. By using the multipoint-measurement capability of Cluster, Marklund et al. (2001) reported the spatial and temporal behavior of a large-amplitude, diverging bipolar electric field structure, located at roughly 4 R_E on auroral field lines, in the vicinity of the transition region of the PSBL and CPS, as seen in the left side of Fig. 50. The structure was monitored for approximately 200 seconds during which it grew in latitudinal width and magnitude, and was accompanied by a widening of the downward current sheet. Using a two-fluid MHD code, Streltsov and Marklund (2006) simulated the evolution of Alfvén waves, launched in the magnetotail, and associated field-aligned currents, and reproduced the observations of the evolution of electric field, as was observed with the four spacecraft of Cluster, as seen in Fig. 50 on the right. In the model,

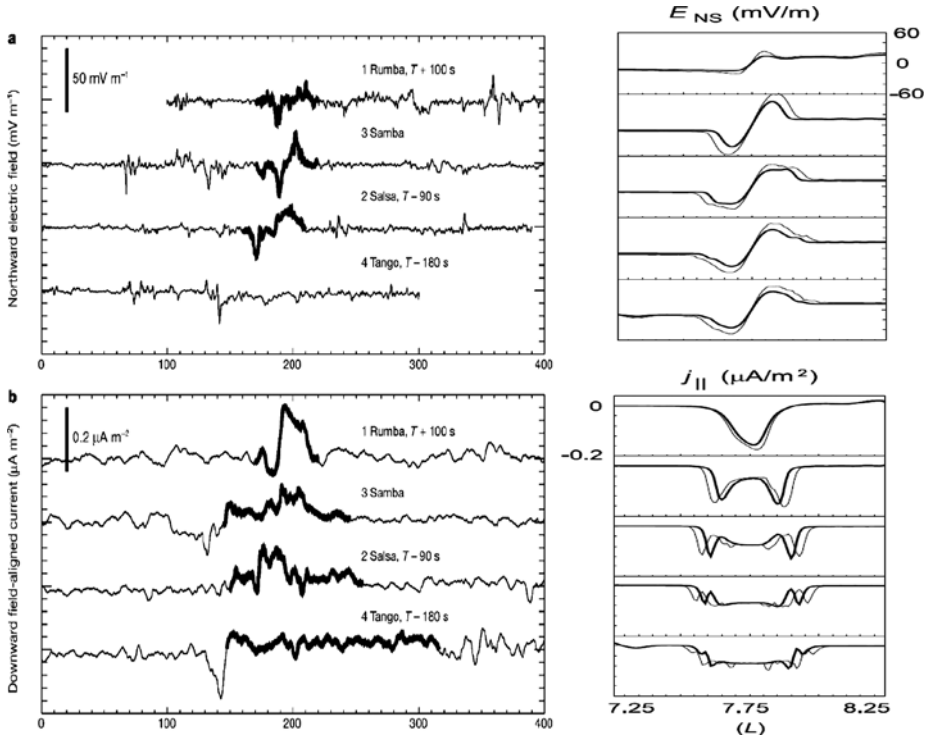

Fig. 50 (*Left*) (from Marklund et al. 2001) North–south electric field, E_{NS}, and parallel current density, $j_{\parallel}$, measured by four Cluster satellites above the nighttime auroral ionosphere on January 14, 2001, near 0430 UT. Positive current corresponds to the downward direction. (*Right*) (from Streltsov and Marklund 2006) Profiles of $j_{\parallel}$ and E_{NS} taken every 45 seconds from the simulation along the virtual satellite trajectory corresponding to the Cluster, January 14, 2001, event. Note that the sign of the current is reversed in comparison to the left figure, positive is upward

the high-altitude diverging electric field resulted from a coupling of Alfvén waves with the conductive ionosphere from where it mapped to Cluster's location. This example indicates strong magnetosphere–ionosphere coupling for an evolving Alfvén wave, and how this coupling affects the evolution and structure of Alfvén waves in the magnetotail. To represent here the opposing point of view, I refer the reader to other studies, like Karlsson et al. (2004) and Johansson et al. (2004), who used Cluster multipoint measurements to argue for the static character of field structures, similar to the event shown in Fig. 50.

Our lack of a complete understanding of the transition from an Alfvén wave to a quasi-static structure under strong M-I coupling results in some ambiguity. In spite of the occasional disagreement among scientists about the identification of Alfvén waves versus quasi-static structures, there are clear particle signatures that have been associated with both of them. Electron fluxes associated with quasi-static structures have a narrow energy range and a broad angular distribution, whereas Alfvén wave-accelerated electrons are field-aligned with a broader and lower energy range. These two electron signatures are associated with different time scales over which changes occur, and can lead to different phenomena. Examples of the co-existence of both electron populations on the same field lines can be found in, for example, Lynch et al. (1999) or Chaston et al. (2002).

Finally, double layers (Block 1972) are an example of the co-existence and causal relationship of electrostatic and Alfvénic structures. Double layers have been invoked as a mechanism to sustain parallel electric fields in both upward (e.g., Mozer and Kletzing 1998) and downward (e.g., Ergun et al. 1998; and Newman et al. 2001) current regions of the auroral zone. A role for Alfvén waves seems to appear for these "electrostatic" structures. It has been suggested by theory/simulations (e.g., Silberstein and Otani 1994; Mishin and Forster 1995; Genot et al. 2004; and Singh 2002) and observations (e.g., Chust et al. 1998; Ergun et al. 2005; and Chaston et al. 2007a) that the field-aligned currents carried by shear Alfvén waves may lead to the formation of some type of double layer on auroral field lines. Similarly, Vaivads et al. (2003) reported simultaneous signatures of both a quasi-static potential and an Alfvén wave in a conjugate study between Cluster located above the auroral acceleration region (at 4.7 R_E) and DMSP located below the auroral acceleration region (at 850 km). The authors proposed that the potential structure might have been part of the low-altitude end of the Alfvén wave.

7.2 Alfvénic Contribution to the Aurora

Observations from spacecraft have demonstrated that there are three main magnetospheric drivers for auroral particle acceleration: field-aligned currents; earthward plasma flow; and Alfvén waves (e.g., Schriver et al. 2003). In this section, I address the question of how much of the aurora is driven by Alfvén waves. To avoid any confusion, it should be stated that auroral arcs are not directly caused by Alfvén waves, but by a sequence of intermediate energy transfer processes from the Alfvén waves to the auroral light. These processes include the field-aligned acceleration of electrons by the parallel electric field in kinetic Alfvén waves, the excitation of ionospheric atoms and molecules, and the emission of photons which constitute the aurora. It is now common to call the parts of the aurora that are excited by electrons that have been accelerated by Alfvén waves, "Alfvén wave aurora" or "Alfvénic aurora", in contrast to the "inverted-V aurora". The simultaneous occurrence of Alfvén waves and field-aligned suprathermal electron bursts are ample in and below the auroral acceleration region (e.g., Knudsen et al. 1992; Boehm et al. 1995; Stasiewicz et al. 1997; Gary et al. 1998; Wahlund et al. 1998; Chaston et al. 2000; Andersson et al. 2002; and Ergun et al. 2005). Through test particle simulations, it has been verified that these suprathermal electrons are accelerated by Alfvén waves (e.g., Kletzing and Hu 2001; and Chaston et al. 2002).

In case studies, see Sect. 3, it has been established that Alfvénic Poynting flux from the outer magnetosphere is sufficient to power the magnetically connected aurora in the ionosphere, especially during active geomagnetic times. For example, Wygant et al. (2000) and Keiling et al. (2002) showed that high-altitude Alfvénic Poynting flux can be up to 10 times larger than the energy flux of conjugate ionospheric electron precipitation. Therefore, in some cases, only ten percent of the wave Poynting flux is needed for auroral particle acceleration. However, these are point measurements and thus only allow a direct comparison along one field line, that is, they do not say anything about the total Alfvén wave contribution over an extended region, let alone the entire oval. To give some answer to the question of how much of the aurora is driven by Alfvén waves, I next review studies that have investigated the Alfvénic contribution to larger regions of the auroral oval.

Keiling et al. (2003b) compared the global distribution of high-altitude electromagnetic energy flow with the kinetic energy associated with electron precipitation causing simultaneous auroral luminosity. The average auroral luminosity in the ionosphere, as seen on the right in Fig. 51, was estimated from 17,372 images of the aurora, taken by the UVI

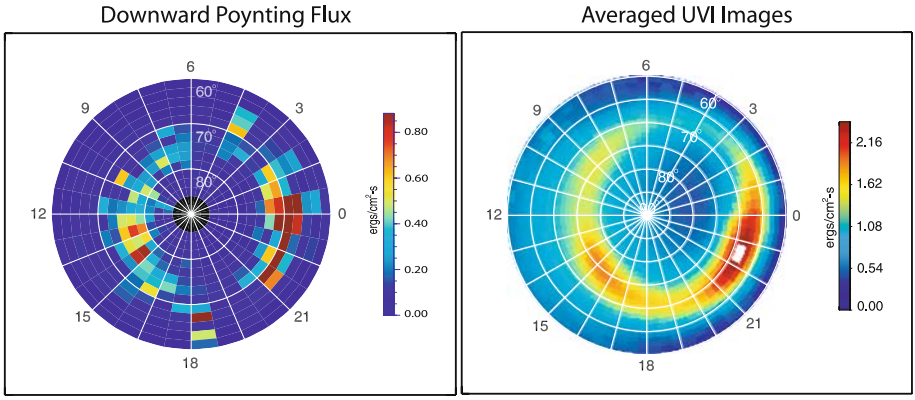

Fig. 51 (*Left*) (from Keiling et al. 2003b) Statistical pattern of the magnetic field-aligned Poynting flux flowing toward the ionosphere as measured at 4–7 R_E (Polar satellite) and mapped onto ionospheric altitude. (*Right*) (from Liou et al. 1997) Averaged auroral luminosity as measured from 17,372 UVI images (Polar satellite)

camera onboard Polar. The energy scale was converted to kinetic energy flux due to precipitating electrons (Torr et al. 1995). The high-altitude (4–7 R_E) wave Poynting flux was determined from one year of Polar electric and magnetic field data in the bandpass from 6 to 120 seconds. The field-aligned Poynting flux was mapped along converging magnetic field lines into the ionosphere at approximately 100 km altitude, so as to compare it with the precipitation energy associated with the auroral luminosity. The Poynting flux values were averaged inside bins of $2^\circ \times 0.75$ hours, as seen on the left in Fig. 51. For the purpose of this review, I restrict the comparison to the nightside. Both distributions have their most intense nightside region located at ~2100–0000 MLT. The aurora in this sector is largely associated with auroral substorms. On average, the *in situ* high-altitude Poynting flux could statistically account for roughly one third of the energy flux required to cause the auroral luminosity, if we keep in mind that the time periods for the comparisons were not the same, and that the statistical fluctuations on the Polar plot are much larger due to a much smaller data base (see Keiling et al. 2003b, for further explanations). Also, it is important to note that the Poynting flux from Polar showed very little reflective power (not shown) which implies that the large majority of the downward Poynting flux crossing the altitude range of Polar was indeed dissipated below the spacecraft (Keiling et al. 2003b). The comparison also shows that the majority, two thirds, of the aurora is caused by non-Alfvénic drivers. One such driver is clearly the inverted-V structure that is routinely observed by low-altitude satellites (e.g., McFadden et al. 1999).

Using the FAST satellite with a 300 to 4400 km altitude range, Chaston et al. (2007b) conducted a 2.3 year statistical study combining measurements of fields and particles. The left side of Fig. 52 shows the statistical distribution of the total electron energy deposition which is highest in the midnight sector. The fraction of this power, which was provided by electron fluxes with distributions consistent with an acceleration by Alfvén waves and which were observed coinciding with Alfvén waves, is shown in the right side of Fig. 52. Near pre-midnight, this fraction is ~50% on average, and, more generally, over the entire high-latitude region has a value of 31% (Chaston et al. 2007b). This result is similar to the estimate of the Polar study, discussed above (Keiling et al. 2003b). Therefore, both the FAST and the Polar study support the view that the Polar Alfvén waves provided the energy for the FAST electrons. Furthermore, Chaston et al. (2007b) differentiated the Alfvén wave

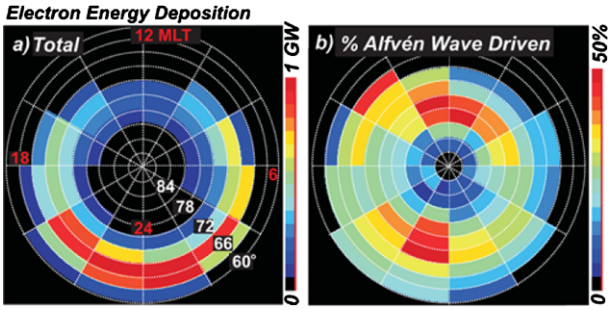

Fig. 52 (from Chaston et al. 2007b) Statistical distributions using FAST data in the altitude range from 300 to 4,400 km. (**a**) Average total electron energy deposition. (**b**) Percentage of the total electron energy flux associated with Alfvénic acceleration

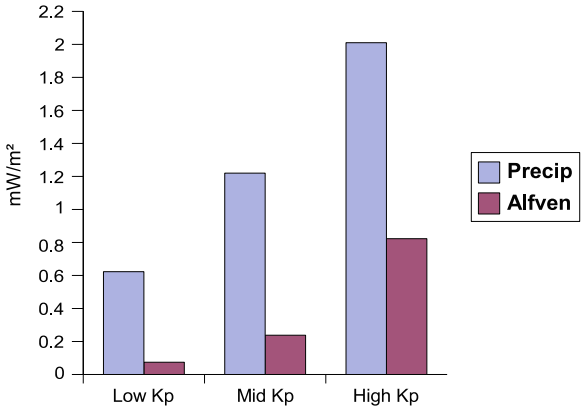

Fig. 53 (from Janhunen et al. 2006) Alfvénic versus total electron precipitation fractions for low, mid and high *Kp* ranges

contribution according to auroral activity and found that the power fraction increased from 25% to 39% as activity increased. It was concluded that, in the vicinity of the pre-midnight auroral oval, Alfvén waves may provide the dominant contribution for powering electron acceleration during active times. The study also showed that at FAST altitudes there is still Alfvén wave activity. In other words, not all Alfvén wave energy recorded above the auroral acceleration region is absorbed by the time the Alfvén waves reach the altitude of FAST. However, the remaining average Alfvén wave power at FAST is only around 10% of the energy flux of the electrons at FAST. Therefore, additional Alfvén wave acceleration below FAST would not significantly change the statistical results of this study.

Utilizing five years of Polar data in the 18–06 MLT sector, and at 65–74° invariant latitude (ILAT), which approximately corresponds to auroral field lines, Janhunen et al. (2006) compared the statistical results of the Poynting flux from Polar with the statistically known amount of total auroral electron precipitation (Hardy et al. 1987), and concluded that the Alfvén wave-induced electron acceleration represents ∼10% of all electron precipitation power during quiet conditions, and increases to ∼40% during disturbed conditions (Fig. 53). These values compare reasonably well with the estimates of Keiling et al. (2003b) and Chaston et al. (2007b).

In summary, the statistical results yield very comparable results. Alfvén waves significantly contribute to the aurora, possibly up to one third on average and possibly up to 50% in the pre-midnight region of the auroral oval. The Alfvénic contribution is dependent on geomagnetic activity with less contribution during quiet times. These results, together with results reviewed in previous sections, show that the substorm aurora is strongly affected by Alfvén waves. On the other hand, it is clear that quasi-static parallel electric fields do

their job of accelerating auroral electrons, as well, and that magnetotail ion beams are also considered drivers of auroral electrons.

It is also important to acknowledge that not all of the high-altitude Alfvénic Poynting flux is transmitted onto the kinetic energy of auroral electrons. For example, some of the wave energy will go into Joule heating, upwardly-accelerated electrons, and ion heating. Therefore, a different question relates to how much of the incoming Alfvénic Poynting flux can be converted into kinetic energy of electrons, both downward and upward moving electrons. This question can best be addressed from the theoretical and numerical side by investigating the efficiency of the energy conversion mechanism. The reader is referred to Chaston et al. (2002), Pilipenko et al. (2004), Lysak and Song (2005), Watt et al. (2005), and Song and Lysak (2006) for information regarding this question.

7.3 Location of Alfvénic Aurora

In previous sections, it has already been noted that only parts of the visible nightside aurora are caused by Alfvén waves. In this section I address the question of where inside the auroral oval the "Alfvénic aurora", see Sect. 7.2 for a definition, occurs. First, it should be noted that the auroral oval is not the only site of the aurora, i.e., some auroral structures lie outside the oval (see review by Frey 2007). Second, although all of the reviewed regions map along magnetic field lines into the ionosphere, only some of the Alfvén waves inside these regions lead to electron energization and visible aurora. Generally, it is assumed that the PSBL and the CPS map into the auroral oval, whereas the lobe and the plasmasphere map poleward and equatorward of the oval, respectively, and are not typically associated with aurora. I have already discussed examples of Alfvén waves in the PSBL and the CPS which lead to Alfvén wave-accelerated electron aurora. In this section, I show additional observations of Alfvén waves, measured in and below the auroral acceleration region, leading to auroras.

The auroral zone shows three characteristic acceleration regions which are dominated by upward field-aligned currents, downward field-aligned currents, or Alfvén waves. Figure 54 shows an example of an auroral zone crossing by the FAST satellite. The region next to the open-closed field line interface (green color in the first panel) is dominated by Alfvénic activity which causes the Alfvénic aurora. This region is magnetically connected to the PSBL where much Alfvénic activity, in particular during disturbed times, has been recorded as well, and this Alfvénic activity has been shown to cause the Alfvénic aurora (see Sect. 3.1). In addition, the electron signature, simultaneously recorded with the Alfvén waves, in and below the auroral acceleration region shows the characteristics of Alfvénic acceleration (e.g., Stasiewicz et al. 2000; and references therein).

Some auroral arcs at or near the equatorward edge of the auroral oval are associated with FLR (e.g., Samson et al. 1991a, 1991b, 1996, 2003; Xu et al. 1993; Trondsen et al. 1997; Rankin et al. 1999a, 1999b, 2000, 2005; Milan et al. 2001; and Wanliss and Rankin 2002). One example was given in Sect. 2.3. Another example is presented in Fig. 55 showing FAST electron and electric field data from a pass through a FLR. This FLR was detected on the ground in the magnetometer and optical data (bottom of Fig. 55). Numerical modeling of *in situ* field signatures confirmed the interpretation of the FLR, see Sect. 7.1 for additional details. Lotko et al. (1998) identified the time between 04:26:06–04:26:10 UT as the high-altitude extension of the auroral arc. This time period is characterized by field-aligned, suprathermal electrons extending to 1 keV, a characteristic for Alfvénic acceleration.

It has been shown that at substorm onset, Alfvén wave-accelerated electrons play a primary role in the auroral surge formation and the break-up aurora which is located deep

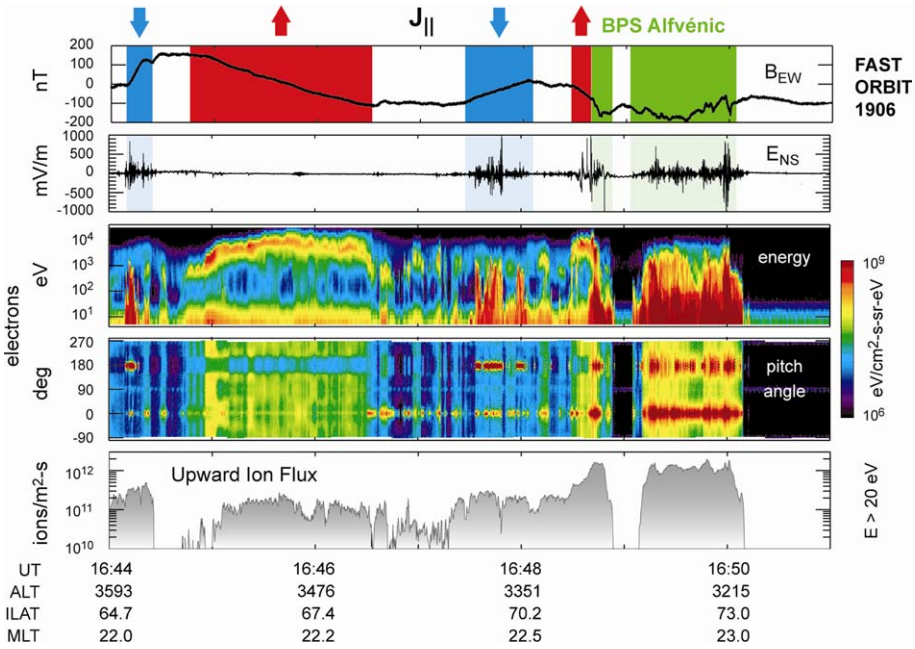

Fig. 54 (from Lotko 2007, adapted from Paschmann et al. 2003) FAST satellite pass on February 13, 1997 across the premidnight northern auroral zone, at an altitude of approximately 0.5 R_E, showing three characteristic acceleration regions: 1) the Alfvénic boundary plasma sheet just equatorward of the polar cap boundary; 2) the upward field-aligned current (inverted-V) region; and 3) the downward field-aligned current region

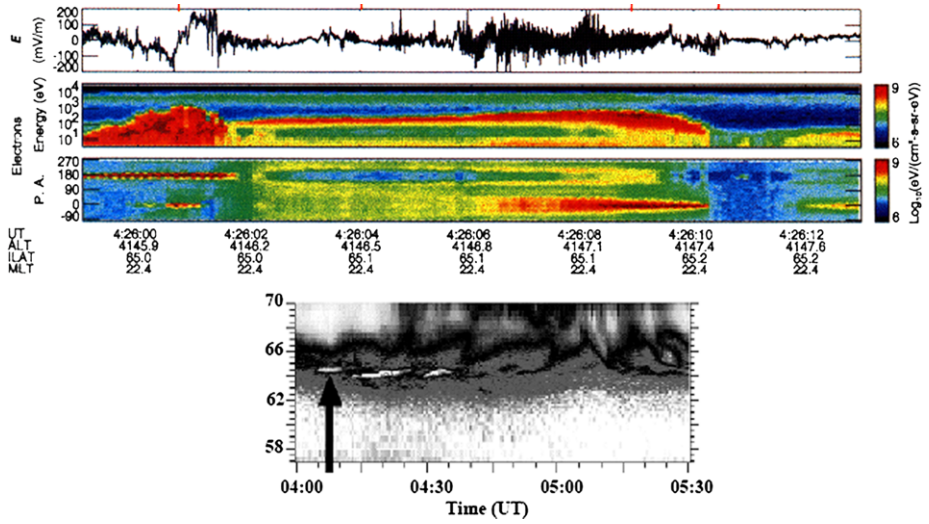

Fig. 55 (*Top*) (from Lotko and Streltsov, 1998) FAST electron and electric field data from a pass through a 1.3-mHz field line resonance (FLR) identified at Gillam. (*Bottom*) (from Samson et al. 2003) Optical emissions at 486.1 nm from the high resolution MPA data of Gillam showing a periodically reforming arc, see *black arrow*, which is conjugate to the FLR observed by FAST

in the region of closed field lines (Mende et al. 2003a). Simultaneous IMAGE FUV (far-ultraviolet) observations and *in situ* FAST observations of a substorm break-up arc, approximately one minute after substorm onset, showed that the most intense poleward surge aurora (dashed lines in Fig. 56) was produced by Alfvén wave-accelerated electrons. Magnetometer data from FAST was also indicative of the presence of Alfvén waves. Equatorward of the surge was a broader region of inverted-V electron precipitation, due to quasi-static electric fields. The numbers at the bottom of Fig. 56 indicate different boundaries. The satellite moved from higher latitude to lower latitude, crossing the open-closed boundary at '5', and later, while deeper inside the auroral oval, the poleward surge was crossed—in other words, the aurora was located well equatorward of the open-closed field line boundary. The study demonstrated that the leading edge of the auroral surge was energized by Alfvén waves rather than by quasi-static field-aligned currents and related electron inverted Vs (Mende et al. 2003a). During later phases of substorm development, the Alfvén wave-accelerated electrons and the corresponding auroral surge were seen closer to the polar cap boundary (also Mende et al. 2002, 2003b, for additional discussions).

In summary, the Alfvénic aurora occurs at the poleward boundary of the auroral oval, the equatorward boundary of the auroral oval, and deep within the auroral oval. It should be added here that Alfvénic fluctuations occur throughout the auroral zone, although they are most commonly found near the polar cap boundary (e.g., Chaston et al. 2003). It is, however, not confirmed for all cases that they produce aurora. Although not reviewed here, because they lack observational confirmation, it is worth noting that other auroral features have been proposed to be caused by Alfvén waves. For example, Liu et al. (2008) proposed that Alfvén waves generated by BBFs are the cause of auroral streamers.

8 Conclusions

The magnetotail is an extremely complex system, and Alfvén waves are essential to its dynamics. Since their predicted presence more than 60 years ago, it is not surprising that Alfvén waves have been observed in so many regions of the magnetosphere. After all, the magnetosphere is not a static system but undergoes periodic changes. Alfvén waves are a primary means to translate these changes to other regions of the magnetosphere. More surprising, perhaps, is the extent to which Alfvén waves participate in so many phenomena. Alfvén waves are associated with magnetospheric phenomena such as auroral arcs, ULF pulsations, reconnection, Alfvén and fast mode-coupling, various FLR, electron acceleration, ion heating, ion outflow, the ionospheric Alfvén resonator, substorm/storm dynamics, resistivity, turbulence, energy transport, the substorm current wedge, the auroral surge, M-I coupling, double layers, the generation of a parallel electric field, and more. These phenomena can be found in different regions of the magnetosphere, as outlined in this review with focus on Alfvén wave observations since 2000 in the CPS, PSBL, plasmasphere, tail lobes, reconnection region, and auroral zone. Key results for each region are listed below.

Central plasma sheet:

- Confirmation for two types of FLR with frequency ranges of 1–7 mHz and 10–40 mHz under different geomagnetic conditions; both types have been observed with a discrete frequency, and frequencies that vary with L value.
- Observation of Pc5 FLR in the CPS whose oscillations were correlated with modulations of auroral luminosity.
- Observation of discrete FLR with a frequency of ~20 mHz associated with substorm and ground Pi2.
- Confirmation that KHI activity at the flank is coupled to the ionosphere via Pc5 FLR.

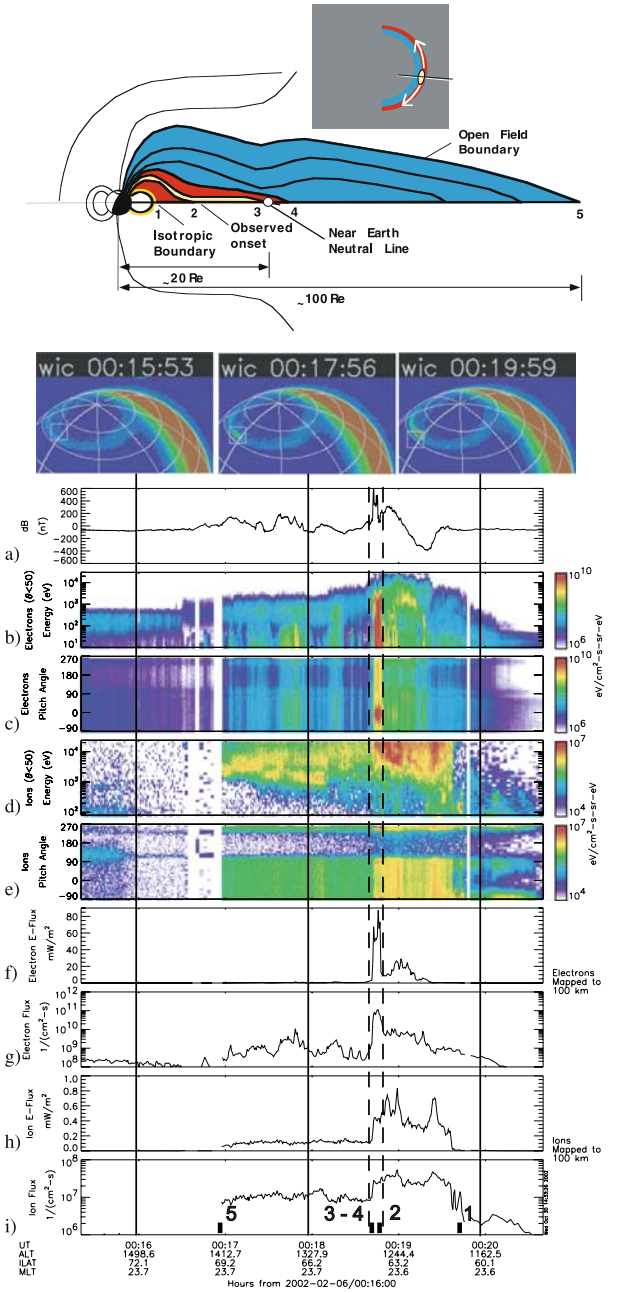

Fig. 56 (from Mende et al. 2003a) FAST crossing of the auroral region during a substorm. The break-up is seen in the space images (from IMAGE). Field and particle data show Alfvén wave-accelerated electrons away from the open-closed field line boundary associated with the break-up arc. The *top* shows a summary sketch of the proposed magnetospheric configuration during this event. The *numbers* refer to the same numbers as in the last panel

- Verification of Alfvén and fast mode coupling in the CPS.
- Observations of very intense Alfvénic Poynting fluxes deep inside the CPS during geomagnetic storms.
- Demonstration that compressional Pi1B pulsations in the tail are associated with Alfvénic Pi1B and electron acceleration in the auroral zone.

- Demonstration that the second amplitude maximum of ground Pi2 pulsations is, at least sometimes, caused by FLR.

Plasma sheet boundary layer:

- Identification of large-amplitude, energetic Alfvén waves in the PSBL, which demonstrates that the PSBL plays a role as a region that carries significant wave energy, in addition to quasi-static FAC energy and particle kinetic energy.
- Dependence of Alfvén wave activity on geomagnetic activity with large-amplitude energetic Alfvén waves occurring during the expansion phase of substorms.
- Evidence that PSBL Alfvén waves drive low-altitude acceleration processes yielding aurora near the poleward border of the auroral oval.
- Correlation of the intensity of Alfvénic Poynting flux in the PSBL and auroral luminosity, while the high-latitude Poynting flux is sufficient to power the magnetically conjugate auroral luminosity.
- Dissipation of Alfvén waves Poynting flux along auroral field lines from high-to low-altitudes while electrons gain energy flux.
- Evidence that kinetic Alfvén waves accelerate electrons above the auroral acceleration region, and possibly all along the PSBL; some evidence for a dissipation layer at 4–5 R_E.
- Identification of many temporal/spatial scales of Alfvén waves with a mixture of Earthward-traveling and reflected waves, depending on the temporal/spatial scale. Larger-scale and smaller-scale waves predominantly travel Earthward and bidirectionally, respectively. The downward component of the Poynting flux is much greater, one to two orders of magnitude, than that of the reflected component.
- Identification of a region with $\mathbf{E} \cdot \mathbf{J} < 0$ (generator region) at $\sim$18 R_E where kinetic energy is converted into Poynting flux.
- Correlation of ion beam energy and Alfvénic Poynting flux, suggesting a causal relationship.

Plasmasphere:

- Identification of traveling and standing (FLR) Alfvén waves in the plasmasphere.
- Association of Alfvén waves inside the plasmasphere with ground Pi2 pulsations.
- Demonstration that Alfvén waves play a role in the plasmasphere as an intermediate energy carrier in the transport of Pi2-related energy from the magnetotail to the ground.

Tail lobe:

- Identification of traveling and standing Alfvén waves with Poynting flux smaller by 2–3 orders of magnitude as compared to that in the neighboring PSBL.
- Alfvénic Poynting flux in the lobes is enhanced by one order of magnitude during storm periods.
- Demonstration that some lobe Alfvén wave activity is associated with substorms and can be used as a substorm indicator.
- Demonstration that lobe Alfvén waves can be recorded on the ground (polar cap) as ULF pulsations.
- Demonstration that lobe Alfvén waves modulate ion energies in the tail.
- Evidence of a loss mechanism of substorm energy via Alfvén waves in the tail lobes streaming along open field lines into the solar wind.

Reconnection region:

- Identification of Alfvén waves with many temporal/spatial scales in the diffusion region (dayside magnetopause).

- Demonstration that Alfvén waves are energy sinks for reconnection.

Alfvénic coupling to the auroral zone:

- Observations of the Alfvénic aurora at the poleward boundary of the auroral oval, the inner boundary of the auroral oval, and deep within the auroral oval.
- Observation that the auroral break-up arc is caused by Alfvén waves.
- Alfvénic contribution to the aurora, possibly up to one third on average and up to 50% in the pre-midnight region of the auroral oval, depending on geomagnetic activity.
- Demonstration of the effects of M-I coupling on the evolution and structure of Alfvén waves in the magnetotail.

There is a growing body of evidence that shows that Alfvén waves are far more abundant in the magnetotail than initially thought, and, at the same time, our knowledge of their roles in the magnetotail is ever increasing. Many roles have been identified, a testimony to the versatility of Alfvén waves. In addition to these specialized roles, Alfvén waves—as any wave—play three fundamental roles as discussed in the Sect. 1. I now finish this review by revisiting these three roles: energy transport, energy dissipation, and energy sink (absorption).

Energy Transport

Alfvén waves participate in many magnetospheric phenomena as an intermediate energy carrier. Therefore, they are *necessary* links in various chains of events, and one could perhaps say that the energy transport in these links is their main role in the magnetotail. With the largest number of spacecraft and extended ground station networks ever devoted to magnetospheric science, it has been possible, in some cases, to follow the energy flow from the magnetopause to the ionosphere, noting that Alfvén waves occur along the way. In particular, the new results have demonstrated the significance of Alfvénic energy transport from the tail towards the ionosphere in creating parts of the aurora. Although the optical aurora uses only a small part of the entire energy budget of the magnetotail, and that other energy carries, such as BBFs, contribute more to the energy transport in the tail than Alfvén waves, Alfvén waves are especially recognized for their versatility—i.e., their participation in a large range of phenomena occurring in many regions of the magnetosphere including both the nightside and the dayside (not reviewed here).

Energy Dissipation

Alfvén waves guided by the Earth's magnetic field are an important mechanism for the coupling of the magnetosphere and the ionosphere. Not only do they carry energy into the coupling region, but they also act as an energy dissipater via the acceleration of particles. The acceleration of electrons by Alfvén waves has long been suggested, and is now firmly established. Furthermore, evidence now suggests that Alfvén waves are one of the major contributors to electron acceleration that leads to the aurora. The heating of ionospheric ions has also been associated with Alfvén waves, and if further confirmed in the future, would provide an additional energy source for ions needed to populate the magnetosphere. Although not reviewed here, Alfvén wave dissipation may lead to the transport of solar wind particles into the magnetosphere via particle acceleration at the dayside magnetopause. Additionally, new evidence indicates that significant wave dissipation occurs in the PSBL via electron acceleration. These direct coupling scenarios add to our understanding of Alfvénic

energy dissipation, which in the past have mostly been associated with Joule heating in the ionosphere via larger-scale ULF Alfvén waves.

The dissipation of Alfvén waves can also create new structures, such as anomalous resistive layers and double layers. In turn, the interaction of Alfvén waves generated in the magnetotail with these structures and the ionosphere modifies the structure and evolution of Alfvén waves themselves. In this sense, magnetotail Alfvén waves can carry information about the low-altitude auroral zone and the ionosphere into the magnetotail.

A different form of dissipation is the loss of Alfvén waves along open lobe field lines into the solar wind. Lobe Alfvén waves occur enhanced during substorms and storms. In addition to those Alfvén waves that move tailward immediately after their generation and are lost to the solar wind, observations show that some Alfvén wave energy that is initially carried towards the ionosphere along the Earth's magnetic field is reflected back and possibly lost to the solar wind, as well. If further confirmed, this form of dissipation provides a new global energy loss mechanism which helps release excess energy.

Energy Sink

Solar wind energy is periodically deposited into the magnetosphere and needs to be released periodically, as well. Several energy sinks during periods of excess energy in the magnetotail have been identified such as Joule heating, the aurora, ring current energization, plasma sheet heating, and plasmoids. These energy partitions do not explicitly mention Alfvén waves, but we now know that Alfvén waves participate in most, if not all, of them as an intermediate energy sink and energy carrier. In addition, Alfvén waves on lobe field lines can provide a release mechanism of excess energy. Therefore, to fully understand the periodic behavior of the magnetotail, it is desirable to quantify the partition of energy in the various energy transfer processes. For example, it is known that Alfvén waves can, at times, dominate the energy partition near-Earth in the PSBL, but are only a small contributor in the entire mid-tail region. New results have confirmed that the reconnection region radiates Alfvén waves, and it is imperative to investigate in the future the energy balance for Alfvén waves and other energy carriers in this region. In spite of the many results reviewed here, we have only just begun to investigate the role of Alfvén waves as energy sinks for the various phenomena. Much work in the future is needed to quantify (i.e., determine the energy balance) all energy transfer processes that involve Alfvén waves. This future work is necessary for a complete understanding of many other phenomena in the magnetosphere. To succeed in this endeavor, we need to know where in the magnetosphere the excitation of Alfvén waves occurs, and what the mechanisms of excitation are. Since Alfvén waves occur along the entire auroral oval and in all magnetotail regions with vastly different properties, it is likely that Alfvén waves are excited in many different places by different mechanisms.

In conjunction with small-scale, broadband kinetic Alfvén waves, pronounced density gradients are observed, suggesting their role in the generation or formation of these waves. The importance of gradients is supported by theory which suggests that density gradients lead to a cascading of energy to smaller perpendicular wavelengths. On the other hand, sinusoidal, monochromatic Alfvén waves are observed in regions with no pronounced density gradients, and some have been shown to be created by mode coupling. Other generation mechanisms such as ion-driven instabilities await concrete observational confirmation. Although not reviewed here, it is worth noting that conductivity changes in the ionosphere can lead to the generation of Alfvén waves with the ability to carry energy into the auroral acceleration region from below, rather than from the outer magnetosphere. In spite of these results, wave generation is the least understood aspect of Alfvén waves, but is a prerequisite

for the abundant Alfvén wave activity in the magnetosphere. Hence, the search for observational evidence, supported by theory and numerical modeling, for the excitation mechanisms of Alfvén waves should be given high priority in the future.

Acknowledgement This work was supported by NASA grant NNG05GL27G-06/08. The author thanks Mark Engebretson for a critical reading of the manuscript.

References

M.H. Acuna et al., Standing Alfvén wave current system at Io—Voyager 1 observations. J. Geophys. Res. **86**, 8513–8521 (1981)

A.T. Aikio et al., On the origin of the high-altitude electric field fluctuations in the auroral zone. J. Geophys. Res. **101**, 27,157–27,170 (1996)

H. Alfvén, Existence of electrodynamic-hydrodynamic waves. Nature **150**, 405–406 (1942)

W. Allan, Plasma energization by the ponderomotive force of magnetospheric standing Alfvén waves. J. Geophys. Res. **98**, 11383 (1993)

W. Allan, A.N. Wright, Magnetotail waveguide: Fast and Alfvén waves in the plasma sheet boundary layer and lobe. J. Geophys. Res. **105**, 317 (2000)

L. Andersson, R.E. Ergun, D. Newman, J.P. McFadden, C.W. Carlson, Y.-J. Su, Phys. Plasmas **9**, 3600 (2002)

V. Angelopoulos, J.A. Chapman, F.S. Mozer, J.D. Scudder, C.T. Russell, K. Tsuruda, T. Mukai, T.J. Hughes, K. Yumoto, Plasma sheet electromagnetic power generation and its dissipation along auroral field lines. J. Geophys. Res. **107**(A8), 1181 (2002). doi:10.1029/2001JA900136

T.M. Bauer, W. Baumjohann, R.A. Treumann, Neutral sheet oscillations at substorm onset. J. Geophys. Res. **100**, 23,737 (1995)

W. Baumjohann, K.-H. Glassmeier, The transient response mechanism and Pi2 pulsations at substorm onset: Review and outlook. Planet. Space Sci. **32**, 1361–1370 (1984)

S.H. Bekhor, The computation of field-line resonance frequencies in general geometries: a tool for improving the understanding of magnetospheric configurations. J. Plasma Phys. **72**, 1–19 (2006). doi:10.1017/S0022377805004150

L.P. Block, Potential double layers in the ionosphere. Cosmic Electrodyn. **3**, 349–376 (1972)

J. Bloxham, S. Zatman, M. Dumberry, The origin of geomagnetic jerks. Nature **420**, 65–68 (2002)

M.H. Boehm et al., High-resolution rocket observations of large-amplitude Alfvén waves. J. Geophys. Res. **95**, 12,157–12,171 (1990)

M.H. Boehm et al., Observations of an upward-directed electron beam with the perpendicular temperature of the cold ionosphere. Geophys. Res. Lett. **22**(16), 2103–2106 (1995)

J.E. Borovsky, Auroral arc thicknesses as predicted by various theories. J. Geophys. Res. **98**, 6101–6138 (1993)

L.J. Cahill et al., Electric and magnetic observations of the structure of standing waves in the magnetosphere. J. Geophys. Res. **91**, 8895–8907 (1986)

C.A. Cattell, M. Kim, R.P. Lin, F.S. Mozer, Observations of large electric fields near the plasma sheet boundary by ISEE-1. Geophys. Res. Lett. **9**, 539–542 (1982)

C.A. Cattell, F.S. Mozer, K. Tsuruda, H. Hayakawa, M. Nakamura, T. Okada, S. Kokubun, T. Yamamoto, Geotail observations of spiky electric fields and low-frequency waves in the plasma sheet and plasma sheet boundary. Geophys. Res. Lett. **21**, 2987–2990 (1994)

C.R. Chappell, Recent satellite measurements of the morphology and dynamics of the plasmasphere. Rev. Geophys. **10**, 951–979 (1972)

C.C. Chaston, C.W. Carlson, R.E. Ergun, J.P. McFadden, Alfvén waves, density cavities and electron acceleration observed from the FAST spacecraft. Phys. Scr. T **84**, 64 (2000)

C.C. Chaston, J.W. Bonnell, L.M. Peticolas, C.W. Carlson, R.E. Ergun, J.P. McFadden, Driven Alfvén waves and electron acceleration: A FAST case study. Geophys. Res. Lett. (2002). doi:10.1029/2001GL013842

C.C. Chaston, J.W. Bonnell, C.W. Carlson, J.P. McFadden, R.E. Ergun, R.J. Strangeway, Properties of small-scale Alfvén waves and accelerated electrons from FAST. J. Geophys. Res. **108**(A4), 8003 (2003). doi:10.1029/2002JA009420

C.C. Chaston, T.D. Phan, J.W. Bonnell, F.S. Mozer, M. Acuña, M.L. Goldstein, A. Balogh, M. Andre, H. Reme, A. Fazakerley, Drift-kinetic Alfvén waves observed near a reconnection X line in the Earth's magnetopause. Phys. Rev. Lett. (2005). doi:10.1103/PhysRevLett.95.065002

C.C. Chaston et al., Ionospheric erosion by Alfvén waves. J. Geophys. Res. (2006a). doi:10.1029/2005JA011367

C.C. Chaston et al., ULF Waves and Auroral Electrons, Magnetospheric ULF Waves: Synthesis and New Directions, in *Geophysical Monograph Series*, vol. 169, ed. by K. Takahashi, P.J. Chi, R.E. Denton, R.L. Lysak (American Geophysical Union, Washington, 2006b), p. 239

C.C. Chaston et al., Large parallel electric fields, currents, and density cavities in dispersive Alfvén waves above the aurora. J. Geophys. Res. (2007a). doi:10.1029/2006JA012007

C.C. Chaston et al., How important are dispersive Alfvén waves for auroral particle acceleration? Geophys. Res. Lett. (2007b). doi:10.1029/2006GL029144

L. Chen, A. Hasegawa, A theory of long-period magnetic pulsations: 1. Steady state excitation of field line resonance. J. Geophys. Res. **79**, 1033 (1974)

S.H. Chen, M.G. Kivelson, On ultralow frequency waves in the lobes of the Earth's magnetotail. J. Geophys. Res. **96**, 15,711–15,723 (1991)

T. Chust, P. Louarn, M. Volwerk, H. de Feraudy, A. Roux, J.-E. Wahlund, B. Holback, Electric fields with a large parallel component observed by Freja spacecraft: Artifacts or real signals? J. Geophys. Res. **103**, 215 (1998)

A.B. Collier et al., Evidence of standing waves during a Pi2 pulsation event observed on cluster. Ann. Geophys. **24**, 2719–2733 (2006)

J. Dandouras et al., A statistical study of plasma sheet dynamics using ISEE 1 and 2 energetic particle flux data. J. Geophys. Res. **91**, 6861–6870 (1986)

J. Dombeck et al., Intense Alfvén waves with compressional mode waves well within the plasma sheet during the main phase of the 21 October 1999 Major Storm and comparison of Major Storm to Non-Storm Substorm PSBL Alfvén wave events, American Geophysical Union, Fall Meeting 2005, abstract #SA13B-05, 2005

J. Dombeck, C. Cattell, J.R. Wygant, A. Keiling, J. Scudder, Alfvén waves and Poynting flux observed simultaneously by Polar and FAST in the plasma sheet boundary layer. J. Geophys. Res. **110**, A12S90 (2005). doi:10.1029/2005JA011269

J.F. Drake, Magnetic reconnection: A kinetic treatment, in *Physics of the Magnetopause. Geophysical Monograph*, vol. 90, 1995

E.M. Dubinin, P.L. Israelevich, N.S. Nikolaeva, Auroral electromagnetic disturbances at an altitude of 900 km: The relationship between the electric and magnetic field variations. Planet. Space. Sci. **38**, 97 (1990)

J.W. Dungey, Electrodynamics of the outer atmosphere, in *Proceedings of the Ionosphere* (Phys. Soc. of London, London, 1955), p. 255

M. Engebretson et al., in *Magnetospheric ULF Waves: Synthesis and New Directions*, ed. by K. Takahashi, P.J. Chi, R.E. Denton, R.L. Lysak. Geophysical Monograph Series, vol. 169 (American Geophysical Union, USA, 2006), pp. 137–156

R.E. Ergun, C.W. Carlson, J.P. McFadden, F.S. Mozer, L. Muschietti, I. Roth, Phys. Rev. Lett. **81**, 826 (1998)

R.E. Ergun, L. Andersson, Y.-J. Su, D.L. Newman, M.V. Goldman, W. Lotko, C.C. Chaston, C.W. Carlson, Localized parallel electric fields associated with inertial Alfvén waves. Phys. Plasmas **12**, 072901 (2005)

G.M. Erickson et al., Electromagnetics of substorm onsets in the near-geosynchronous plasma sheet. J. Geophys. Res. **105**, 25265–25290 (2000)

D.H. Fairfield, T. Mukai, M. Brittnacher, G.D. Reeves, S. Kokubun, G.K. Parks, T. Nagai, H. Matsumoto, K. Hashimoto, D.A. Gurnett, T. Yamamoto, Earthward flow bursts in the inner magnetotail and their relation to auroral brightenings, AKR intensifications, geosynchronous particle injections and magnetic activity. J. Geophys. Res. **104**, 355–370 (1999)

C.-G. Fälthammar, Plasma physics from laboratory to cosmos—the life and achievements of Hannes Alfvén. IEEE Trans. Plasma Phys. **25**(3) (1997)

H.U. Frey, T.D. Phan, S.A. Fuselier, S.B. Mende, Continuous magnetic reconnection at Earth's magnetopause. Nature **426**, 533 (2003)

H.U. Frey, Localized aurora beyond the auroral oval. Rev. Geophys. (2007). doi:10.1029/2005RG000174

M. Fujimoto, T. Nagai, N. Yokokawa, Y. Yamade, T. Mukai, Y. Saito, S. Kokubun, Tailward electrons at the lobe-plasma sheet interface detected upon polarizations. J. Geophys. Res. **106**, 21,255 (2001)

H. Fukunishi, Polarization changes of geomagnetic Pi 2 pulsations associated with the plasmapause. J. Geophys. Res. **80**, 98–110 (1975)

J.B. Gary et al., Identification of auroral oval boundaries from in situ magnetic field measurements. J. Geophys. Res. **103**, 4187 (1998)

W. Gekelman, Review of laboratory experiments on Alfvén waves and their relationship to space observations. J. Geophys. Res. **104**, 14,417–14,435 (1999)

V. Genot et al., Alfvén wave interaction with inhomogeneous plasmas: acceleration and energy cascade towards small-scales. Ann. Geophys. **22**(6), 2081–2096 (2004)

K.-H. Glassmeier, C. Carsten, R. Cramm et al., Magnetospheric field line resonances: A comparative planetology approach. Surv. Geophys. **20**, 61–109 (1999)
C.K. Goertz, Kinetic Alfvén waves on auroral field lines. Planet. Space Sci. **32**, 1387–1392 (1984)
C.K. Goertz, R.W. Boswell, Magnetosphere-ionosphere coupling. J. Geophys. Res. **84**, 7239–7246 (1979),
D.A. Gurnett et al., Correlated low-frequency electric and magnetic noise along the auroral field lines. J. Geophys. Res. **89**, 8971–8985 (1984)
M. Hamrin, O. Marghitu, K. Rönnmark et al., Observations of concentrated generator regions in the nightside magnetosphere by Cluster/Fast conjunctions. Ann. Geophys. **24**, 637–649 (2006)
A. Hardy, M.S. Gussenhoven, R. Raistrick, W.J. McNeil, J. Geophys. Res. **92**, 12275 (1987)
A. Hasegawa, Particle acceleration by MHD surface wave and formation of aurora. J. Geophys. Res. **811**, 5083–5090 (1976)
D. Hayward, J.W. Dungey, An Alfvén wave approach to auroral field-aligned currents. Planet. Space Sci. **31**, 579 (1983)
W.J. Hughes, The effect of the ionosphere on long period magnetospheric micropulsations. Planet. Space Sci. **22**, 1167 (1974)
W.J. Hughes, R.J.L. Grard, A second harmonic geomagnetic field line resonance at the inner edge of the plasma sheet: GEOS 1, ISEE 1, and ISEE 2 observations. J. Geophys. Res. **89**, 2755–2764 (1984)
P. Janhunen, A. Olsson, J. Hanasz, C.T. Russell, H. Laakso, J.C. Samson, Different Alfvén wave acceleration processes of electrons in substorms at 4–5 R_E and 2–3 R_E radial distance. Ann. Geophys. **22**, 2213–2227 (2004)
P. Janhunen et al., Statistics of a parallel Poynting vector in the auroral zone as a function of altitude using Polar EFI and MFE data and Astrid-2 EMMA data. Ann. Geophys. **23**, 1797–1806 (2005)
P. Janhunen et al., Alfvénic electron acceleration in aurora occurs in global Alfvén resonosphere region. Space Sci. Rev. **122**, 89–95 (2006). doi:10.1007/s11214-006-7017-5
T. Johansson et al., Intense high-altitude auroral electric fields—temporal and spatial characteristics. Ann. Geophys. **22**, 2485–2495 (2004)
T. Karlsson et al., Separating spatial and temporal variations in auroral electric and magnetic fields by Cluster multipoint measurements. Ann. Geophys. **22**, 2463–2472 (2004)
A. Keiling, J.R. Wygant, C. Cattell, M. Temerin, F.S. Mozer, C.A. Kletzing, J. Scudder, C.T. Russell, W. Lotko, A.V. Streltsov, Large Alfvén wave power in the plasma sheet boundary layer during the expansion phase of substorms. Geophys. Res. Lett. **27**, 3169 (2000)
A. Keiling et al., Properties of large electric fields in the plasma sheet at 4–7 R_E measured with Polar. J. Geophys. Res. **106**, 5779 (2001a)
A. Keiling, J.R. Wygant, C. Cattell, K.-H. Kim, C.T. Russell, D.K. Milling, M. Temerin, F.S. Mozer, C.A. Kletzing, Pi2 pulsations observed with the Polar satellite and ground stations: Coupling of trapped and propagating fast mode waves to a midlatitude field line resonance. J. Geophys. Res. **106**, 25,891 (2001b)
A. Keiling, J.R. Wygant, C. Cattell, W. Peria, G. Parks, M. Temerin, F.S. Mozer, C.A. Kletzing, Correlation of Alfvén wave poynting flux in the plasma sheet at 4–7 R_E with ionospheric electron energy flux. J. Geophys. Res. **107**(A7), 1132 (2002). doi:10.1029/2001JA900140
A. Keiling, K.-H. Kim, J.R. Wygant, C. Cattell, C.T. Russell, C.A. Kletzing, Electrodynamics of a substorm-related field line resonance observed by the Polar satellite in comparison with ground Pi2 pulsations. J. Geophys. Res. **108**(A7), 1275 (2003a). doi:10.1029/2002JA009340
A. Keiling et al., Global morphology of wave Poynting flux: Powering the aurora. Science **299**, 383 (2003b). doi:10.1126/science.1080073
A. Keiling, G.K. Parks, J.R. Wygant, J. Dombeck, F.S. Mozer, C.T. Russell, A.V. Streltsov, W. Lotko, Some properties of Alfvén waves: Observations in the tail lobes and the plasma sheet boundary layer. J. Geophys. Res. **110**, A10S11 (2005). doi:10.1029/2004JA010907
A. Keiling, G.K. Parks, H. Reme, I. Dandouras, M. Wilber, L. Kistler, C. Owen, A.N. Fazakerley, E. Lucek, M. Maksimovic, N. Cornilleau-Wehrlin, Energy-dispersed ions in the plasma sheet boundary layer and associated phenomena: Ion heating, electron acceleration, Alfvén waves, broadband waves, perpendicular electric field spikes, and auroral emissions. Ann. Geophys. **24**, 2685–2707 (2006)
M.C. Kelley, D.J. Knudsen, J.F. Vickrey, Poynting flux measurements on a satellite: A diagnostic tool for space research. J. Geophys. Res. **96**, 201–207 (1991)
L. Kepko, M.G. Kivelson, K. Yumoto, Flow bursts, braking, and Pi2 pulsations. J. Geophys. Res. **106**, 1903–1916 (2001)
L. Kepko et al., ULF waves in the solar wind as direct drivers of magnetospheric pulsations. Geophys. Res. Lett. **29**, 1197 (2002). doi:10.1029/2001GL014405
K.-H. Kim, K. Takahashi, D.-H. Lee, N. Lin, C.A. Cattell, A comparison of Pi2 pulsations in the inner magnetosphere and magnetic pulsations at geosynchronous orbit. J. Geophys. Res. **106**, 18,865 (2001)

M.G. Kivelson, D.J. Southwood, Coupling of global magnetospheric MHD eigenmodes to field line resonances. J. Geophys. Res. **91**, 4345–4351 (1986)
C.A. Kletzing, S. Hu, Alfvén wave generated electron time dispersion. Geophys. Res. Lett. **28**, 693–696 (2001)
C.A. Kletzing, C. Cattell, F.S. Mozer, S.-I. Akasofu, K. Makita, Evidence for electrostatic shocks as the source of discrete auroral arcs. J. Geophys. Res. **88**, 4105–4113 (1983)
C.A. Kletzing et al., The electrical and precipitation characteristics of morning sector Sun-aligned auroral arcs. J. Geophys. Res. **101**, 17,175–17,189 (1996)
C.A. Kletzing, S. Hu, Alfvén wave generated electron time dispersion. Geophys. Res. Lett. **28**, 693–696 (2001)
D.J. Knudsen et al., Alfvén waves in the auroral ionosphere—A numerical model compared with measurements. J. Geophys. Res. **97**, 77–90 (1992)
H. Laakso, D.H. Fairfield, C.T. Russell et al., Field-line resonances triggered by a northward IMF turning. Geophys. Res. Lett. **25**, 2991–2994 (1998)
L.J. Lanzerotti et al., Storm time Pc 5 magnetic pulsation at the equator in the magnetosphere and its latitude dependence as measured on the ground. J. Geophys. Res. **79**(16), 2420–2426 (1974)
M.R. Lessard et al., Simultaneous satellite and ground-based observations of a discretely driven field line resonance. J. Geophys. Res. **104**, 12361–12371 (1999)
M.R. Lessard, E.J. Lund, S.L. Jones, R.L. Arnoldy, J.L. Posch, M.J. Engebretson, K. Hayashi, Nature of Pi1B pulsations as inferred from ground and satellite observations. Geophys. Res. Lett. **33**, L14108 (2006). doi:10.1029/2006GL026411
S. Levin, K. Whitley, F.S. Mozer, A statistical study of large electric field events in the Earth's magnetotail. J. Geophys. Res. **88**, 7765–7768 (1983)
K. Liou et al., Synoptic auroral distribution: A survey using Polar ultraviolet imagery. J. Geophys. Res. **102**, 27197–27206 (1997)
W.W. Liu et al., Theory and observation of auroral substorms: A magnetohydrodynamic approach. J. Geophys. Res. **100**, 79 (1995)
W.W. Liu et al., Observation of isolated high-speed auroral streamers and their interpretation as optical signatures of Alfvén waves generated by bursty bulk flows. Geophys. Res. Lett. **35**, L04104 (2008). doi:10.1029/2007GL032722
W. Lotko, A.V. Streltsov, Magnetospheric resonance, auroral structure and multipoint measurements. Adv. Space Res. **20**(4/5), 1067–1073 (1997)
W. Lotko, A.V. Streltsov, C.W. Carlson, Discrete auroral arc, electrostatic shock and suprathermal electrons powered by dispersive, anomalously resistive field line resonances. Geophys. Res. Lett. **25**, 4449–4452 (1998)
W. Lotko, The magnetosphere–ionosphere system from the perspective of plasma circulation: A tutorial, J. Atmos. Sol.-Terr. Phys. special issue on "Global Aspects of Magnetosphere-Ionosphere Coupling" (2007)
P. Louarn, J.-E. Wahlund, T. Chust, H. de Feraudy, A. Roux, B. Holback, P.O. Dovner, A.I. Eriksson, G. Holmgren, Observations of kinetic Alfvén waves by the Freja satellite. Geophys. Res. Lett. **21**, 195–205 (1994)
A.T.Y. Lui, C.Z. Cheng, Resonance frequency of stretched magnetic field lines based on a self-consistent equilibrium magnetosphere model. J. Geophys. Res. **106**, 25 793–25 802 (2001)
K.A. Lynch et al., Multiple-point electron measurements in a nightside auroral arc: Auroral turbulence II particle observations. Geophys. Res. Let. **26**, 3361–3364 (1999)
R.L. Lysak, Theory of auroral zone PiB pulsation spectra. J. Geophys. Res. **93**, 5942–5946 (1988)
R.L. Lysak, Electrodynamic coupling of the magnetosphere and ionosphere. Space Sci. Rev. **52**, 33–87 (1990)
R.L. Lysak, The relationship between electrostatic shocks and kinetic Alfvén waves. Geophys. Res. Lett. **25**(12), 2089–2092 (1998)
R.L. Lysak, C.T. Dum, Dynamics of magnetosphereionosphere coupling including turbulent transport. J. Geophys. Res. **88**, 365 (1983)
R.L. Lysak, W. Lotko, On the dispersion relation for shear Alfvén waves. J. Geophys. Res. **101**, 5085 (1996)
R.L. Lysak, Y. Song, Nonlocal interactions between electrons and Alfvén waves on auroral field lines. J. Geophys. Res. **110**, A10S206 (2005). doi:10.1029/2004JA010803
A.J. Mallinckrodt, C.W. Carlson, Relations between transverse electric field sand field-aligned currents. J. Geophys. Res. **83**, 1426–1432 (1978)
I.R. Mann, I. Voronkov, M. Dunlop et al., Coordinated ground-based and Cluster observations of large amplitude global magnetospheric oscillations during a fast solar wind interval. Ann. Geophys. **20**, 405–426 (2002)

O. Marghitu et al., Experimental investigation of auroral generator regions with conjugate Cluster and FAST data. Ann. Geophys. **24**, 619–635 (2006)
G.T. Marklund et al., Temporal evolution of the electric field accelerating electrons away from the auroral ionosphere. Nature **414**, 724 (2001)
N.C. Maynard, W.J. Burke, E.M. Basinska, G.M. Erickson, W.J. Hughes, H.J. Singer, A.G. Yahnin, D.A. Hardy, F.S. Mozer, Dynamics of the inner magnetosphere near times of substorm onset. J. Geophys. Res. **101**, 7705–7736 (1996)
J.P. McFadden, C.W. Carlson, R.E. Ergun, Microstructure of the auroral acceleration region as observed by FAST. J. Geophys. Res. **104**, 1445–14480 (1999)
D.B. Melrose, Energy propagation into a flare kernel during a solar flare. Astrophys. J. **387**, 403–413 (1992)
S.B. Mende et al., IMAGE and FAST observations of substorm recovery phase aurora. Geophys. Res. Lett. (2002). doi:10.1029/2001GL013027
S.B. Mende, C.W. Carlson, H.U. Frey, L.M. Peticolas, N. Østgaard, FAST and IMAGE-FUV observations of a substorm onset. J. Geophys. Res. **108**(A9), 1344 (2003a). doi:10.1029/2002JA009787
S.B. Mende, C.W. Carlson, H.U. Frey, T.J. Immel, J.-C. Gerard, Image FUV and in situ FAST particle observations of substorm aurorae. J. Geophys. Res. **108**(A4), 8010 (2003b). doi:10.1029/2002JA009413
S.E. Milan et al., Auroral forms and the field-aligned current structure associated with field line resonances. J. Geophys. Res. **106**, 25825–25833 (2001)
E.V. Mishin, M. Forster, 'Alfvénic shocks' and low-altitude auroral acceleration. Geophys. Res. Lett. **22**, 1745–1748 (1995)
M. Morooka et al., Cluster observations of ULF waves with pulsating electron beams above the high latitude dusk-side auroral region. Geophys. Res. Lett. **31**, L05804 (2004). doi:10.1029/2003GL017714
F.S. Mozer et al., Observations of paired electrostatic shocks in the polar magnetosphere. Phys. Rev. Lett. **38**, 292–295 (1977)
F.S. Mozer, ISEE-1 observations of electrostatic shocks on auroral zone field lines between 2.5 and 7 Earth radii. Geophys. Res. Lett. **8**, 823–826 (1981)
F.S. Mozer, C.A. Kletzing, Direct observation of large, quasi-static, parallel electric fields in the auroral acceleration region. Geophys. Res. Lett. **25**, 1629–1632 (1998)
T. Nagatsuma et al., Field-aligned currents associated with Alfvén waves in the poleward boundary region of the nightside auroral oval. J. Geophys. Res. **101**, 21,715 (1996)
D.L. Newman, M.V. Goldman, M. Spector, F. Perez, Phys. Rev. Lett. **86**, 1239 (2001)
M.T. Nose et al., ULF pulsations observed by the ETS-VI satellite: Substorm associated azimuthal Pc 4 pulsations on the nightside. Earth Planets Space **50**, 63 (1998)
D.M. Ober et al., Electrodynamics of the poleward auroral border observed by Polar during a substorm on April 22, 1998. J. Geophys. Res. **106**, 5927 (2001)
J.V. Olson, Pi2 pulsations and substorm onsets: A review. J. Geophys. Res. **104**, 17499–17520 (1999)
H. Osaki, K. Takahashi, H. Fukunishi, T. Nagatsuma, H. Oya, A. Matsuoka, D.K. Milling, Pi2 pulsations observed from the Akebono satellite in the plasmasphere. J. Geophys. Res. **103**, 17,605 (1998)
G. Paschmann, S. Haaland, R. Treumann (eds.), *Auroral Plasma Physics* (Kluwer, Boston, 2003)
V.A. Pilipenko, E. Fedorov, M.J. Engebretson, K. Yumoto, Energy budget of Alfvén wave interactions with the auroral acceleration region. J. Geophys. Res. **109**, A10204 (2004). doi:10.1029/2004JA010440
V.A. Pilipenko, N.G. Mazur, E.N. Federov, M.J. Engebretson, D.L. Murr, Alfvén wave reflection in a curvilinear magnetic field and formation of Alfvénic resonators on open field lines. J. Geophys. Res. **110**, A10S05 (2005)
I.J. Rae et al., Evolution and characteristics of global Pc5 ULF waves during a high solar wind speed interval. J. Geophys. Res. **110**, A12211 (2005). doi:10.1029/2005JA011007
R. Rankin, J.C. Samson, V.T. Tikhonchuk, Discrete auroral arcs and nonlinear dispersive field line resonances. Geophys. Res. Lett. **26**, 663–666 (1999a)
R. Rankin et al., Auroral density fluctuations on dispersive field line resonances. J. Geophys. Res. **104**, 4399 (1999b)
R. Rankin et al., Shear Alfvén waves on stretched magnetic field lines near midnight in Earth's magnetosphere. Geophys. Res. Lett. **27**, 3265 (2000)
R. Rankin et al., Magnetospheric field line resonances: Ground-based observations and modeling. J. Geophys. Res. (2005). doi:10.1029/2004JA010919
B.N. Rogers et al., Role of dispersive waves in collisionless magnetic reconnection. Phys. Rev. Lett. **87**, 195004 (2001)
J.M. Ruohoniemi, R.A. Greenwald, K.B. Baker, J.C. Samson, HF radar observations of Pc 5 field line resonances in the midnight/early morning MLT sector. J. Geophys. Res. **96**, 15 697–15 710 (1991)
T. Saito, Geomagnetic pulsations. Space Sci. Rev. **10**, 319–412 (1969)
O. Saka et al., Ground-satellite correlation of low-altitude Pi2 pulsations: A quasi-periodic field line oscillation in the magnetosphere. J. Geophys. Res. **101**, 15433 (1996)

T. Sakurai, R.L. McPherron, Satellite observations of Pi 2 activity at synchronous orbit. J. Geophys. Res. **88**, 7015–7027 (1983)
J.C. Samson et al., Latitude-dependent characteristics of long-period geomagnetic micropulsations. J. Geophys. Res. **76**, 3675–3683 (1971)
J.C. Samson, T.J. Hughes, F. Creutzberg, D.D. Wallis, R.A. Greenwald, J.M. Ruohoniemi, Observations of a detached discrete arc in association with field line resonances. J. Geophys. Res. **96**, 15,683–15,695 (1991a)
J.C. Samson, R.A. Greenwald, J.M. Ruohoniemi, T.J. Hughes, D.D. Wallis, Magnetometer and radar observations of magnetohydrodynamic cavity modes in the earth's magnetosphere. Can. J. Phys. **69**, 929–937 (1991b)
J.C. Samson, D.D. Wallis, T.J. Hughes, F. Creutzberg, J.M. Ruohoniemi, R.A. Greenwald, Substorm intensification and field line resonances in the nightside magnetosphere. J. Geophys. Res. **97**, 8459–8518 (1992a)
J.C. Samson, B.G. Harrold, J.M. Ruohoniem, R.A. Greenwald, A.D.M. Walker, Field line resonances associated with MHD waveguides in the magnetosphere. Geophys. Res. Lett. **19**, 441–444 (1992b)
J.C. Samson, L.L. Cogger, Q. Pao, Observations of field line resonances, auroral arcs, and auroral vortex structures. J. Geophys. Res. **101**, 17 373 (1996)
J.C. Samson, R. Rankin, V. Tikhonchuk, Optical signatures of auroral arcs produced by field-line resonances: comparison w!ith satellite observations and modeling. Ann. Geophys. **21**, 933–945 (2003)
J.-A. Sauvaud et al., Case studies of the dynamics of ionospheric ions in the Earth's magnetotail. J. Geophys. Res. **109**, A01212 (2004). doi:10.1029/2003JA009996
D. Schriver et al., FAST/Polar conjunction study of field-aligned auroral acceleration and corresponding magnetotail drivers. J. Geophys. Res. **108**(A9), 8020 (2003). doi:10.1029/2002JA009426
V.S. Semenov et al., A comparison and review of steady-state and time-varying reconnection. Planet. Space Sci. **40**, 63–87 (1992)
M. Silberstein, N.F. Otani, Computer simulation of Alfvén waves and double layers along auroral field lines. J. Geophys. Res. **99**, 6351 (1994)
H.J. Singer, D.J. Southwood, R.J. Walker, M.G. Kivelson, Alfvén wave resonances in a realistic magnetospheric magnetic field geometry. J. Geophys. Res. **86**, 4589 (1981)
N. Singh, Spontaneous formation of current-driven double layers in density depletions and its relevance to solitary Alfvén waves. Geophys. Res. Lett. **29**(7), 1147 (2002). doi:10.1029/2001GL014033
Y. Song, Theoretical constraints on mechanisms for the substorm current wedge, in *Substorms-4*, ed. by S. Kokubun, Y. Kamide (Terra Scientific, Tokyo, 1998), p. 543
Y. Song, R.L. Lysak, Current dynamo effect of 3-d time-dependent reconnection in the dayside magnetopause. Geophys. Res. Lett. **16**, 911 (1989)
Y. Song, R.L. Lysak, Displacement current and the generation of parallel electric fields. Phys. Rev. Lett. (2006). doi:10.1103/PhysRevLett.96.145002
D.J. Southwood, Some features of field line resonances in the magnetosphere. Planet. Space Sci. **22**, 483 (1974)
K. Stasiewicz et al., Cavity resonators and Alfvén resonance cones observed by Freja. J. Geophys. Res. **102**, 2565 (1997)
K. Stasiewicz et al., Small scale Alfvénic structure in the aurora. Space Sci. Rev. **92**, 423–533 (2000)
T. Streed, C. Cattell, F. Mozer, S. Kokubun, K. Tsuruda, Spiky electric fields in the magnetotail. J. Geophys. Res. **106**, 6275–6289 (2001)
A.V. Streltsov, W. Lotko, Small scale "electrostatic" auroral structures and Alfvén waves. J. Geophys. Res. **104**, 4411–4426 (1999)
A.V. Streltsov, W. Lotko, Reflection and absorption of Alfvénic power in the low altitude magnetosphere. J. Geophys. Res. **108**(A4), 8016 (2003). doi:10.1029/2002JA009425
A.V. Streltsov, W. Lotko, Multiscale electrodynamics of the ionosphere-magnetosphere system. J. Geophys. Res. (2004). doi:10.1029/2004JA010457
A.V. Streltsov, G. Marklund, Divergent electric fields in downward current channels. J. Geophys. Res. (2006). doi:10.1029/2005JA011196
P.R. Sutcliffe, The association of harmonics in Pi2 power spectra with the plasmapause. Planet. Space Sci. **23**, 1581 (1975)
T. Takada, K. Seki, M. Hirahara, T. Terasawa, M. Hoshino, T. Mukai, Two types of PSBL ion beam observed by Geotail: Their relation to low frequency electromagnetic waves and cold ion energization. Adv. Space Res. **36**, 1883–1889 (2005a)
T. Takada, K. Seki, M. Hirahara, M. Fujimoto, Y. Saito, H. Hayakawa, T. Mukai, Statistical properties of low-frequency waves and ion beams in the plasma sheet boundary layer: Geotail observations. J. Geophys. Res. **110**, A02204 (2005b). doi:10.1029/2004JA010395

T. Takada et al., Alfvén waves in the near-PSBL lobe: Cluster observations. Ann. Geophys. **24**, 1001–1013 (2006)
K. Takahashi, ULF waves: 1997 IAGA Division 3 reporter review. Ann. Geophys. **16**, 787–803 (1998)
K. Takahashi et al., AMPTE/CCE observations of substorm-associated standing Alfvén waves in the midnight sector. Geophys. Res. Lett. **15**, 1287–1290 (1988)
K. Takahashi, S.-I. Ohtani, B.J. Anderson, Statistical analysis of Pi 2 pulsations observed by the AMPTE CCE spacecraft in the inner magnetosphere. J. Geophys. Res. **100**, 21 929–21 941 (1995)
K. Takahashi, B.J. Anderson, S. Ohtani, Multisatellite study of nightside transient toroidal waves. J. Geophys. Res. **101**, 24 815–24 825 (1996)
K. Takahashi, P.J. Chi, R.E. Denton, R.L. Lysak, eds, *Magnetospheric ULF Waves: Synthesis and New Directions*. Geophysical Monograph Series, vol. 169 (2006)
P.K. Toivanen, D.N. Baker, W.K. Peterson, X. Li, E.F. Donovan, A. Viljanen, A. Keiling, J.R. Wygant, C.A. Kletzing, Plasma sheet dynamics observed by the Polar spacecraft in association with substorm onsets. J. Geophys. Res. **106**, 19,117–19,130 (2001)
P.K. Toivanen et al., Polar observations of transverse magnetic pulsations initiated at substorm onset in the high-latitude plasma sheet. J. Geophys. Res. **108**(A7), 1267 (2003). doi:10.1029/2001JA009141
S. Tomczyk et al., Alfvén waves in the solar corona. Science (2007). doi:10.1126/science.1143304
R.B. Torbert, F.S. Mozer, Electrostatic shocks as the source of discrete auroral arcs. Geophys. Res. Lett. **5**, 135–138 (1978)
M.R. Torr et al., A far ultraviolet imager for the International Solar-Terrestrial Physics Mission, in *The Global Geospace Mission*, ed. by C.T. Russell (Kluwer Academic, Norwell, 1995), pp. 459–495
T.S. Trondsen et al., Asymmetric multiple auroral arcs and inertial Alfvén waves. Geophys. Res. Lett. **24**, 2945–2948 (1997)
C.Y. Tu, E. Marsch, MHD structures waves and turbulence in the solar wind: Observations and theories. Space Sci. Rev. **73**, 1 (1995)
T. Uozumi, K. Yumoto, H. Kawano et al., Characteristics of energy transfer of Pi 2 magnetic pulsations: Latitudinal dependence. Geophys. Res. Lett. **27**, 1619–1622 (2000)
T. Uozumi, K. Yumoto, H. Kawano et al., Propagation characteristic of Pi 2 magnetic pulsations observed at ground high latitudes. J. Geophys. Res. **109**, A8 (2004). doi:10.1029/2003JA009898
O.L. Vaisberg, L.A. Avanov, J.L. Burch, J.H. Waite Jr., Measurements of plasma in the magnetospheric lobes. Adv. Space Res. **18**, 63 (1996)
A. Vaivads et al., What high altitude observations tell us about the auroral acceleration: A Cluster/DMSP conjunction, Geophys. Res. Lett. **30**, 1106 (2003). doi:10.1029/2002GL016006
A. Vaivads, Y. Khotyaintsev, M. Andre et al., Structure of the magnetic reconnection diffusion region from four-spacecraft observations. Phys. Rev. Lett. **93**, 10 (2004). doi:10.1103/PhysRevLett.93.105001
A. Vaivads et al., Microphysics of magnetic reconnection. Space Sci. Rev. **122**, 19–27 (2006). doi:10.1007/s11214-006-7019-3
J. Vogt, G. Haerendel, Reflection and transmission of Alfvén waves at the auroral acceleration region. Geophys. Res. Lett. **25**, 277 (1998)
J. Vogt, Alfvén wave coupling in the auroral current circuit. Surv. Geophys. **23**, 335–377 (2002)
M. Volwerk, P. Louarn, T. Chust, A. Roux, H. Feraudy, Solitary kinetic Alfvén waves: A study of the Poynting flux. J. Geophys. Res. **101**, 13,335 (1996)
J.-E. Wahlund et al., On ion acoustic turbulence and the nonlinear evolution of kinetic Alfvén waves in aurora. Geophys. Res. Lett. **21**, 1831–1834 (1994)
J.-E. Wahlund et al., Broadband ELF plasma emission during auroral energization 1. Slow ion acoustic waves. J. Geophys. Res. **103**(A3), 4343–4376 (1998)
A.D.M. Walker et al., STARE auroral radar observations of Pc 5 geomagnetic pulsations. J. Geophys. Res. **84**, 3373–3388 (1979)
A.D.M. Walker, J.M. Ruohoniemi, K.B. Baker, R.A. Greenwald, J.C. Samson, Spatial and temporal behavior of ULF pulsations observed by the Goose Bay HF radar. J. Geophys. Res. **97**, 12 187 (1992)
J.A. Wanliss, R. Rankin, Auroral substorm dynamics and field line resonances. Earth Planets Space **54**, 927–932 (2002)
J.A. Wanliss, R. Rankin, J.C. Samson, V.T. Tikhonchuk, Field line resonances in a stretched magnetotail: CANOPUS optical and magnetometer observations. J. Geophys. Res. **107**(A7), 1100 (2002). doi:10.1029/2001JA000257
M.R. Warner, D. Orr, Time of flight calculations for high latitude geomagnetic pulsations. Planet. Space Sci. **27**, 679–689 (1979)
C.L. Waters et al., Low latitude geomagnetic field line resonance: Experiment and modeling. J. Geophys. Res. **99**, 17,547–17,558 (1994)
C.L. Waters, J.C. Samson, E.F. Donovan, The temporal variation of the frequency of high latitude field line resonances. J. Geophys. Res. **100**, 7987–7996 (1995)

C.E.J. Watt et al., Self-consistent electron acceleration due to inertial Alfvén waves. J. Geophys. Res. (2005). doi:10.1029/2004JA010877
D.R. Weimer, D.A. Gurnett, Large-amplitude auroral electric fields measured with DE 1. J. Geophys. Res. **98**, 13,557–13,564 (1993)
A.N. Wright et al., Phase mixing and phase motion of Alfvén waves on tail-like and dipole-like magnetic field lines. J. Geophys. Res. **104**, 10,159 (1999)
J.R. Wygant et al., Polar spacecraft based comparisons of intense electric fields and Poynting flux near and within the plasma sheet-tail lobe boundary to UVI images: An energy source for the aurora. J. Geophys. Res. **105**, 18,675 (2000)
J.R. Wygant et al., Evidence for kinetic Alfvén waves and parallel electron energization at 4–6 R_E altitudes in the plasma sheet boundary layer. J. Geophys. Res. **107**(A8), 1201 (2002). doi:10.1029/2001JA900113
B.-L. Xu et al., Observations of optical aurora modulated by resonant Alfvén waves. J. Geophys. Res. **98**, 11,531–11,541 (1993)
Y. Yamade, M. Fujimoto, N. Yokokawa, M.S. Nakamura, Field-aligned currents generated in magnetotail reconnection: 3D Hall-MHD simulations. Geophys. Res. Lett. **27**, 1091 (2000)
T.K. Yeoman, M. Lester, Characteristics of MHD waves associated with storm sudden commencements observed by SABRE and ground magnetometers. Planet. Space Sci. **38**, 603–616 (1990)
T.K. Yeoman, D. Orr, Phase and spectral power of mid-latitude Pi2 pulsations: Evidence for a plasmaspheric cavity resonance. Planet. Space Sci. **37**, 1367 (1989)
T.K. Yeoman et al., Polarization, propagation and MHD wave modes of Pi2 pulsations: SABRE/SAMNET results. Planet. Space Sci. **39**, 983–998 (1991)
L.M. Zelenyi, E.E. Grigorenko, A.O. Fedorov, Spatial-temporal ion structures in the Earth's magnetotail: Beamlets as a result of nonadiabatic impulse acceleration of the plasma. JETP Lett. **80**, 663–673 (2004)
Y. Zheng et al., Coordinated observation of field line resonance in the mid-tail. Ann. Geophys. **24**, 707–723 (2006)
C.W.S. Ziesolleck, D.R. McDiarmid, Auroral latitude Pc5 field line resonance: Quantized frequencies, spatial characteristics, and diurnal variation. J. Geophys. Res. **99**, 5817–5830 (1994)